ABSTRACT

Title of Document: THERMOPLASTIC MICROFLUIDIC TECHNOLOGIES FOR PORTABLE AND DISPOSABLE BIOANALYTICAL AND DIAGNOSTIC PLATFORMS

Omid David Rahmanian, Ph.D. 2015

Directed By: Professor Don L. DeVoe
Department of Mechanical Engineering

Portable and cost-effective medical diagnostic technologies that require minimal external infrastructure for their operation are highly desirable for on-field military operations, defense against acts of bioterrorism, and infectious disease screening in resource-limited environments. Miniaturized Total Analysis Systems (μTAS) have the potential to fulfill this un-met need via low-cost, portable, and disposable point-of-care (POC) diagnostic devices. Inherent advantages of μTAS systems can be utilized to transform diagnostic technologies that currently require significant investment in centralized laboratories and highly trained personnel into automated, integrated, and miniaturized platforms.

This dissertation addresses the development of microfabrication techniques and resulting component technologies that are realized in low-cost thermoplastic substrates.

A thermoplastic microfabrication technique termed *orogenic microfabrication*, based on a non-reversible solvent-assisted swelling mechanism, is developed to provide unique capabilities for microscale and nanoscale patterning in rigid thermoplastics with minimal infrastructure. Orogenic microfabrication is compatible with multiple masking techniques including photolithography, chemical surface modification, contact and noncontact spotting, and inkjet deposition techniques, with each masking method offering unique influence on resulting orogenic structures that can be applied to microfluidic and μTAS systems. Direct ink masking is further explored as a low-cost rapid prototyping tool for fabrication of simple microfluidic devices where channel formation and bonding are combined into a single step, resulting in fully enclosed microfluidic channels within 30 minutes.

Chemical surface passivation by UV-ozone treatment is utilized in combination with orogenic swelling and thermocompression bonding to develop single-use burst valves with tunable burst pressures. In addition to assisting in on-chip fluid manipulation, the normally closed burst valves enable on-chip reagent packaging and hermetic sealing of bioactive material in lyophilized format, and can be used for delivery of stored reagents for a range of disposable point-of-care assays.

On-chip integrated micropumps are also developed, using simple fabrication process compatible with conventional thermoplastic fabrication techniques such as direct micromilling or injection molding. Direct displacement of liquid reagents using screw-assisted pumping can be operated either automatically or manually, with on-demand delivery of liquid reagents in a wide range of flow rates typically used in microfluidic applications.

Collectively, the technologies developed in this dissertation may be applied to the future development of simple, disposable, and portable diagnostic devices that have the potential to be operated without off-chip instrumentation. On-chip storage of buffers and reagents in either dry or liquid format, and on-demand delivery of liquid reagents is packaged in a miniaturized, portable, and automated platform that can be operated in resource-constrained settings by practitioners with minimal expertise.

THERMOPLASTIC MICROFLUIDIC TECHNOLOGIES FOR PORTABLE AND DISPOSABLE BIOANALYTICAL AND DIAGNOSTIC PLATFORMS

By

Omid David Rahmanian

Dissertation submitted to the Faculty of the Graduate School of the
University of Maryland, College Park, in partial fulfillment
of the requirements for the degree of
Doctor of Philosophy
2015

Advisory Committee:
Professor Don L. DeVoe, Chair
Professor John Fisher
Professor Srinivasa R. Raghavan
Dr. Robert Ulrich
Professor Ian White

Dedication

To the memory of my mother Forough Sohaylian, who is lovingly remembered everyday.

Acknowledgements

I would like to express my sincere gratitude to my Advisor, Prof. Don DeVoe, whose enthusiasm, support, and guidance has been ever present throughout my graduate studies. It is a privilege to call him my mentor as he has had a profound influence in my career.
I would also like to thank the members of my committee, Profs. John Fisher, Srinivasa Raghavan, Ian White, and Dr. Robert Ulrich for their invaluable guidance.

Many Thanks to my colleagues at Maryland MEMS and Microfluidics Laboratory for their support, friendship, and the good times we have had together.

This work would have been impossible if not for the love and support of my family. I am forever grateful for the sacrifices my parents Hossein and Forough made allowing me to follow my dreams. Tarane and Payam, I am extremely lucky to have such loving and caring role models.

Last, but certainly not least, I would like to thank Parastou for her boundless love, inspiration, and support.

Table of Contents

List of Tables

List of Figures

Chapter 1: Introduction

1.1 Brief history of microfluidics

The origins of microfluidics field can be traced back to mid 1970s, where scientist at Stanford University developed a silicon-based gas chromatographer[1]. By 1990s the concept of miniaturized total chemical analysis systems (μTAS) was pioneered by Manz et al[2], who argued for faster and more efficient separations in chromatography when the system is miniaturized to take advantage of the inherit benefits of smaller scales. But it wasn't until late 1990s and the development of soft lithography[3] and use of polydimethylsiloxane (PDMS) that microfluidics began to flourish as an enabling technology and became widely adopted for fabricating devices in both academia as well as early industry. Since then, tremendous progress has been made in the field and the impact of microfluidics can be seen in various scientific disciplines such as biology[4,5], medicine[6,7], chemistry[8], physics[9,10], and forensics[11,12].

1.2 Common substrates used in microfluidic devices

Since many of the early microfluidics fabrication technologies were borrowed from the microelectromechanical systems (MEMS) industry, glass and silicon were initially the substrate of choice in the microfluidics community[13].Besides the convenience of adopting a well-characterized substrate, glass and silicon offered desired properties for various microfluidic applications[14,15]. However, several disadvantages of glass and silicon, combined with the superior ease and low-cost of device fabrication with elastomers, resulted in the majority of researchers to adopt PDMS as the main microfluidic substrate. In addition, inherent characteristics of

PDMS, mainly its optical transparency, facile tuning of surface hydrophilicity, ability to reversibly (and irreversibly) bond to glass, and its elasticity were highly desired characteristics that were utilized in a plethora of applications[4,16,17]. However, unlike the MEMS industry where silicon has remained as the mainstay material, as the microfluidics technology developed further, the materials used for device fabrication has also undergone a large transition and has expanded well beyond PDMS. Among others, several plastic materials such as Polystyrene (PS)[18,19], polymethylmethacrylate (PMMA)[20,21], polycarbonate (PC)[22], cyclic olefin (co) polymers (COC/COP)[23] have been heavily used as substrates in various microfluidic platforms. Since the number of substrates for microfluidic devices has rapidly increased in the past two decades, one of the key factors that must be considered early in the research process is the choice of substrate material for the particular application in mind[24,25]. For example in cell biology research, polystyrene is highly preferable to other plastics despite its challenges in microfabrication. On the other hand, despite the ease of fabricating devices with PDMS, characteristics such as leaching of un-crosslinked monomers, and absorption of small molecules makes use of PDMS as a substrate detrimental to cell studies[26].

1.3 Application of microfluidics in point-of-care diagnostics

One of the first potential applications of microfluidics has been in point-of-care (POC) diagnostics. Defined as diagnostic tests performed at or near site of a patient[27], microfluidic-enabled diagnostic platforms hold significant promise to make a meaningful impact in global health[28,29], particularly in resource-constrained settings such as sub-Saharan Africa and active war zones, where access to centralized

laboratories and well-equipped hospital with trained personnel is highly scarce. A schematic of an of an ideal point-of-care diagnostic device as depicted in Figure 1.1 has to be capable of handling minute volumes of samples, processing measurements

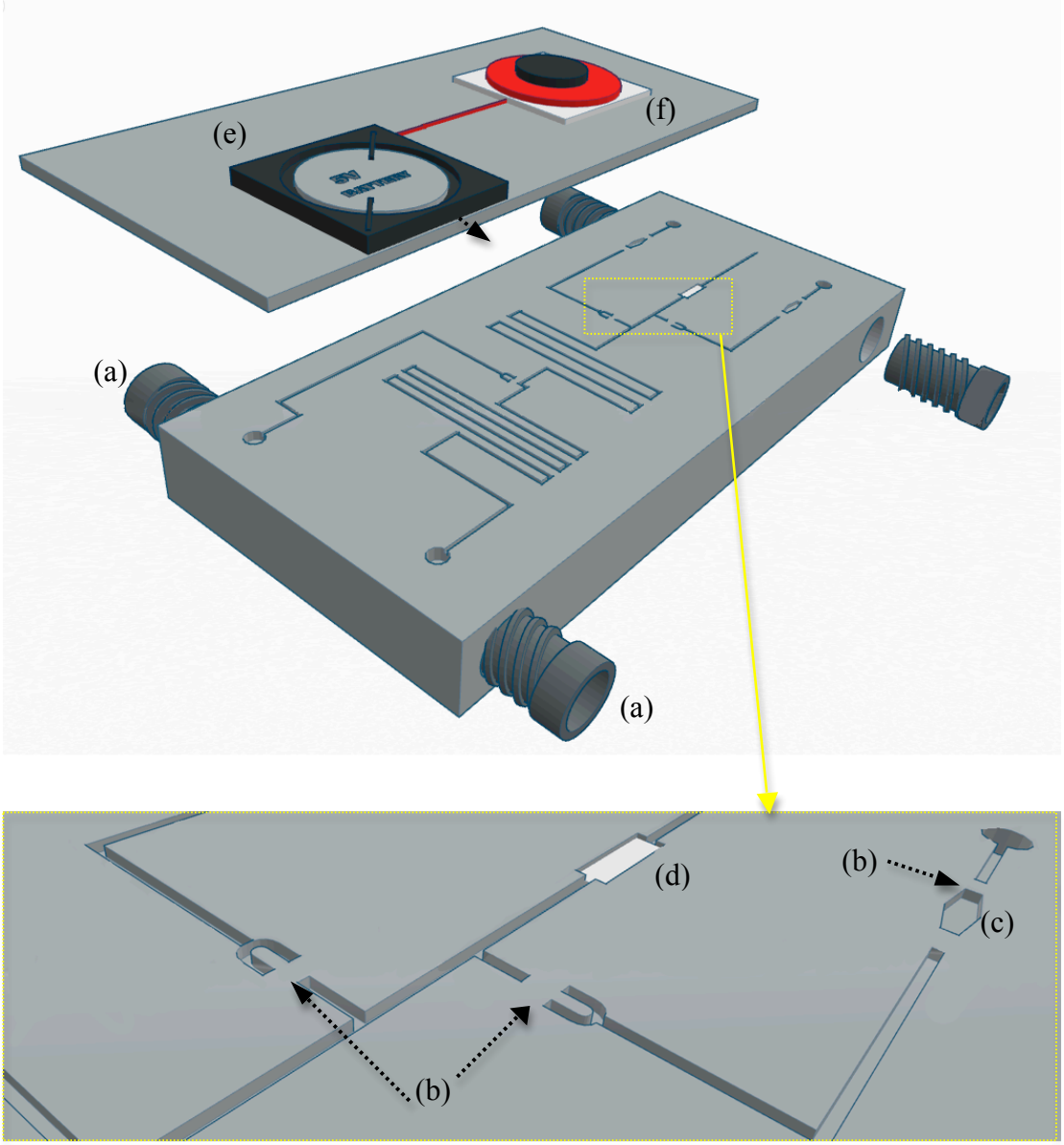

Figure 1.1 Schematic of ideal microfluidic diagnostic device for use at the point-of-care. A two-layer design is shown where bottom layer houses all the fluidic circuitry, integrated manually-actuated pumps (a), normally-closed valves (b), hermetically sealed reagent storage reservoirs(c), and a detection element (d). While sealing the microfluidic circuitry, top layer also houses integrated optics (e) as well as a battery (f) for remote operation.

from complex fluidic samples in a relatively fast and efficient manner, be automated and operable without the need of a trained user. In addition, the device needs to be portable, low-cost, and rugged. Lastly, the diagnostic device should be free of off-chip instrumentations, compatible with biological samples, and capable of storing all bioactive reagents necessary for performing diagnostic assays without compromising the integrity or activity of the reagents. Keeping all above requirements in mind, as mentioned previously, one of the first key decisions for POC diagnostic devices is the choice of material, which will ultimately dictate many of the characteristics of the device including its optical properties, adhesion of biomolecules, and achievable flow rate [30].

Cyclic olefin polymers (COP) are a class of thermoplastics that are increasingly popular as substrates in microfluidic devices, and in particular for POC diagnostic applications. Inherent characteristics of COP, mainly its transparency in both visible and UV light, low water absorption, biological inertness, exceptional dimensional stability, minimal gas permeability, and compatibility with a wide range of acids, bases, and alcohols makes COP and ideal substrate for POC diagnostic applications. In Addition, mature rapid prototyping techniques such as injection molding[31] and hot embossing[32] can be utilized for high-throughput manufacturing of COP devices in a cost-effective manner. However since the use of COP is relatively new in the field of microfluidics, creative and novel engineering approaches are required to develop and implement fluidic components such as mixers, valves, and pumps for processing and manipulation of small volumes of fluids within the microfluidic device.

1.4 Approach and organization of dissertation

The goal of the research presented in this dissertation is to explore innovative fabrication techniques for thermoplastic microfluidic platforms. With the application of point-of-care diagnostics in mind, we aim to develop novel techniques that allows us to readily integrate some of the essential components of a point-of-care diagnostic device, mainly microfluidic channels, valves, and pumps into a truly portable, low-cost, and disposable package, operable with minimal off-chip instrumentation. Collectively, the advances reported in this thesis will results in a simple, low-cost thermoplastic device that can potentially be operated by a practitioner with little or no experience in the laboratory methods in diagnosis of multiple analytes from complex fluidic samples. This dissertation is organized into six Chapters. In the following Chapter (Chapter 2) Cyclic Olefin polymers (COP) are discussed as ideal substrates for point-of-care diagnostic devices. Besides their low cost and relative ease in manufacturability, wider variety of desirable physical and chemical characteristics of COPs are presented. Furthermore, a novel fabrication technique, coined "Orogenic Microfabrication" is described, allowing for facile fabrication of a wide variety of micro and nano scale features, that are otherwise difficult to produce using conventional thermoplastic fabrication methods. In addition, a wide variety of masking techniques are explored, and unique advantages of each of these masking techniques are presented. Chapter 2 is adapted from Rahmanian et al.[33] In Chapter 3, direct ink masking is utilized in order to fabricated fully-sealed all thermoplastic microfluidic devices using the orogenic microfabrication process. This low-cost technique is ideal for rapid prototyping of thermoplastic microfluidic devices with a

design-to-device cycle of approximately 30minutes. Chapter 3 is adapted from Rahmanian et al.[34] In Chapter 4 that is adapted from Rahmanian et al.[35], we use indirect masking method of UV-Ozone patterning, coupled with orogenic microfabrication to develop single-use normally-closed burst valves in thermoplastic devices. Tuning of burst pressure and use of burst valves to achieve hermetically sealed reservoir for storage of dried reagents in COP devices is also demonstrated. Lastly, in Chapter 5, a facile fabrication technique is developed for miniaturization and integration of micropumps in thermoplastic microfluidic devices capable of volumetric flow rates of nanoliters per minute, up to tens of microliters per minute. The integrated micropumps directly support on chip storage of lyophilized and liquid reagents, and can be utilized for rapid reconstitution of lyophilized and hermetically sealed bioactive reagents when coupled with burst valves.

Chapter 2: Orogenic Microfabrication: An Irreversible solvent-assisted swelling mechanism for patterning of thermoplastics polymer surfaces

2.1 Summary

This Chapter presents a series of experiments that were completed through combined efforts with Dr. Chien-Fu Chen at the University of Maryland College Park and is adapted from a published article in which Dr. Chen and I share first authorship. Dr. Chen performed the work regarding direct photoresist masking, and that of UV/ozone surface passivation masking. Analysis and manuscript preparation were the result of a combined effort from both parties.

In this Chapter, an entirely new method for the fabrication of microscale features in thermoplastic substrates is presented. Unlike traditional thermoplastic microfabrication techniques reviewed in previous section, in which bulk polymer is displaced from the substrate by machining or embossing, a unique process termed orogenic microfabrication has been developed in which selected regions of a thermoplastic surface are raised from the substrate by an irreversible solvent swelling mechanism. The orogenic technique allows thermoplastic surfaces to be patterned using a variety of masking methods, resulting in three-dimensional features including microchannel that would be difficult to achieve through traditional microfabrication methods. Using cyclic olefin polymer as a model thermoplastic material, several variations of this process are described to realize growth heights ranging from several

nanometers to tens of micrometers, with patterning techniques include direct photoresist masking, patterned UV/ozone surface passivation, elastomeric stamping, and noncontact spotting. Orogenic microfabrication is also demonstrated by direct inkjet printing as a facile photolithography-free masking method for rapid desktop thermoplastic microfabrication.

2.2 Cyclic olefin (co)polymers in Microfluidics

2.2.1 Introduction to Cyclic olefin (co)polymers

Thermoplastics are a class of polymers that demonstrate a unique softening behavior when heated above glass transition temperatures, while retaining the ability to return to their original chemical states when cooled.[36] Unlike elastomers, thermoplastics remain chemically and dimensionally stable over a wide range of temperatures and pressures and allow softening and reshaping upon applying heat and pressure. These characteristics has made thermoplastics, in particular cyclic olefin (co)polymers (COP) as attractive materials for the fabrication of a variety of microsystems, with applications including micro-optical components[37], micro cantilever chemical sensors[38], microstructure biomimetic surfaces[39,40], and microfluidic chips[31]. In the following section, a brief review of the physical and chemical properties of COPs are discussed, followed by a brief review of currently available methods for fabrication of COP devices used in microfluidic platforms.

2.2.2 Chemical and Physical properties of cyclic olefin polymers

Cyclic olefin (co)polymers are commercially available through several companies such as TOPAS, APEL, and Zeonor (Zeonex), with COP resin and plaques used

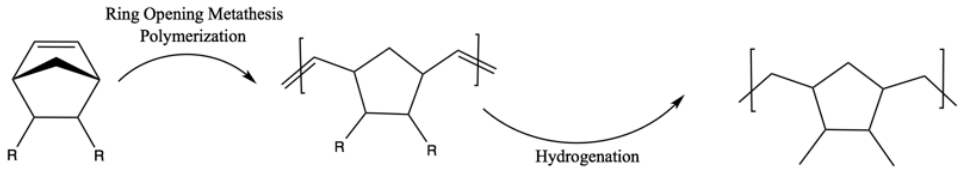

Figure 2.1 Typical polymerization scheme for cyclic olefin polymer, reproduced from Ref. 41

throughout this dissertation obtained from Zeon Chemicals (Zeonor). It is important to note that although COP and COC are often used interchangeably in literature, cyclic olefin polymers are chemically different from cyclic olefin copolymers, and hence the two materials exhibit different characteristics. According to literature, the polymerization process Zeon chemicals uses for COP synthesis includes a ring-opening metathesis polymerization of the cyclic monomer followed by hydrogenation

Table 2.1 Common physical and chemical characteristics of commercially available cyclic olefin polymers reproduced from Ref. 23,36,41

Heat distortion temp (ºC)	70-170
Density g/cm3	1.01-1.08
Light transmission %	90-93
Refractive index	1.51-1.54
Glass transition temperature (ºC)	70-177
Water contact angle (º)	93-116
Biological compatibility	Exceptionally inert
Flexural modulus (MPa)	1600-3450
Tensile strength (MPa)	45-78
Water absorption (%)	<0.01
Birefringence	Low

as shown in Figure 2.1. Since during polymerization bulky cyclic olefin units are randomly or alternately attached to the backbone of the polymer, COPs show high glass transition temperatures, are optically clear, and demonstrate low shrinkage, low moisture absorption, and are amorphous[41]. Cyclic olefin copolymers however are a

product of copolymerization of cyclic norbornene with ethylene. Since repeating units of COPs are all cyclic, fewer low-molecular-weight additives are typically present in COPs, providing greater optical properties, better chemical uniformity, and fewer leaching of low-molecular-weight materials when compared with COC. Some of these advantageous physical and chemical properties of COPs are listed in table 1.1. Also, as a result of the unique polymerization technique used, Low water absorption, resistance to acids, bases, as well as polar solvents are exclusive to cyclic olefin polymers and are not found in other common polymer substrates used in microfluidics such as PMMA, PC, or PS[23] as depicted in table 1.2. Lastly, Optical clarity of COPs, both in the visible and UV light are highly attractive properties for microfluidic devices, in particular for point-of-care diagnostics applications where optical clarity and low auto fluorescence are critical for detection purposes.

Table 2.2 Comparison of COP's chemical resistance to common microfluidic substrates, reproduced from Ref. 23

	COP	**PMMA**	**PC**	**PS**
`	+	o	+	+
Acids, strong and conc.	+	-	-	o
Alcohols, aliphatic	+	-	o	+
Aldehydes	o	o	o	-
Bases	+	o	-	+
Esters	+	-	-	-
Hydrocarbons, aliphatic	-	o	o	-
Hydrocarbons, aromatic	-	-	-	-
Ketones	o	-	-	-

2.2.3 Conventional replication techniques for cyclic olefin polymers

Thermoplastic microfabrication has been widely explored using replication methods including hot[42] or cold[20] embossing, injection molding[43], and hot roller microprinting[32], as well as serial fabrication methods such as direct laser machining[22,44] and micromilling[45]. Each of these techniques involves the removal or displacement of material from desired regions within the substrate through thermal or mechanical means. Below is a brief description of some of these replications methods and their benefits for use in thermoplastic microfluidic device fabrication.

2.2.3a Injection molding The process of micro-injection molding has been adopted and miniaturized from the plastic industry to fabricate micron sized features on a variety of thermoplastics substrates[43] including COPs. A typical process involves using a variotherm setup to melt thermoplastic polymer resins at temperatures above their glass transition temperature T_g and pressurize the resulting viscous polymer into a hot or cold mold containing the desired micron-scale features. After cooling of the apparatus below the glass transition temperature of thermoplastic, the mold is opened up to eject the molded thermoplastic. Since a single thermo cycling process only takes few minutes[46], the automated process is highly cost-effective for high-throughput manufacturing of microfluidic devices. However, start-up cost and complexity of the process[31] are among disadvantages preventing a broader adoption of injection molding in academic settings and prototype evaluations.

2.2.3b Hot Embossing The process of hot-embossing is relatively similar to injection molding, however due to a more simplified process, comparatively low-cost for master molds, and larger range of suitable materials hot embossing has been more

widely used for fabrication of thermoplastic microfluidic devices in both academia and industry[31]. In a typical process, a hydraulic press is used to pressurize a mold against a thermoplastic film while the apparatus is being heated above the softening temperature of the thermoplastic to replicate mold features into the softened substrate. After Cooling, opening the hydraulic press results in withdrawal of the mold from the thermoplastic. Although batch fabrication can limit the use of hot embossing beyond device prototyping, hot roller embossing[32] proves to be a potential process for high-throughput mass fabrication of thermoplastics microfluidic devices.

2.2.3c Micromilling Unlike hot embossing or injection molding where a master mold is required for pattern replication by displacement of softened thermoplastic substrate, micromilling typically use a computerized numerical control (CNC) milling machine for direct removal of desired patterns from a thermoplastic substrate. Since the pattern feature is fed to the CNC machine by computer-aided-design (CAD) software, tinkering and manipulation of microfluidic features is relatively easy, rendering direct milling as a suitable fabrication method for rapid prototyping without the need to invest in expensive molds.

2.2.4 Conventional bonding techniques for cyclic olefin polymers

Sealing of microchannels and other microfluidic elements in thermoplastic substrates, regardless of the replication technique, involves bonding of a capping layer to the layer containing microchannels[36]. While there are several direct and indirect bonding techniques available for thermoplastic substrates reviewed elsewhere[36], here we briefly describe the process for thermal fusion bonding and solvent bonding, two of the most common techniques used for bonding of thermoplastics including COP.

2.2.4a Thermal bonding During thermal bonding, the mating substrates are heated slightly above their glass transition temperature T_g while a pressure is applied to increase the contact surface area between the mating substrates.[36] Combination of the applied pressure and temperature results in flow and interdiffusion of polymer at the mating interface, where polymer chains fuse together resulting in a strong cohesive bond at the interface. Selection of bonding temperatures and pressures are highly dependent on the type of thermoplastic, and require optimization to avoid deformation of the microfluidic features due to bulk polymer flow, a major challenge of thermal fusion bonding technique[47].

2.2.4b Solvent-assisted bonding Solvent bonding takes advantage of the solubility of polymers in selected solvents to create a solvated polymer layer at the interface between two mating thermoplastic substrates. A suitable solvent can be determined by considering Hildebrandt parameter of solvents and thermoplastics, which provides a numerical estimation for the attraction of solvents to the thermoplastic of choice. For example, cyclohexane and decalin have previously been used for bonding of COP substrates with solubility parameters of 16.7 and 8.7 $[J/cm^3]^{1/2}$ respectively. Solvated surface of thermoplastics present loose and mobile polymer chains at the mating interface, resulting in "intertwining of chains across the interface" when two solvated thermoplastics are brought into intimate contact and pressurized in a hydraulic press. The strength of the bond achieved during solvent bonding is exceptionally strong[36], close to the bond of polymer chains in the bulk of the polymer.

2.3 Introduction to "Orogenic" microfabrication

Here we report an entirely different approach to forming microscale features in

thermoplastics termed orogenic microfabrication, wherein selected regions of a COP thermoplastic surface are raised from the bulk substrate through an irreversible solvent swelling mechanism. The term orogenic ("mountain forming") is used to differentiate the process from conventional thermoplastic microfabrication methods, reviewed in section 2.2, based on material removal or displacement rather than surface growth. The orogenic process comprises selective exposure of a thermoplastic surface to a suitable organic solvent, resulting in controlled and irreversible swelling of the exposed regions, as depicted in Figure 2.2. As the polymer expands due to solvent uptake, mobile polymer chains rearrange within the polymer matrix, resulting in permanent volume change within the plasticized regions even after the solvent has been fully removed from the bulk polymer. Unlike solvent-assisted microcontact molding[48], a version of soft lithography in which solvent exposure is used to soften a thermoplastic substrate to enable replica molding from an elastomer template, and capillary imprint lithography[49,50], which employs thermally induced capillary flow to reshape a polymer surface using a mold, orogenic microfabrication involves patterned surface growth to achieve the desired features. For amorphous nonpolar thermoplastics, a chemical typically acts as a good solvent for the polymer when the cohesive energy densities for each molecular system are nearly equal[51]. The Hildebrandt solubility parameter, defined as the square root of the cohesive energy density[52], provides a suitable metric for selecting an appropriate solvent for the orogenic process. Here we explore the process using cyclic olefin polymer (COP), a class of thermoplastics commonly produced by a ring-opening metathesis polymerization of the cyclic monomer followed by hydrogenation[41] as discussed in

section 2.2. Cyclohexane was selected as a suitable organic solvent, with a Hildebrandt parameter that differs from that of COP by 6%[36]. By choosing a solvent/polymer system with a small difference in Hildebrandt parameters, solvent permeation is sufficient to allow controlled rearrangement of the polymer chains, without excessive solvation that could otherwise result in complete dissolution of the polymer surface.

Orogenic patterning through selective exposure of COP surfaces to cyclohexane vapor is explored using various masking methods, including direct photolithographic masking, selective chemical surface passivation, and both contact and noncontact pattern transfer methods. Depending on the masking technique employed, different microstructure morphologies can be achieved for the same initial mask patterns. In particular, direct photolithography using photoresist as a masking layer is found to result in solvent-initiated bulk swelling and concomitant polymer flow across the thermoplastic surface that expands pattern linewidths during vertical surface growth, limiting the achievable aspect ratios for the resulting features. In contrast, masking regions of the COP surface through selective exposure to a combination of UV light and ozone (UV/O_3) generates polar oxygen-containing surface groups that effectively resist the absorption of nonpolar solvents into the polymer matrix, resulting in a reduction in pattern linewidths below the initially masked dimensions. Photolithography-free masking by microcontact printing and noncontact spotting is explored as a simple and low-cost approach to orogenic microfabrication using glycerol as a liquid-phase masking layer. Finally, inkjet printing is demonstrated as a facile approach to mask patterning enabling exceptionally rapid design-to-device

cycle times. The combination of these methods enables fabrication of a range of unique microstructures that would be challenging to realize using traditional thermoplastic microfabrication techniques based on material removal rather than surface growth.

2.4 Experimental section

2.4.1 materials and reagents

Methanol and 2-propanol were purchased from Fisher Scientific (Pittsburgh, PA). Cyclohexane and glycerol were purchased from Sigma-Aldrich (St. Louis, MO). Zeonor 1060R COP plates (2 mm thick) were procured from Zeon Chemicals (Louisville, KY). Wafer dicing tape was purchased from Semi- conductor Equipment Corporation (Moorpark, CA).

2.4.2 Photoresist Patterning

Thermoplastic plates were cut into 2 in-square chips which were deburred to remove machining debris from the chip edges. The chips were sequentially sonicated in

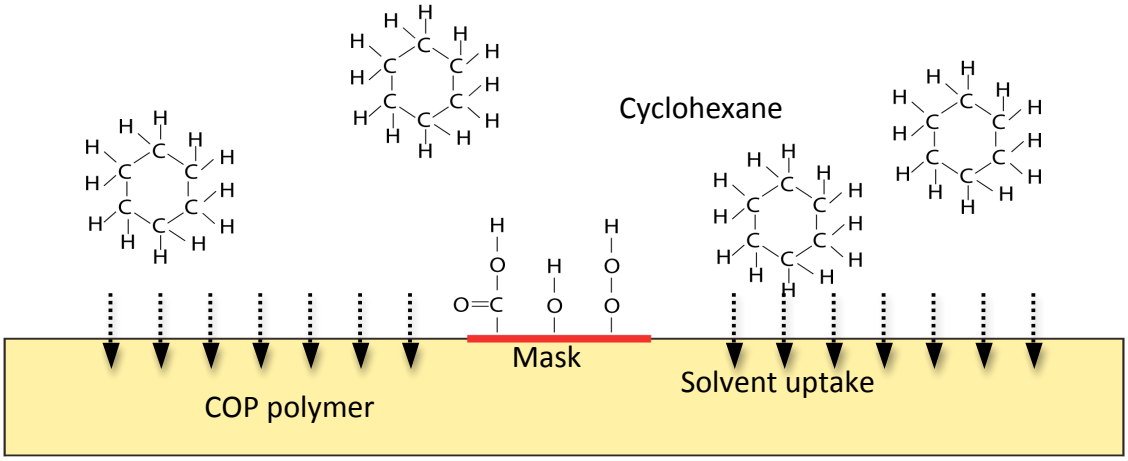

Figure 2.2 Schematics of orogenic microfabrication, a masked COP chip is exposed to cyclohexane vapor, allowing the exposed areas to irreversibly swell as a result of controlled solvent uptake

methanol, 2-propanol, and DI water for 5 min, and then degassed overnight at 60 °C under vacuum. Shipley 1813 positive photoresist was spin-coated on the polymer chip surface to a thickness of approximately 1.5 μm, and patterned by contact photolithography through a chromium coated glass plate mask using a UV flood exposure tool (PRX1000; Tamarack Scientific, Corona, CA). After exposure and photoresist development, the chips were rinsed with DI water, blown to dry with N_2, and baked on a 60 °C hot plate for at least 8 h to dehydrate the thermoplastic and densify the patterned photoresist.

2.4.3 UV/Ozone Passivation

Following photolithography, COP chips were loaded into a commercial UV/O_3 exposure system (PSD-UV; Novascan Technologies, Ames, IA) and subjected to a 30 min exposure. After UV/O_3 treatment, the polymer chips were submerged in methanol and sonicated for 1 min to remove photoresist, rinsed sequentially by 2-propanol and DI water, and dried at room temperature under a stream of N_2

2.4.4 Glycerol Patterning

For microcontact printing with an elastomer stamp, a PDMS layer with 200 μm diameter circular posts were fabricated using a plastic mold formed by CNC milling. Glycerol was spin-coated onto a silicon wafer to a thickness of approximately 5 μm, and the PDMS stamp was pressed into the thin layer of glycerol and applied to the COP chip surface manually to transfer the patterned glycerol film. For masking by noncontact spotting, a single hair strand was dipped in glycerol and dragged along the COP chip surface to deposit discrete droplets with a distribution of diameters ranging

from several micrometers to several hundred micrometers. Droplet diameters were measured optically prior to solvent exposure and post exposure electron microscopy.

2.4.5 Inkjet Printing

Inkjet printing was performed using a flatbed direct-to-substrate desktop printer (Direct Color Systems, Rocky Hill, CT) employing an Epson piezoelectric print head, with a proprietary ink based on a mixture of propyl glycol monomethyl ether and 2-butyl ethanol as a carrier. Although the printer supports thick substrates, a thin (100 μm) COP foil was used here to ensure future compatibility with standard paper feed systems in consumer-level inkjet printers.

2.4.6 Solvent Exposure

The masked thermoplastic chips were positioned at the top of a sealed glass dish partially filled with cyclohexane, with the chip surfaces 5 cm from the liquid solvent. Wafer dicing tape was used to hold the chips in place while also serving to seal the opening of the dish. The cyclohexane was heated to 30 °C to generate an estimated equilibrium vapor pressure of 14 kPa[53]. For photoresist patterning, solvent exposure was performed in an enclosed oven to uniformly heat the entire assembly in order to reduce condensation of liquid solvent at the edges of the photoresist patterns. For solvent exposure using UV/O_3, glycerol, and inkjet masks, the solvent dish was placed on a hot plate. After timed solvent exposure, the chips were promptly removed from the sealed chamber and dried under a stream of N_2 to encourage removal of residual solvent from the bulk polymer. For photoresist masks, the resist was removed by a sequential methanol and DI water rinse. For glycerol and inkjet masks, the masking layers were removed by a DI water rinse.

2.5 Results and Discussion

2.5.1 Photoresist Masking:

In order to evaluate the relationship between solvent exposure time and polymer surface growth, photoresist was used to mask regions of the COP surface from exposure to solvent vapor. Lines and spaces of varying width were patterned in a photoresist layer deposited on a set of COP chips, followed by timed vapor-phase exposure to the cyclohexane solvent. Measurements of polymer height changes were performed by stylus profilometry after orogenic growth. Like many glassy polymers, COP exhibits case II solvent diffusion characteristics[54], in which a sharp solvent front separates the swollen and unexposed regions of the polymer. This phenomenon is

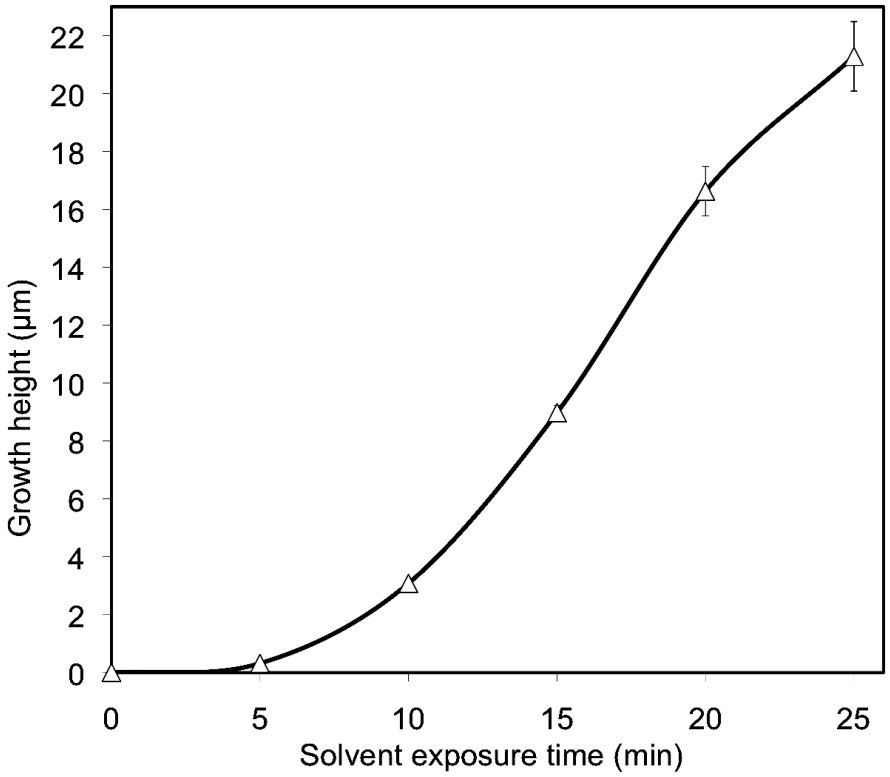

Figure 2.3 Relationship between COP surface growth height and solvent vapor exposure time for patterns significantly larger than the growth height. Submicrometer heights can be reliably achieved for short (<5 min) exposures, while longer exposure times of 60 min yield growth heights above 50 µm (n =5).

largely due to a concentration-dependent viscous flow rate and results in a linear rate of solvent intrusion into the polymer[55]. Using the COP/cyclohexane system, short solvent exposure times below 5 min were found to result in submicrometer growth heights, with gradually increasing grow rates. As depicted in Figure 2.3, for solvation times between 5 and 25 min, a nearly constant growth rate consistent with case II diffusion was observed. For significantly longer solvent exposure times between 25 and 60 min, the growth rate was slightly reduced, with an average growth height of

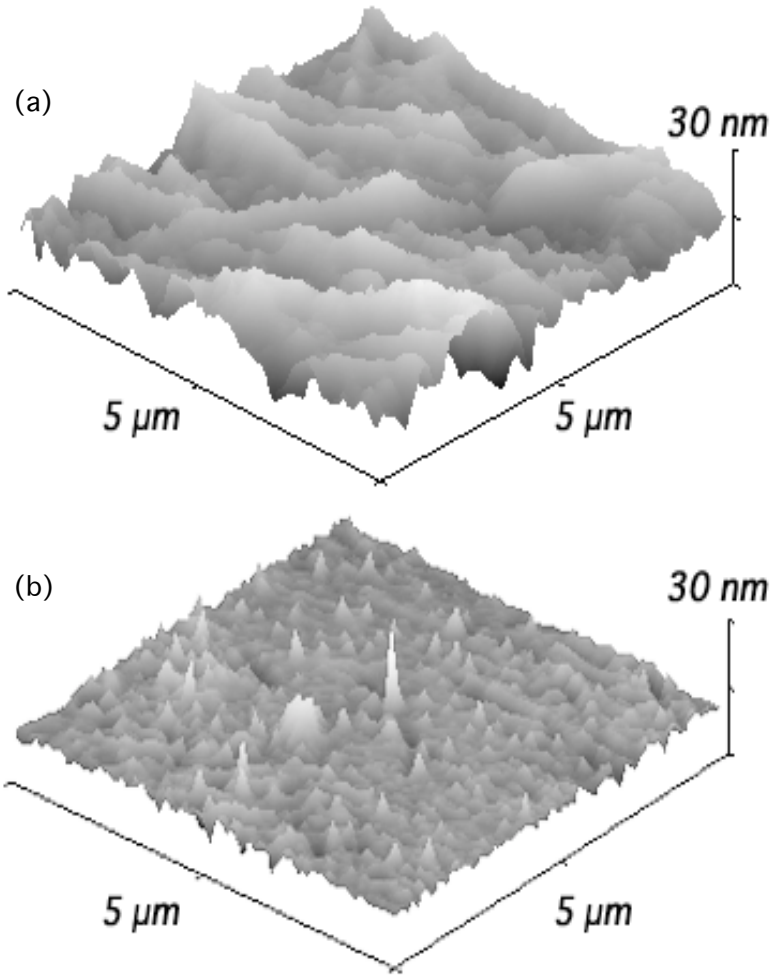

Figure 2.4 AFM profilometry data revealing a significant reduction in surface roughness during the transition from (a) a native COP surface prior to solvent exposure, to (b) a solvent-treated COP surface following 30 min exposure.

51 μm achieved for the maximum tested exposure time of 60 min. These results were highly repeatable across multiple chips (n = 5), with less than 10% variation in growth heights for all repeated experiments. Furthermore, the final heights of the solvated surfaces are very stable, with no measurable changes in geometry for chips stored at room temperature over a period of several weeks. Surface roughness of the solvated polymer was significantly reduced compared to the native surfaces as depicted in Figure 2.4, and no change in optical clarity or surface damage such as crazing was observed for any of the growth conditions explored in the study.

In addition to solvent exposure time, variations in mask dimensions can also affect the polymer growth height. A characteristic feature of the polymer swelling process is the formation of regions adjacent to the mask boundaries where polymer is first depleted and then piled up, resulting in distinct raised bulges near the mask edges. This behavior is clearly visible in the profilometry traces presented in Figure 2.5 for both positive (line) and negative (space) photoresist mask patterns. For large features, that is, when the mask opening is significantly larger than the width of the pile-up zone, polymer swelling far from the mask boundaries is independent of pattern resolution and raised areas in the field exhibit growth heights consistent with Figure 2.3. However, when the mask opening approaches twice the width of the pile-up zone, the superimposed polymer fronts result in growth heights that can be significantly larger than those predicted for larger mask openings. For example, as shown in Figure 2.5 COP chip patterned with a 200 μm wide photoresist space and exposed to solvent vapor for 10 min results in a peak height over 3 times larger than a patterned photoresist line of the same width.

Minimum feature size is limited primarily by the desired growth height. Solvent is absorbed isotropically into the polymer matrix, and thus solvent is taken up by the polymer beneath the photoresist along the perimeter of the unmasked regions. As solvent is absorbed beneath the photoresist mask, the lateral dimensions of the resulting swelled polymer pattern increase, resulting in a minimum feature size of approximately twice the growth height. In this sense, the process is similar to thermal oxidation of silicon, where the formation of a characteristic "bird's beak" profile results from the growth of silicon dioxide beneath the edge of a nitride masking film. This phenomenon is more clearly seen for smaller masking patterns, as depicted in

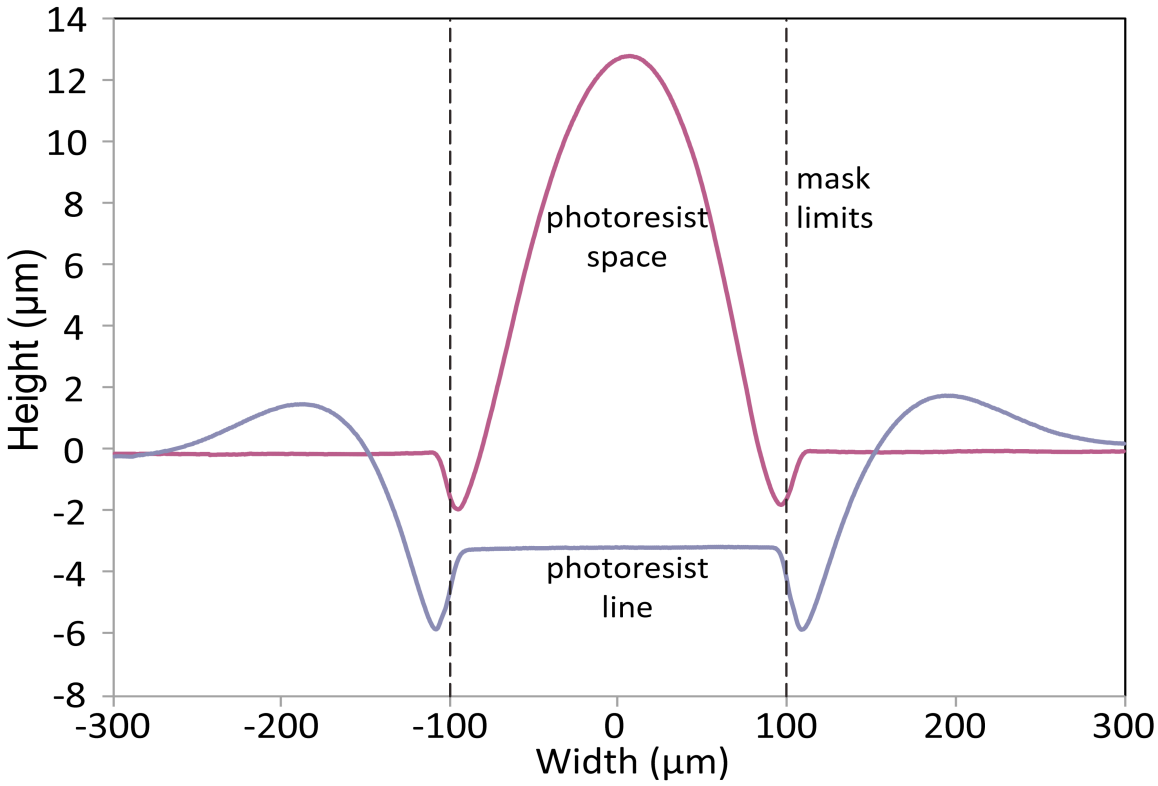

Figure 2.5 Profilometry traces revealing line and space cross sections formed by 10 min orogenic growth of a COP surface masked with photoresist, using approximately 200 µm wide positive (line) mask features and negative (space) mask features.

2.6 which shows the results of orogenic growth through a photoresist mask patterned with a periodic grid of 5 μm spaces. In this case, the raised features exhibit lateral expansion of approximately twice the growth height of 3.1 μm.

Regardless of the dimensions of the mask lines or spaces, as the growth height of the polymer surface increases, the solvated polymer eventually flows over the physical photoresist mask. As a result, the maximum growth height was found to be dependent on the patterned mask dimensions, with smaller mask openings resulting in lower growth heights due to lateral flow of a larger proportion of the solvated polymer. The transition from vertical growth to lateral flow over the mask occurs earlier for smaller mask openings due to earlier wetting of the photoresist surface by solvated polymer. Because the free polymer interface at the mask edge is driven to minimize its surface area by surface tension, it forms a curved boundary that tends toward a circular cross section as more solvated polymer is extruded from the bulk substrate. For a given solvent exposure time, higher curvature occurs at smaller mask

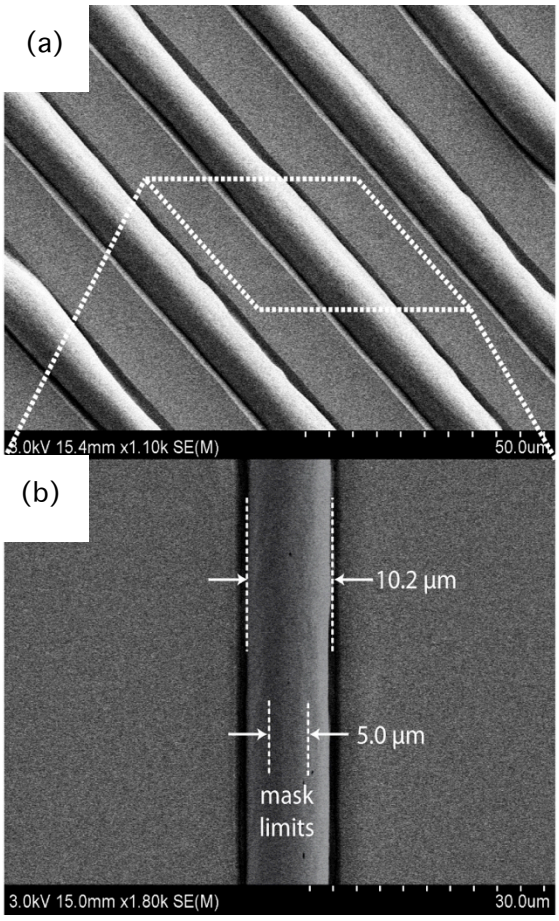

Figure 2.6 Thermoplastic features resulting from orogenic growth through a photoresist mask patterned with a periodic grid of 5 μm spaces and growth height of 3.1 μm, revealing lateral solvent uptake by polymer beneath the masking layer.

openings. As a result, solvated polymer is forced to contact the upper photoresist surface earlier in the growth process, wetting the photoresist and leading to polymer flow over the exposed surface. Thus, predicting polymer swelling height and shape for the case of photoresist masking requires careful evaluation of this resolution-dependent transition between non-wetting and wetting growth modes. An example of a pattern defined using a 50 μm wide photoresist line and exposed to solvent vapor for 15 min is shown in Figure 2.7a. The orogenic feature expands beyond the initially masked region, resulting in a final structure over 70 μm wide with significantly reduced height of the raised polymer surface. This flow of solvated polymer over the masking layer produces a region of polymer separated from the substrate by a 1.5 μm tall gap defined by the thickness of the photoresist mask.

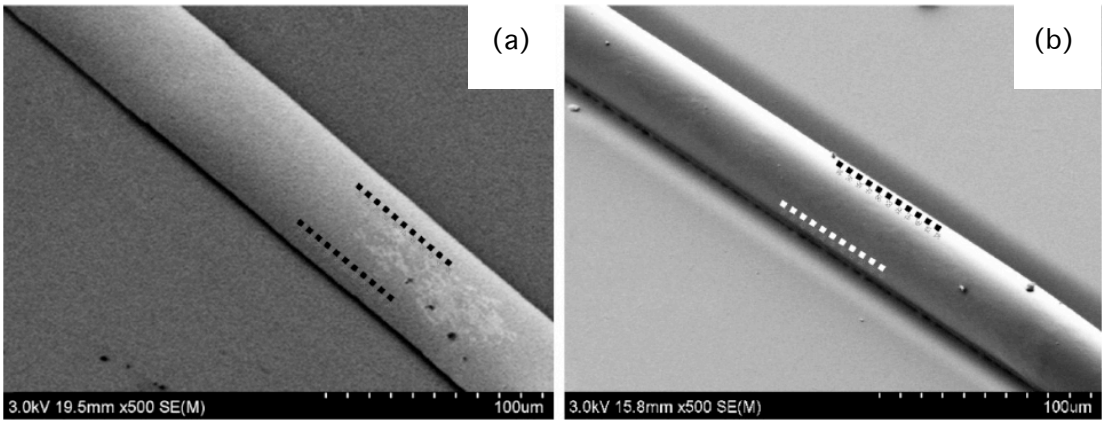

Figure 2.7 SEM images of orogenically grown lines using 50 μm mask features by (a) direct photoresist masking and (b) UV/O3 passivation. While lateral polymer flow leads to expansion of the line width for the case of photoresist masking, the UV/O3 masked line remains constrained by the oxidized surface. Approximate mask limits are shown with dotted lines in each case.

2.5.2 UV/Ozone masking:

As an alternative to masking with a physical photoresist layer, patterned orogenic growth can also be achieved by modifying the chemistry of the polymer surface to

prevent solvent absorption in selected areas. While specific chemical groups can be attached to thermoplastics by methods such as photografting, a simpler approach to generating a solvent-resistant surface is through localized oxidation. We hypothesized that the presence of a dense layer of polar oxygen groups on the surface would prevent a nonpolar solvent from penetrating into the bulk substrate. This concept was explored by exposing the COP surfaces to a controlled dose of UV/O_3. The exposure of thermoplastics to UV/O_3 is known to generate free radicals that can react with oxygen, resulting in surface species containing carboxyl, hydroxyl, or peroxide groups[56]. For example, it has previously reported that UV/O_3 exposure of COP can more than triple the surface concentration of oxygen-containing species[47]. Indeed, initial tests revealed that UV/O_3 treatment times longer than 20 min were sufficient to completely prevent the absorption of cyclohexane into the exposed polymer. Solvent swelling of surfaces patterned by UV/O_3 exhibit very different characteristics compared with the case of photoresist masking. Unlike the case of a physical photoresist mask, the high surface energy of the chemically modified COP surfaces prevents flow of solvated polymer over the mask. In this case, the morphology of the raised features is defined by surface tension driven shaping of the solvated polymer. As a result of the lateral constraint during polymer growth, large growth heights may be achieved for small mask openings that would otherwise result in significant polymer flow over a physical photoresist masking layer. In principle, the swelling height and shape can be predicted given knowledge of the solvent exposure time, the resulting volume of solvated polymer, and mask dimensions. Because gravitational body forces acting on the solvated polymer are significantly smaller than surface

tension at the size scales of interest in this work, the morphology of the resulting polymer structures may be determined based solely on surface tension driven shaping

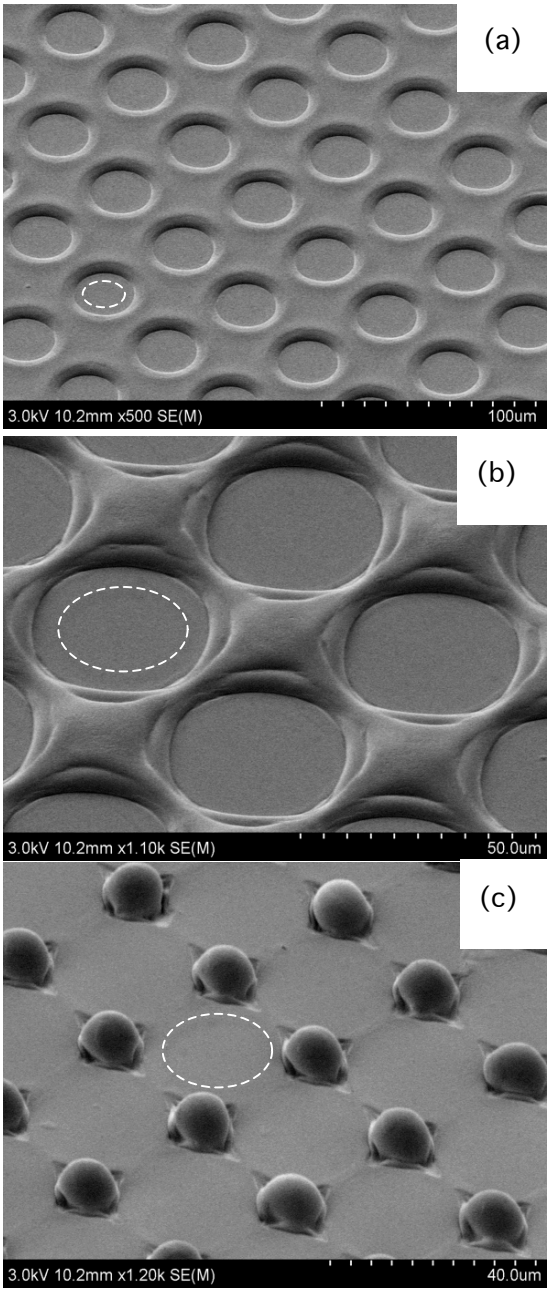

Figure 2.8 Arrays of circular mask features with progressively smaller edge-to-edge spacing of (a) 30 μm, (b) 20 μm, and (c) 10 μm following 10 min solvent exposure. The flat circular valleys passivated by UV/O_3 exposure expand during orogenic growth, leading to the formation of discrete posts for the case of 10μm spacing. Approximate sizes of the initial UV/O_3 mask regions are shown in each image (dashed circles).

of the solvated material. As predicted using this simple model, sufficiently long solvent doses and small mask openings result in polymer features with nearly circular cross sections. For example, when using linear 50 μm wide mask openings with a 15 min solvent dose, resulting in a total growth height of 43 μm due to polymer pile-up at the mask edges, structures with partial cylinder cross sections are achieved Figure 2.7b.

In addition to preventing flow of polymer over the oxidized field, it is surprising to note that UV/O_3 masking results in final line widths that are smaller than the original mask openings. This phenomenon is independent of solvation time and surface growth height, and the resulting reduction in pattern width has been observed consistently for a variety of designs. For example, Figure 2.8 presents SEM images for a set of circular arrays with decreasing edge-to-edge spacing between adjacent array elements. During the 10 min solvent exposure used to define these features, the masked regions expand approximately 5 μm in all directions, thereby reducing the widths of raised features between the circles. For the case of 10 μm spacing shown in Figure 2.8c, the expanding effective mask areas have overlapped, resulting in an array of discrete posts. In all cases the transitions between the initial masked areas and final patterns are indistinguishable. The mechanism for the observed increase in masking may be related to solvent-induced migration of charged surface species generating during UV/ O_3 treatment. The ability to reproducibly form raised surface features below the resolution of the photolithographic mask represents an intriguing option for thermoplastic micro- fabrication.

2.5.3 Pattern Transfer Masking:

While photolithographic patterning using photoresist or UV/O_3 masking layers can provide high resolution control over the microstructure geometry, the orogenic process is also compatible with direct masking using pattern transfer via selective deposition of a physical solvent barrier, for example by spotting or stamping a suitable material on the chip surface. Microcontact printing based on elastomeric stamping is an important soft lithography technique that offers the ability to achieve low-cost microscale and nanoscale patterns using a variety of materials with a simple master template, commonly fabricated from PDMS. When using substrates such as

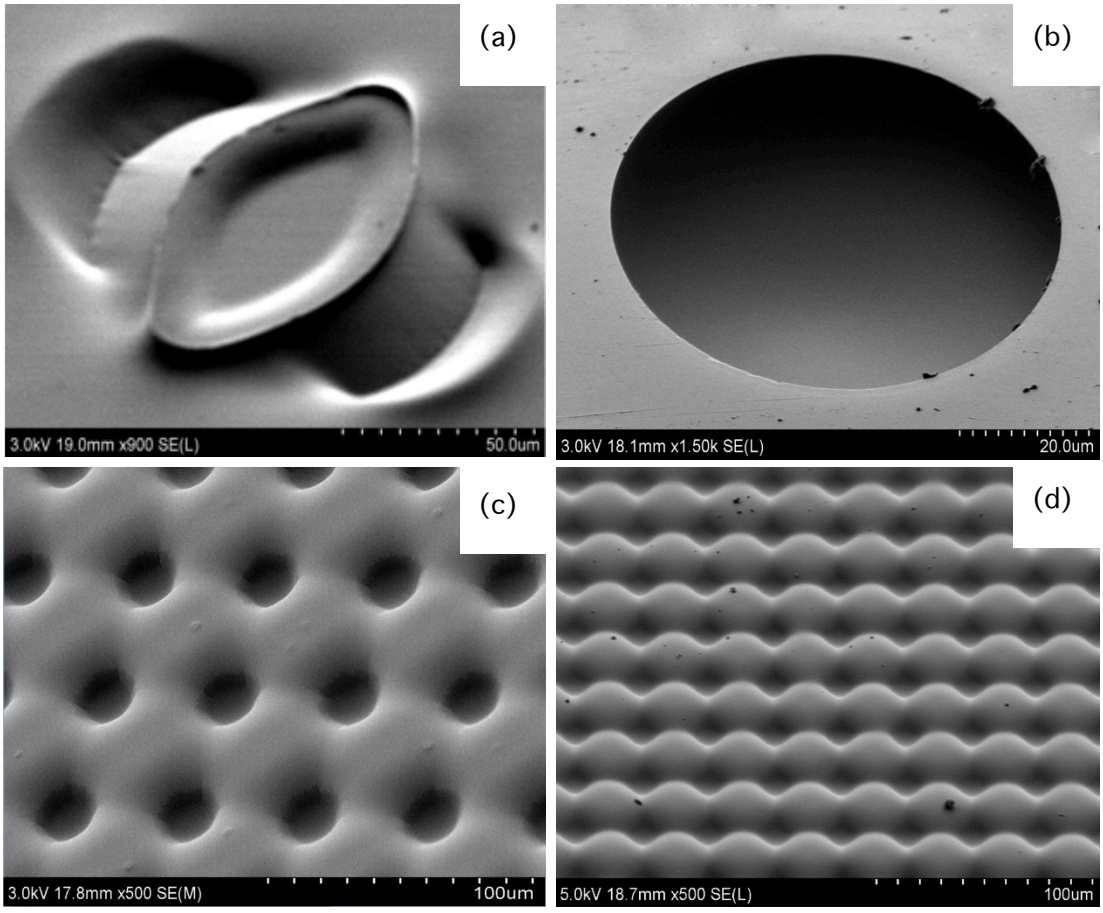

Figure 2.9 Orogenic features patterned in COP thermoplastic chips using different masking techniques: (a) glycerol microcontact printing using a PDMS stamp, (b) glycerol spotting and UV/O_3 masking using (c) light field and (d) dark field masks.

glass or silicon, microcontact printing can be used to transfer patterned monolayers to the surface with a minimum resolution limited only by the elastomer stamp itself. Unlike these common substrates used in microcontact printing which support the transfer of chemical monolayers, for example, through covalent attachment to silanol or thiol groups, thermoplastics are relatively inert and do not present suitable chemical handles for monolayer anchoring. Furthermore, surface modifications to promote this functionality can potentially inhibit the desired solvent absorption within unmasked areas. As an alternate approach, the transfer of thick glycerol films by elastomeric stamping was investigated as a viable method for microcontact printing of a masking layer prior to orogenic growth. The high viscosity of glycerol and

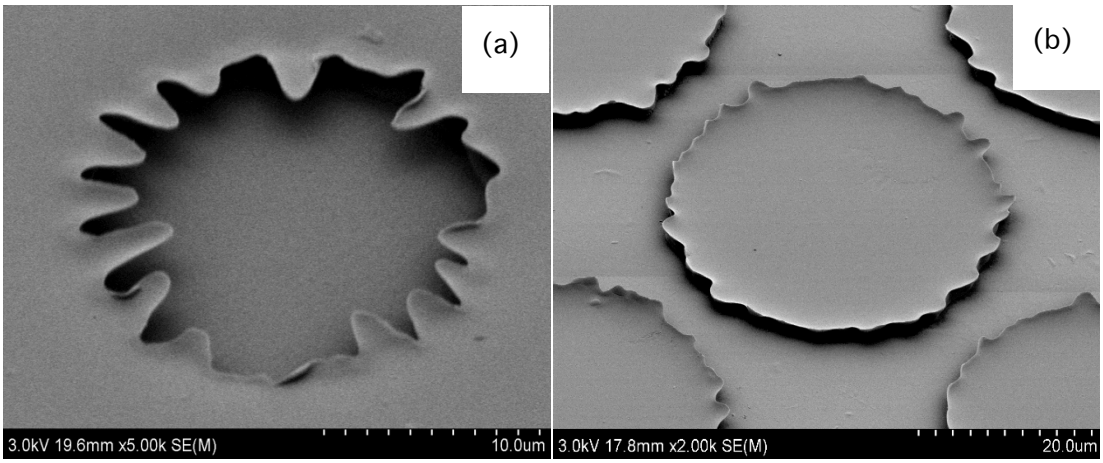

Figure 2.10 Orogenic features patterned in COP thermoplastic chips using photoresist masking using (a) light field and (b) dark field masks

moderate hydrophobicity of the COP surface was found to prevent dispersion of the transferred glycerol patterns after spotting, with resolution limits on the order of 50 μm. However, removal of the stamp tended to create uneven distributions of glycerol on the COP due to surface tension effects. This behavior resulted in complex but reproducible structures following orogenic growth, such as the feature stamped with a circular PDMS post shown in Figure 2.9a. Although this capability could potentially

be harnessed to realize unique three-dimensional thermoplastic microstructures, a mechanistic understanding needed to relate stamp geometry, non-uniformities in the distribution of transferred glycerol, and the resulting orogenic patterns is lacking. To achieve uniform patterns of well-defined features, noncontact spotting of glycerol droplets was explored as an efficient and flexible masking technique that avoids glycerol redistribution during microcontact printing. Droplets with diameters ranging from 5−100 μm were deposited on a COP chip and exposed to cyclohexane vapor for up to 20 min. Just as with photoresist masking, the solvated polymer increasingly encroached over the glycerol droplets with longer solvation times, resulting in nearly hemispherical chambers partially enclosed within the substrate (Figure 2.9b). It is notable that the smooth rim morphology achieved with noncontact spotting is very different from edges of features patterned using circular photoresist masks, with the latter case resulting in polytomous extrusions around the rim. Examples of these extrusions are shown in Figure 2.10a and b for the case of light field and dark field photoresist masking, respectively. For comparison, similar light and dark field features patterned by UV/O_3 masking are presented in Figure 2.9c and d. In these latter cases, no encroachment of the solvated polymer into the masked regions is observed, consistent with the results described in Figure 2.8.

2.5.4 Inkjet Printing

Inkjet printing is commonly used for the deposition of macroscale patterns of biological materials such as oligonucleotides[57] or proteins for rapid microarray preparation. Here we have adapted standard inkjet printing technology for deposition a removable masking layer, consisting of dye or pigment components within an oil-

based ink, to enable patterned orogenic growth of the deposition substrate. The use of an oil-based ink was dictated by the moderate hydrophobicity of common thermoplastics including COP, requiring a non-aqueous carrier to prevent the ink from beading on the polymer surface and losing printing resolution before drying. After orogenic growth, the ink is easily removed from the chip surface by brief sonication in water.

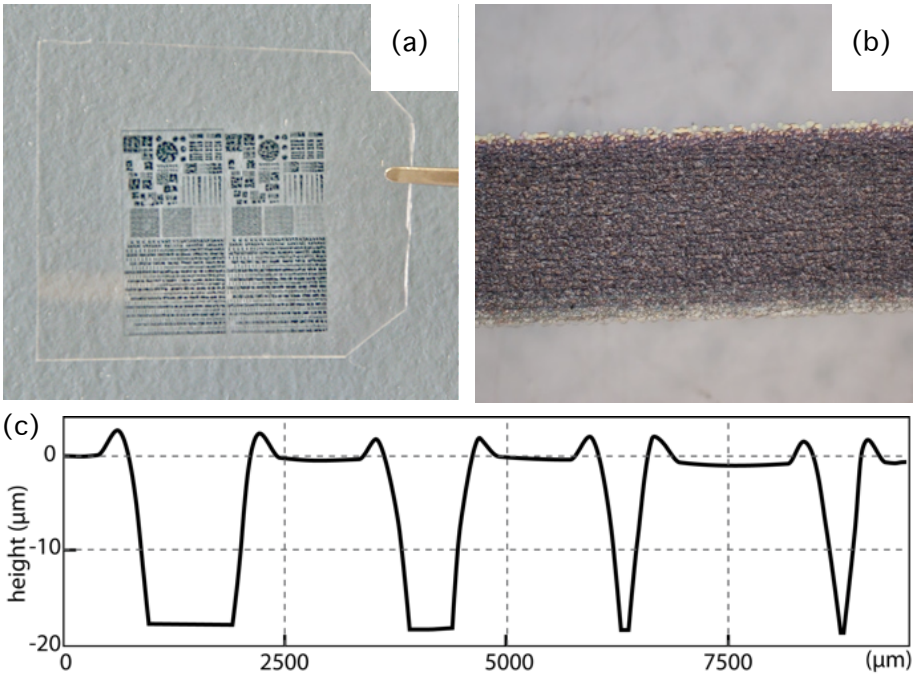

Figure 2.11 (a) Inkjet printed COP film chip and (b) micrograph of a 400 μm wide line of oil-based ink on the COP surface showing uniform coverage and minimal dispersion. (c) Profilometry traces from a series of inkjet printed line features, 100−400 μm wide, following 15 min orogenic growth and removal of ink from the chip surface.

An image of a thin COP foil containing an inkjet printed mask design is shown Figure 2.11a, together with a micrograph of a 400 μm wide ink line on the foil surface in Figure 2.11b. The ink used in this work exhibits no significant lateral dispersion over the chip surface and provides nearly uniform ink distribution over the patterned line. Variations in ink coverage near the edges of printed features are common, resulting in

sloped sidewalls as apparent from the stylus profilometry traces in Figure 2.11c measured from a set of inkjet printed line features ranging in width from 100 to 400 μm following 15 min orogenic growth. The raised regions also exhibit distinct shoulders near the mask edges, similar to the results of photoresist masking shown in Figure 2.5. While the observed sidewall slope and overall resolution constraints of consumer-level inkjet printers limits the range of dimensions that can be realized with the inkjet masking method, this approach eliminates the need for direct photolithography or microcontact stamp preparation.

Conclusions

Overall, the orogenic process offers unique capabilities for patterning microscale and nanoscale features in rigid thermoplastics using a simple solvent swelling technique. The process is differentiated from traditional methods of thermoplastic patterning by the use of controllable solvent swelling rather than material removal or mechanical displacement to achieve a range of three-dimensional surface features. The surface growth process is compatible with multiple masking techniques, including direct photolithography, chemical surface modification, microcontact stamping, noncontact spotting, and inkjet deposition as demonstrated in this work. The selection of masking method is seen to have a significant impact on the resulting surface structure, with resolution limits, sidewall angles, and overall morphology affected by interactions between the mask layer and the solvent swelling process. A variety of unique features can be realized with different masking methods, with potential applications in the fabrication of thermoplastic microwell arrays, microfluidic systems, micro optical components, and beyond. The application of consumer-level inkjet printing for

orogenic masking is particularly attractive for rapid manufacturing enabling concept-to-device cycle times in a true low-cost and scalable desktop process. Furthermore, the use of direct-to-substrate inkjet systems for mask deposition may be extended to the fabrication of complex micropatterns on nonplanar thermoplastic substrates, and many of the masking methods explored in this work can be readily combined with more traditional approaches to thermoplastic microfabrication to further expand the range of patterning options for these materials. It should also be noted that while the orogenic process has been explored here using COP as a model thermoplastic material, the concept may be extended to other polymers with the selection of suitable solvents and exposure conditions.

Chapter 3: Orogenic microfabrication as a tool for rapid prototyping of thermoplastic microfluidic devices

3.1 Summary

A unique technique for the rapid fabrication of thermoplastic microfluidic chips is described. The method enables the realization of fully-sealed microchannels in around one hour while requiring only minimal infrastructure by taking advantage of orogenic microfabrication, (Chapter 2) allowing raised features to be patterned on the surface of homogeneous thermoplastic materials. Patterning is achieved without photolithography by simply drawing the desired microchannel pattern onto the polymer surface using a suitable ink as a masking layer, either manually or under robotic control, followed by timed exposure to solvent vapor to yield a desired depth for the masked channel features. The channels are then permanently sealed through solvent bonding of the microchannel chip to a mating thermoplastic substrate. As with the previous Chapter, the process is demonstrated using cyclic olefin polymer as a thermoplastic material, with fully operational microfluidic devices fabricated following a true desktop manufacturing model suitable for rapid prototyping.

The Chapter is adapted from a published article in the journal of Lab-on-a-Chip.

3.2 Introduction

Simple and rapid desktop manufacturing processes capable of decreasing the cost, time, and labor associated with microfluidic system fabrication are highly desirable for device prototyping and low volume production. While a range of substrate materials including glass, silicon, and thermoplastics have been widely used for

microfluidic applications, device prototyping continues to be widely performed using polydimethylsiloxane (PDMS) elastomer. As discussed earlier, the popularity of PDMS for microfluidic systems is due in part to the relative ease and speed of fabrication afforded by this soft lithography technique[3]. However, PDMS suffers from a number of disadvantages that limit its utility in many applications, including low stiffness, high gas permeability, high water absorption, and incompatibility with many common solvents used in biomolecular assays[58]. More fundamentally, although within certain constraints a PDMS chip may be prototyped from design to final sealed device within several days, elastomer micromolding processes remain far from meeting the goals of true desktop manufacturing, with the micro fabrication of templates needed for PDMS molding often requiring significant infrastructure, time, and labor.

As an alternative to PDMS micromolding, a variety of desktop manufacturing approaches have been explored toward the realization of direct-write processes that require neither photolithography nor molding templates. Examples include laser printing of thick toner ink on glass or plastic substrates to define microchannel walls[57,59–61], computer-controlled deposition of wax channel sidewalls on glass substrates[62], and the use of programmable vinyl decal cutters (cutter plotters) to create patterned adhesive films that may be bonded to a secondary substrate[63,64]. However, in each of these processes the resulting chips are formed from heterogeneous materials with different physical and chemical properties, complicating surface functionalization or passivation required for many bio-analytical systems. The multifunctional materials systems can also introduce challenging chemical, solvent,

and biomolecule compatibility issues. In the case of cutter plotters, a further constraint is that closed channel loops cannot be implemented due to the nature of the adhesive transfer process.

With the emergence of thermoplastics as a leading material system for microfluidic devices, there is a particular need for desktop manufacturing processes capable of realizing homogeneous thermoplastic chips with flexible geometric control and high-resolution patterning. Thermoplastic microfabrication has been reported using a variety of replication methods including hot[42] or room temperature[20] embossing, injection molding[65], and thermoforming[66]. More recently, hot roller embossing into polymer foils using high-throughput reel-to-reel processing promises further reductions in fabrication costs for mass produced thermoplastic microfluidics[21,67]. In addition to replication-based fabrication, thermoplastics are also amenable to direct machining techniques such as laser ablation and mechanical micromilling[31,68–70]. However, for both replication-based methods and direct patterning, thermoplastic microfabrication continues to require significant infrastructure investment, time, and effort[68]. Although the use of cutter plotters to directly scratch microchannels into bulk thermoplastic surfaces has been reported as a way to avoid these constraints, the method provides limited control over channel geometry, resolution, and surface quality[62].

In this Chapter we describe a new process utilizing orogenic microfabrication, enabling rapid desktop manufacturing of sealed microfluidic chips fabricated from homogeneous thermoplastic substrates. While traditional thermoplastic microchannel

fabrication involves the removal or displacement of bulk polymer from the substrate by machining or embossing, in this work we leverage orogenic microfabrication (Chapter 2) that allows selected regions of a thermoplastic surface to be raised from the substrate by irreversible solvent swelling[33]. Unlike solvent assisted microcontact molding[48] and capillary force lithography[49,50], where solvent-softened thermoplastics are shaped using a molding template, the orogenic microfabrication technique employs direct patterning and surface growth without the need for a microfabricated template. As described in detail in previous Chapter, in the orogenic process, regions of the surface masked with a material that serves as a barrier to solvent transport into the substrate are prevented from swelling. As the exposed polymer regions expand during solvent uptake, the mobile polymer chains rearrange to produce a permanent volume change within the plasticized regions. The volume change is permanent after removal of solvent from the bulk polymer. For a given thermoplastic, selection of an appropriate solvent for orogenic patterning is driven by consideration of the solubility parameters for the thermoplastic and solvent, with more rapid solvent absorption occurring for smaller differences between the solubility parameters for each material. The masking layer must be selected to provide an effective barrier to the chosen solvent, thereby preventing solvent from reaching the masked thermoplastic surface. In Chapter 2 we explored the use of both chemical and physical masking layers for orogenic growth of cyclic olefin polymer (COP) substrates, including direct photoresist masking, patterned UV/ozone surface passivation, and both elastomeric stamping and non-contact spotting of glycerol as a liquid-phase masking material, to determine the relationships between mask material, solvent exposure conditions, and

orogenic growth.

In the present Chapter, an ink mask deposited from a high-resolution pen nib is used to define microchannel features within COP substrates. Because the deposited ink mask directly defines the microchannel geometry, the desired patterns are defined by simply drawing the microchannel designs directly onto a COP substrate prior to solvent exposure and surface growth. Because the exposed surface is swollen with solvent upon completion of the orogenic growth step, the resulting microchannel substrate may be permanently sealed by mating the substrate with a second COP chip containing pre-drilled fluidic access ports, resulting in room temperature solvent bonding[54,71,72] between the layers. While lateral channel dimensions are controlled by the deposited ink pattern, channel height is controlled by the solvent exposure time. By using water-soluble ink, the masking layer can be removed after bonding by perfusing water through the sealed micro channels. The method provides a simple path for realizing sealed microfluidic chips within homogeneous thermoplastic substrates, with exceptionally rapid design-to-device cycle times on the order of 30–90 min using minimal infrastructure in a true desktop manufacturing process. The ‘‘pen microfluidics’’ fabrication technique is demonstrated here using both hand-drawn ink patterns and computer-generated designs deposited using a robotic pen plotter.

3.3 Experimental section

3.3.1 Materials and methods

Zeonor 1060R COP plates (2 mm thick) were purchased from Zeon Chemicals (Louisville, KY). Reagent grade cyclohexane was purchased from Sigma-Aldrich (St.

Louis, MO). Wafer dicing tape was purchased from Semiconductor Equipment Corporation (Moorpark, CA). Ink from a commercial wet-erase marker (Expo vis-`a-vis purple ink marker; Sanford Corp., Oak Brook, IL) was used for masking. High-resolution masking was performed using a Pigma Micron pen with a 200 mm diameter nib (Sakura Color Products, Osaka, Japan).

3.3.2 Microchannel Fabrication:

COP chips were diced to the desired size and sequentially cleaned by methanol, isopropanol, and DI water, followed by N_2 drying and overnight degassing at 75 ºC under vacuum. Ink from the high-resolution pen was removed, and the nib was thoroughly cleaned by sequential sonication in methanol, isopropyl alcohol, and DI water. After cleaning, the ink reservoir was refilled with ink from a wet-erase marker cartridge. Selective masking was realized by directly drawing patterns onto a COP chip, resulting in lines of various widths depending on the nib width on the pen. For simple straight channels, a straight-edged guide was used to assist in drawing the mask by hand. For precise patterning, a 3-axis desktop CNC milling machine (MDX-650, Roland DGA, Irvine, CA) was modified with a penholder, allowing direct and automated transfer of a computer-generated mask layout to the COP chip.

3.3.3 Microchannel fabrication:

The apparatus used for solvent exposure followed previous reports[33,45,73]. Briefly, a glass dish containing a small volume of cyclohexane was heated to 30 ºC on a hotplate. The masked COP substrate was positioned face down at the top of the glass dish, with a sheet of solvent-resistant dicing tape used to hold the chip in place while also serving to prevent the escape of cyclohexane vapor from the dish. The solvent

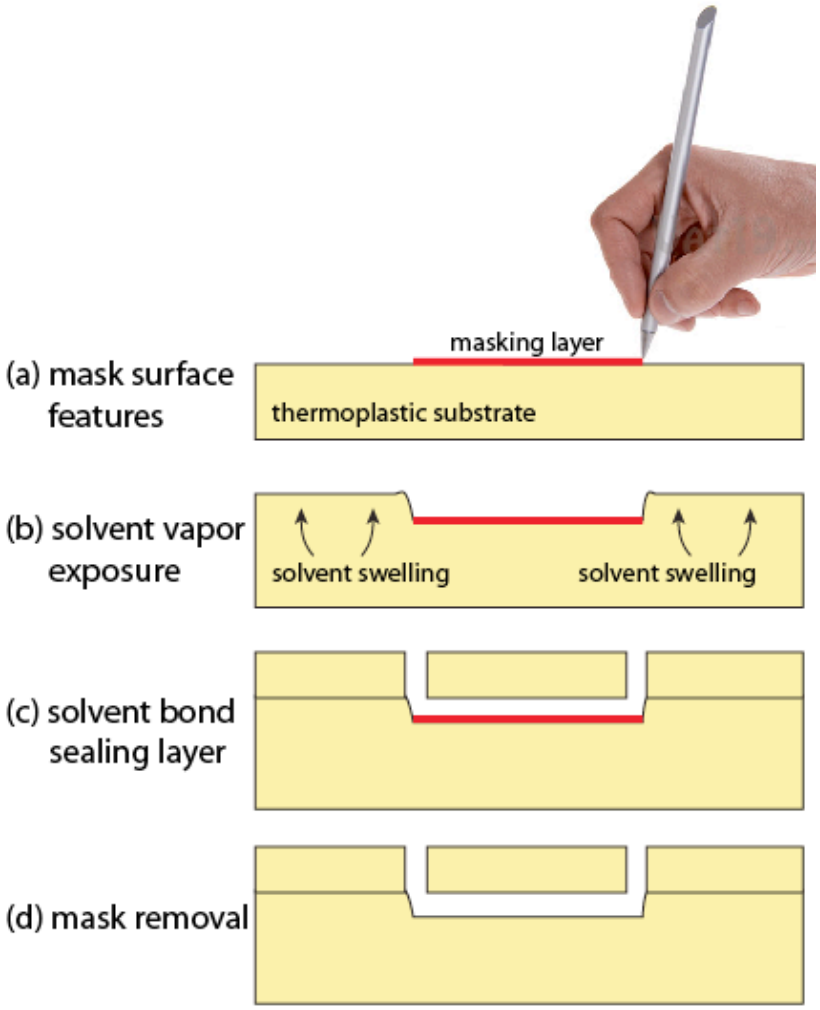

Figure 3.1 Overview of the pen microfluidics fabrication process. (a) An ink mask is drawn on a COP chip surface. (b) Vapor-phase solvent exposure results in patterned growth of the COP surface by solvent swelling. (b) Bonding is realized by bringing the patterned surface into contact with a sealing layer, followed by solvent bonding using a desktop laminator. (d) The water-soluble ink masking layer remaining within the sealed microchannel is removed by pumping aqueous buffer through the channel.

volume was selected to define a 5 cm gap between the liquid solvent surface and the COP chip. After exposure to solvent vapor for the desired time, the COP chip was promptly removed from the solvent dish and brought into aligned contact with a mating COP sealing layer. Each multilayer chip assembly was then bonded by either using a hot press (AutoFour/15, Carver, Wabash, IN) at a pressure of 500 psi or by running the chip through a desktop laminator (model PL1200, NSC International, Hot

Springs, AR) to apply consistent moderate pressure to the mating surfaces, resulting in a permanent solvent bond between the layers. In both methods, bonding was performed at room temperature. Before bonding, fluidic access ports were milled in the COP sealing chip using a 125 mm diameter end mill. For completed microfluidic chips, interfacing between the access ports and off-chip syringe pumps was realized by inserting needle tubing segments (Hamilton Syringe, Reno, NV) into the access ports following a previously reported method.[8]

3.4 Results and discussion

3.4.1 Microchannel patterning via orogenic growth

Cyclic olefin polymers are attractive materials for microfluidic applications due to a range of favorable properties including high optical clarity and low autofluorescence. In comparison with PDMS as an alternative material for rapid prototyping of microchannels, COP offers important advantages such as exceptionally dimensional stability, low water absorption, low gas permeability, and good chemical compatibility with a wide range of alcohols, acids, and bases[41]. In Chapter 2 it was established that COP materials can exhibit large and permanent surface swelling during gas phase cyclohexane absorption, with achievable growth heights above 50 mm. By masking the COP surface with a solvent-impermeable material, selective patterning of solvent absorption provides a means to form complex raised structures in the COP substrate. In the following Chapter, we explore the application of this orogenic microfabrication process to sealed microchannel fabrication using commercially available ink deposited from a pen as a masking layer. The basic process is described in Figure 3.1. Ink from a pen with a fine-tip felt nib is written

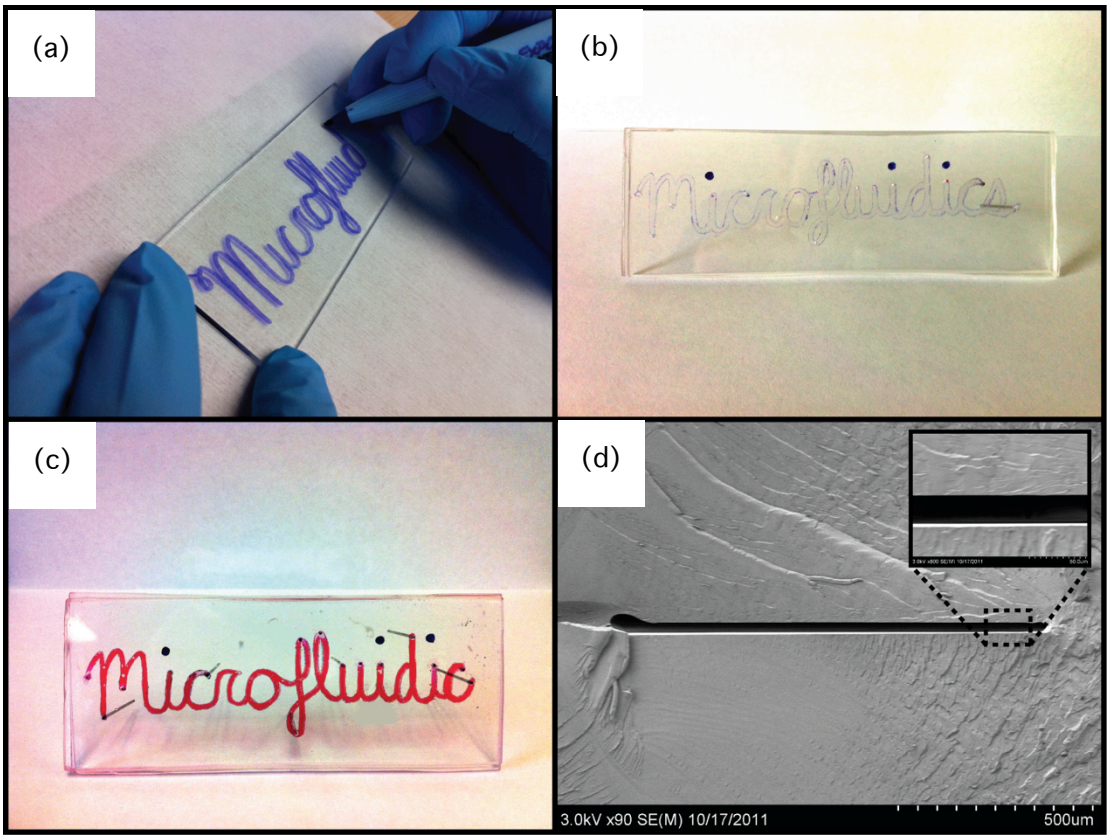

Figure 3.2: (a) Manual writing with a wet-erase pen onto a COP chip, followed by 15 min orogenic growth and solvent bonding, and sequential injection of (b) water and (c) red food coloring through the resulting microchannel network. (d) SEM image revealing the cross-section of the sealed microchannel.

onto a COP surface by manual or computer-controlled deposition, followed by exposure to solvent vapor for a specified time required to grow the surface outside of the masked regions by the desired channel height. The solvated surface is then brought into contact with a mating sealing layer comprising a COP chip with pre-drilled fluid ports, resulting in a permanent solvent bond between the layers due to the presence of solvent within the field of the microchannel substrate. Uniform sealing pressure is applied, and the masking ink is removed from the sealed channels by flushing aqueous buffer through the chip. Depending on the desired channel height, the entire process from mask patterning to sealed chip is typically completed within

30–90 min.

3.4.2 Selection of masking ink

Inks are colloidal systems of insoluble pigments or soluble dyes dispersed in an aqueous or organic solvent. For printing on moderately hydrophobic materials such as thermoplastics, inks based on less polar organic solvents are preferred to prevent beading of ink on the polymer surface. Modern inks are complex, with additional components including pH modifiers, dispersants to prevent colloid aggregation, humectants to control drying rate, polymer binders and resins, anti foaming agents, surfactants, and modifiers to control viscosity[74].Common organic solvents include propylene glycol, propyl alcohol, toluene, and glycoethers, with a wide range of pigments or dyes used depending on the desired color, such as eosin (red), copper phthalocyanine or triphenylmethane (blue), titanium dioxide (white), and carbon black (black)[74,75]. Unfortunately, the detailed chemistries of commercial inks are generally proprietary, with little information available beyond basic solvent content as determined from manufacturer MSDS data[76]. In the absence of detailed ink composition data, a wide variety of over 20 different commercial inks were experimentally evaluated for use in the pen microfluidics process. During these initial experiments, it was observed that orogenic growth on a COP surface patterned with different inks resulted in different growth heights due to varying levels of resistance to solvent penetration through the masking layer. In some cases large growth heights could be achieved, but only with pinholes forming in the masking layer, resulting in rough channel surfaces. In other cases, smoother channel surfaces were observed, but with maximum growth heights ranging from 20-40 mm regardless of the solvent

exposure time, suggesting that cyclohexane was able to uniformly penetrate the ink after sufficient time had elapsed. Of the tested inks, purple ink from a wet-erase marker designed for writing on plastic overhead transparencies was found to be most effective for inhibiting solvent uptake. The solvent system for the selected ink is based on water and propylene glycol[76]. Since wet-erase marker solvent content is identical for all of the tested colors, the superior solvent-blocking property of the purple ink is presumably due to the dye used to define this particular ink color. However, other inks may also be used for effective masking within the constraints presented by the observed growth height limitations.

3.4.3 Microchannel width

The dimensions of microchannels fabricated in the orogenic process are defined by mask linewidths, with minimum channel widths limited by the pen nib dimensions. Using commercially available wet-erase markers, masking linewidths slightly below 1 mm were reliably formed by manual writing. For example, Figure 3.2a depicts a chip defined using an ink pattern drawn with ~1 mm lines. After drawing the ink

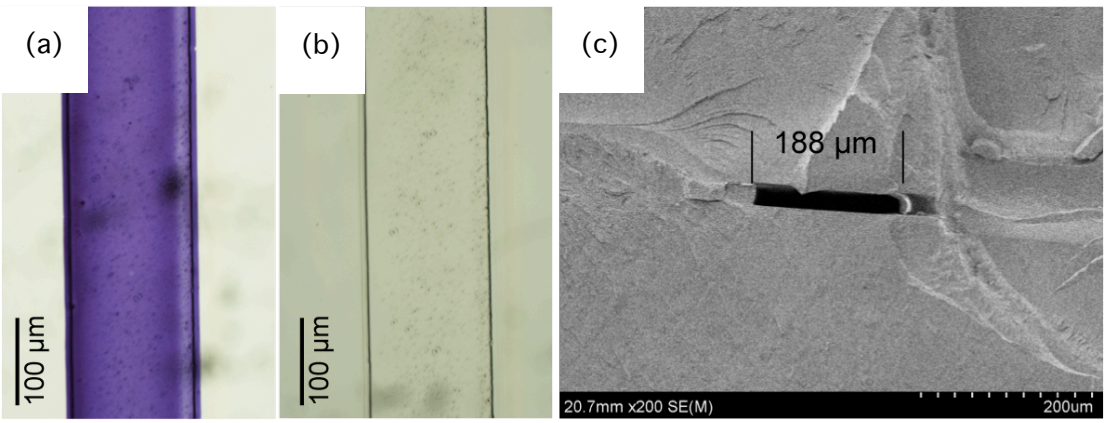

Figure 3.3 Bright field images of a microchannel formed in a COP chip by orogenic growth with a manually-drawn ink mask (a) immediately after microchannel sealing and (b) following buffer rinsing to remove the water-soluble ink. (c) Cross-sectional SEM image of a typical microchannel, 188 µm wide and 22 µm tall.

mask, exposing the chip to solvent vapor for 15 min, and sealing the channel, the water-soluble ink was removed by flushing the channels with DI water (Figure 3.2b) followed by injection of red food coloring (Figure 3.2c) to demonstrate that the channels remain open throughout the process. While low aspect ratio mm-scale channels have been explored for various applications, channels with smaller lateral dimensions are desirable in many microfluidic systems. To achieve smaller mask linewidths, wet-erase marker ink was removed from the native casing and injected into a refillable fiber-tip marker with a reported 200 mm nib diameter. While higher-resolution markers with nib dimensions as small as 30 mm are available, our tests with markers smaller than 200 mm were inconsistent due to irreproducible ink deposition. An example of a straight microchannel fabricated by masking with a marker possessing a nominal nib diameter of 200 mm is shown in Figure 3.3, with a measured channel width of 188 mm after sealing.

3.4.4 Microchannel height

For the channels shown in Figures 3.2 and 3.3, chip bonding was performed using a hot press after 15 min orogenic growth, resulting in an average channel height of 22 mm in each case. As mentioned in previous Chapter, 60 min exposures yielded an average growth height of 51 mm, with nearly linear growth between 5–60 min. These growth heights were measured with respect to the masked surface far from the mask boundaries. However, a region of piled-up polymer forms at these boundaries (Figure 2.5), resulting in localized hillocks of polymer that typically protrude out of the plane of the chip by 40y50% of the overall growth height. Because these raised hillocks act as stress concentration points during chip bonding, application of a high bonding

force during channel sealing serves to deform the solvated hillocks, forcing polymer from the raised regions to flow into the open microchannels. In the case of high

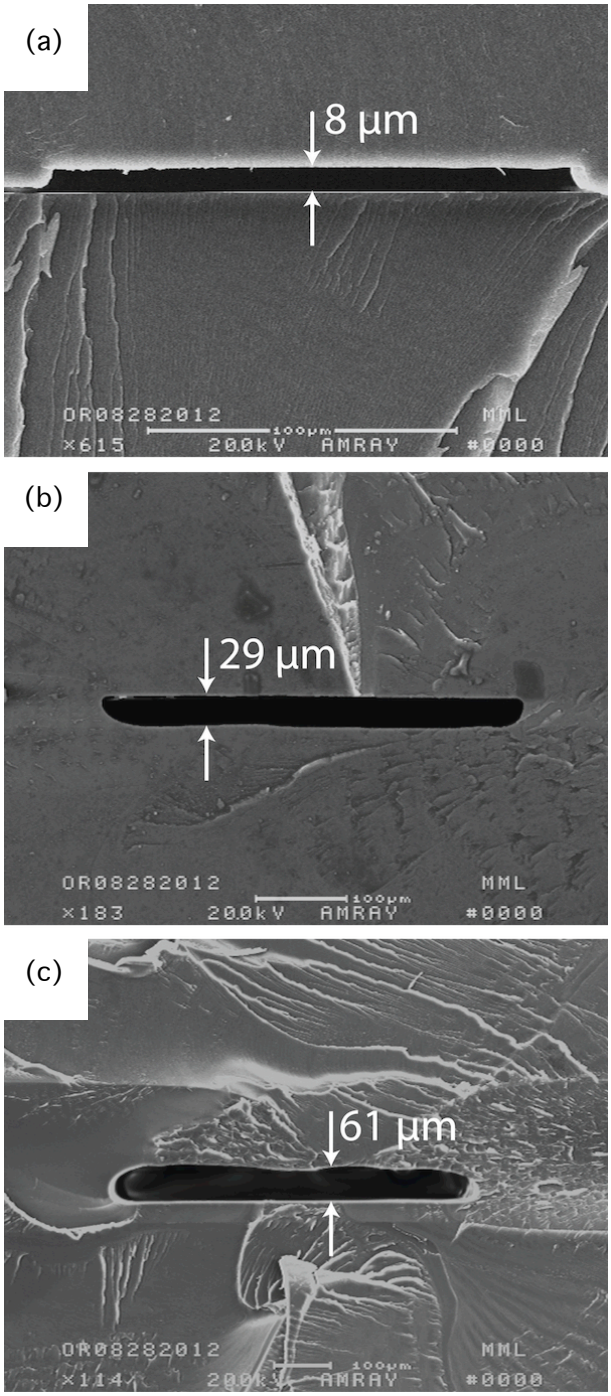

Figure 3.4 Cross-sectional views of channels fabricated using (a) 8 min, (b) 30 min, and (c) 60 min solvent exposure times, resulting in channel heights of 8 µm, 29 µm, and 61 µm, respectively. In case (a), chip bonding was performed using a hot press, while in cases (b) and (c) a low-pressure lamination process was used for bonding to minimize channel height reduction.

pressure bonding using a hot press, this polymer reflow results in nearly vertical sidewalls as the hillock volume is displaced into the open channel. This phenomenon can be clearly seen in Figure 3.3.

By extending the solvent exposure time, deeper channels with higher aspect ratios can be achieved. However for channels taller than ~25 mm, swelling of the unmasked regions during extended solvent exposure generates taller hillocks at the edge of the masked area that can uncontrollably fold or collapse into the microchannel when bonding at high pressure, resulting in clogging of the channel by the displaced polymer. To address this problem while making the overall fabrication process compatible with a true desktop manufacturing model, lower bonding pressure was applied using a desktop laminator. The use of the desktop laminator was found to result in significantly less deformation of the raised hillocks, yielding slanted and smooth channel sidewalls without clogging.

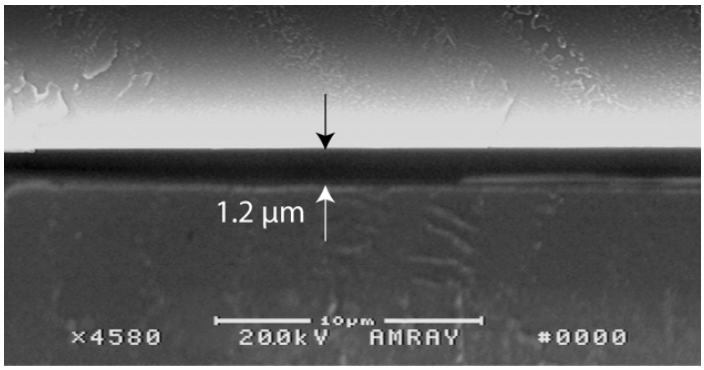

Figure 3.5 Example of a 1.2 µm tall microchannel with fabricated using a 3 min solvent exposure time. While submicron channel features have been fabricated, solvent exposure times below 3 min result in compromised bond strength for the sealed chips.

Examples of channels fabricated using different solvent exposure times and bonding methods are presented in Figure 3.4. It is significant that final channel heights are higher than reported orogenic growth heights reported in Chapter 2. For example, in the case of a 15 min solvent exposure time, leading to an orogenic growth height of 17 mm, a final channel height of 22 mm is observed (e.g. Figure 3.3). Similarly, a 60

min exposure expected to yield a 51 mm growth height results in a channel height of 61 mm (Figure 3.4c). The enhanced channel height is believed to be largely due to the presence of the solvent-swollen polymer hillocks at the mask edge following orogenic growth. A further factor that may contribute to the increased channel height is that solvent absorbed by the orogenically-patterned chip can transfer into the sealing layer during the bonding process, leading to swelling and additional growth of the sealing layer where the chips are in contact. Regardless of the solvent exposure time and bonding method, the final sealing interface is highly planar, with good sealing in the field far from the channels. Bonding strength of the final sealed chips is excellent, with typical burst pressures above 15 MPa as measured using a liquid chromatography pump connected to the chips through high pressure needle ports[45]. One consideration regarding the orogenic process is whether the solvent-swollen surfaces exhibit different mechanical, chemical, or optical properties compared to the native polymer. Because the swollen polymer possesses a lower density, it is likely that characteristics such as refractive index and bulk modulus are modified during growth. It should be noted that this same issue applies to any thermoplastic surfaces that have been solvent treated during a solvent bonding process, and in fact the orogenically-patterned channels are expected to present surfaces closer to the native polymer since the top and bottom of each channel are protected from solvent exposure during the growth and bonding steps.

The ink-masking method may also be used to fabricate very low aspect ratio channels through the application of reduced solvent exposure times. Short solvent exposures can produce consistent and controllable growth heights below 200 nm, while

maintaining a smooth polymer surface with average surface roughness below 3 nm as reported in Chapter 2 (Figure 2.4). In principle, this approach can provide a facile alternative to current methods for two-dimensional nanofluidic device fabrication[77–83], since the absence of solvent within the channel regions prevents channel collapse during bonding. However, solvent exposure time also impacts bond strength of the sealed chips, setting a lower limit on achievable channel depth for functional chips. For example, the 1.2 mm deep channel shown in Figure 3.5, achieved using a solvent exposure time of 3 min, was found to be near the minimum dimension that could be successfully fabricated without chip delamination during cleavage in preparation for microscopy. Thus while submicron channels are feasible, further efforts are needed to evaluate the limitations of this process.

3.4.5 Computer-controlled patterning

While manual mask drawing may be suitable for simple microfluidic designs, automated robotic control over mask patterning is necessary more typical applications where pattern accuracy and precision are important considerations. A goal of this Chapter is to demonstrate the pen microfluidic technique as a low-cost desktop manufacturing platform enabling thermoplastic microfluidic fabrication without significant infrastructure investment. To remain aligned to the concept, we evaluated to use of a pen plotter for low-cost automated mask deposition as a replacement for manual drawing. Pen plotters use an automated stage to move a pen cartridge across a drawing surface to create line art. Compared to inkjet printing, an advantage of pen plotting is that a wide range of ink compositions may be used, since the ink is not limited by the viscosity constraints encountered in both piezoelectric and thermal

inkjet printing. While consumer-level desktop pen plotters have not been commercially available since the widespread adoption of inkjet and laser printers, an equivalent platform can be assembled by adding a penholder to an alternative 3-axis robotic positioning system. For example, low-cost vinyl cutter plotters (decal cutters) commonly offer 3-axis position control with high positioning resolution on the order of 10-20 mm[84]. Similarly, inexpensive desktop CNC milling machines are available from multiple vendors with suitable positioning accuracy and resolution.

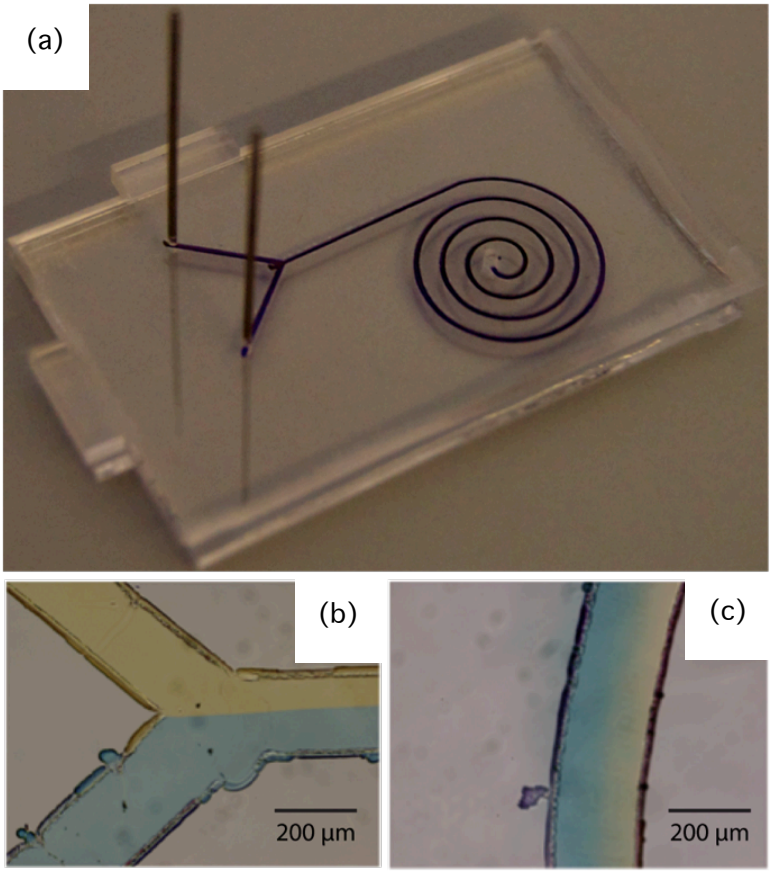

Figure 3.6 Spiral diffusive micromixer fabricated using computer-controlled mask definition. (a) Image of the fully-bonded chip before flushing ink from the enclosed microchannel, and images of dye solutions (b) at the confluence of the injected dye streams and (c) within an arm of the spiral showing formation of a smooth dye gradient due to diffusive mixing.

To demonstrate this latter concept, a spiral diffusive mixer design was patterned by mounting a pen on the tool holder of a desktop CNC machine, with the resulting sealed chip shown in Figure 3.6. The substrate was exposed to solvent vapor for 15 min, and aligned and bonded to a COP sealing layer with pre-drilled fluid ports. In this device, fluidic access was achieved by inserting stainless steel needle segments into the ports for low dead volume interfacing[45]. To demonstrate operation of this device, colored dye solutions were injected through the inlets, with well-defined laminar flow observed at the confluence of the injected streams (Figure 3.6b) and formation of a smooth color gradient by diffusion within the downstream arm of the spiral ([Figure 3.6). Although portions of the channels exhibited variations in width due to uneven ink deposition during mask patterning, as evident in Figure 3.6b, the flow profile within the channels did not appear to be impacted by these defects.

3.5 conclusions

A rapid desktop manufacturing method for thermoplastic microfluidic devices has been developed, utilizing commercially available inks as a masking layer for orogenic patterning of the thermoplastic substrates. The photolithography-free fabrication approach combines channel formation and bonding into a single step, where the solvent permeated surface can be permanently bonded to a cap layer to form fully enclosed channels. For manual patterning, the sealed all-thermoplastic chips containing microchannels with lateral dimensions on the order of several hundred microns and heights up to 60 mm may be manufactured with minimal infrastructure consisting of a pen, a solvent dish, and a desktop laminator. Precise computer-generated mask patterns have also been demonstrated by using a modified desktop

CNC tool as a pen plotter. The masking ink may also be patterned by inkjet deposition using a commercial piezoelectric print head, following appropriate modification of the ink viscosity. The simplicity of this approach allows a user to directly define channel features on a thermoplastic substrate, with total cycle times between 30–90 min from initial design concept to final device. This process offers a unique and exceptionally rapid approach to prototyping patterned and sealed microfluidic devices from homogeneous thermoplastic substrates.

Chapter 4: Single-use burst valves in thermoplastic microfluidic devices enabling on-chip reagent storage

4.1 Summary

A simple and reliable method for fabricating single-use normally closed burst valves in thermoplastic microfluidic devices is presented, using a process flow that takes advantage of orogenic growth (Chapter 2) and is readily integrated into established workflows for the fabrication of thermoplastic microfluidics. An experimental study of valve performance reveals the relationships between valve geometry and burst pressure. The technology is demonstrated in a device employing multiple valves engineered to actuate at different inlet pressures that can be generated using integrated manual pumps. On-chip storage and reconstitution of fluorescein salt sealed within defined reagent chambers are demonstrated. By taking advantage of the low gas and water permeability of cyclic olefin polymer, the robust burst valves allow on-chip hermetic storage of reagents, making the technology well suited for the development of integrated and disposable assays for use at the point of care.

This Chapter is adapted from a published article in the journal of Microfluidics and Nanofluidics.

4.2 Introduction

Microfluidic systems aimed for use at the point of care offer great promise for integrating and miniaturizing multiple discrete functional assay steps within inexpensive and disposable packages. While significant advances have been made toward realizing functional microfluidic diagnostics for use in point-of-care settings,

the miniaturization of integrated instrumentation for introducing assay reagents remains a challenging issue and is often a bottleneck in achieving true portable and disposable platforms. As a potential solution to this challenge, single-use normally closed valves integrated directly into the microfluidic system can enable on-chip storage of assay reagents within hermetically sealed compartments, supporting on-demand release without the need for external fluidic interfacing. This capability is of particular importance for point-of-care diagnostics and other analytical applications in low resource settings[30,85]. Although a wide range of microfluidic valves actuated through a variety of transduction mechanisms have been reported[86] , the development of normally closed valves that can be easily integrated into disposable devices remains a challenge. For example, while normally closed PDMS-based valves have been widely explored[87–92] , these components either require external pressure sources and pneumatic valves for their operation, or rely on internal pressure-induced deformation of an elastic substrate above an initially closed, but unbonded, valve interface. In each of these cases, valve operation depends on the use of an elastomeric substrate, and thus, these approaches cannot be readily implemented using thermoplastic materials that are ideally suited for low-cost and robust disposable devices. Hydrophobic valves, commonly used in lab-on-a-cd platforms[93,94], rely on the presence of an air/water interface and thus cannot provide hermetic sealing of fluids. Several different types of active valves employing materials including hydrogels[17,95], polymers monoliths[95,96], waxes[97,98] , and ink[99] have been described, but these materials require external stimuli such as pH shift, light, or heat to actuate, often employ complex fabrication processes that are not amenable to low-cost diagnostics,

and can suffer from issues with biocompatibility, contamination, and unwanted interaction with bioactive materials. Here we demonstrate a new approach to the integration of single-use normally closed burst valves in thermoplastic microfluidic devices that are directly compatible with thermoplastic fabrication of cyclic olefin polymer (COP) devices. The integration of burst valves into thermoplastic microfluidics presents a particular challenge, since established thermoplastic bonding methods have been developed with the goal of providing a permanent seal between the microfluidic substrates. The approach presented here takes advantage of orogenic microfabrication technique explored in Chapter 2, a selective solvent swelling technique[33,34] that allows small open pockets to be created within a surrounding substrate sealed by solvent bonding. By fabricating two discontinuous microchannels in the substrate prior to solvent bonding and positioning the unbonded pocket between the proximal ends of these channels, a continuous bridge supporting fluid flow between the channels is formed. Subsequent thermocompression bonding of the device closes this pocket, which is fabricated with a nominal height of several micrometers, generating an interfacial bond that is weaker than the surrounding solvent bonded substrate. The thermally bonded region acts as a robust single-use pressure-controlled valve, preventing fluid flow in its initial state, but permanently opening upon application of a pre-defined pressure within one of the discontinuous channels. This approach is conceptually similar to the successful realization of normally closed valves in elastomeric polydimethylsiloxane (PDMS) substrates through the selective patterning of unbonded valve regions[92], but with the ability to tune the burst pressure with the addition of a thermal bonding step, and to achieve a

permanently open channel following valve actuation, while taking advantage of the favorable properties of thermoplastic materials for microfluidic applications. In this Chapter, we detail the valve fabrication process and pressure-controlled actuation mechanism and investigate the relationships between valve design parameters and the resulting burst pressure and operational back pressure for the fabricated valves. Fabricated valves with actuation pressures in the range of 1–2 MPa and negligible back pressure are realized. Furthermore, by combining burst valves with integrated screw pumps, we explore the packaging of different solutions on chip, followed by selective valve actuation and flow control using a simple manual pumping technique. Lastly, on-chip packaging, sealing, reconstitution, and release of dehydrated fluorescein salt are investigated to demonstrate the utility of the burst valves for on-chip storage of assay reagents within thermoplastic devices.

4.3 Experimental section

4.3.1 Materials and Reagents

Thermoplastic 1020R COP plaques (2 mm thick) were purchased from Zeon chemicals (Louisville, KY). Reagent grade cyclohexane was obtained from Sigma (St. Louis, MO) Wafer dicing tape was acquired from Semiconductor Equipment Corporation (Moorpark, CA). Needle tubing segments (gauge 22 s, 710 μm o.d. 150 μm i.d.) were purchased from Hamilton Syringe (Reno, NV) Stainless steel machine screws (3 mm diameter, 350 μm pitch) were purchased from Small Parts (Miami Lakes, FL).

4.3.2 Microfluidic chip fabrication

Microchannels were directly milled into a COP plate using a computer numerical control (CNC) milling machine (MDX-650A; Roland, Lake Forest, CA). Inlet/outlet ports and on-chip reagent reservoirs were milled using the same CNC tool using 650 μm and 2-mm-diameter drill bits, respectively. The inlet reservoirs were then self-tapped to form threaded ports using a stainless steel screw. The machined chips were sonicated in deionized (DI) water for approximately 10 min to clear debris and sequentially cleaned by methanol, isopropanol, and DI water, followed by drying in nitrogen gas and overnight degassing at 75 °C under vacuum.

4.3.3: Burst valve fabrication and bonding

The burst valve integration process is fully compatible with conventional thermoplastic chip fabrication based on solvent bonding. As described in Figure 4.1, the surface of a COP chip containing microchannels is covered with a sheet of dicing tape patterned with holes aligned to the desired burst valve regions. The chip is placed in a UV-ozone (UVO) system (PDS-UV, Novascan Technologies, Ames, IA) for 20 min (Figure 4.1b). After removing the blue tape, vapor phase solvent bonding[33,34,73] is used to bond the chip to a mating COP plaque (Figure 4.1c,d). Briefly, a glass dish containing 200 ml of cyclohexane was heated to 30 °C in an oven. The UVO-exposed COP chip was positioned face down at the top of the glass dish, with a sheet of solvent resistant tape to hold the chip in place, 5 cm away from the liquid cyclohexane surface. The fabrication process allows for either the chip containing microchannels or the COP capping layer to be exposed to solvent during bonding process. For cases where reagents are integrated into the microchannel substrate, exposure of the capping layer is preferred to prevent unwanted exposure of

reagents to potentially harmful solvents. After exposure to solvent vapor for 5 min (Figure 4.1c), the microchannel substrate was promptly removed from the solvent dish and brought into aligned contact with its mating COP lid substrate containing inlet and outlet ports (Figure 4.1d). The assembly was then placed in a hot press (AutoFour/15, Carver, Wabash, IN) at a pressure of 3,500 kPa for 1 min at room temperature to promote intimate substrate contact during the solvent bonding process. Following minimum 8-h incubation at room temperature to allow evaporation of solvent, the open-valve regions were thermally bonded at an elevated temperature of 95 °C and pressure of 4,800 kPa for 10 min (Figure 4.1e)

4.3.4: Valve actuation and measurements

High-pressure needle ports[45] were used to interface the chip with an analytical liquid chromatography pump (PU-2089; Jasco, Easton, MD) providing precise volumetric flow rates and pressure measurements with 0.1 MPa resolution during device characterization. A constant flow rate was applied to the inlet, and the applied pressure was continually monitored using the pump. Valve actuation was readily determined by a large drop in back pressure and immediate visible release of liquid downstream of the valve. Valve actuation was also accompanied by a characteristic audible signal resulting from the sudden failure of the weak thermal bond at the valve interface. Back pressure was measured 1 min after initial opening of the valve while pumping DI water through the valve at 2 µl/ min. Steady-state inlet pressure is typically observed following 20 s after valve actuation. For manual valve actuation, small volumes of water spiked with food coloring were pipetted into the reagent reservoirs. Stainless steel screws were gently inserted to seal the reservoirs by turning

approximately one half turn after seating each screw against its mating threads. Valve actuation was performed by manually rotating the screws with a small screwdriver. For devices prepared with sealed fluorescein salt, syringe pumps (Harvard Apparatus)

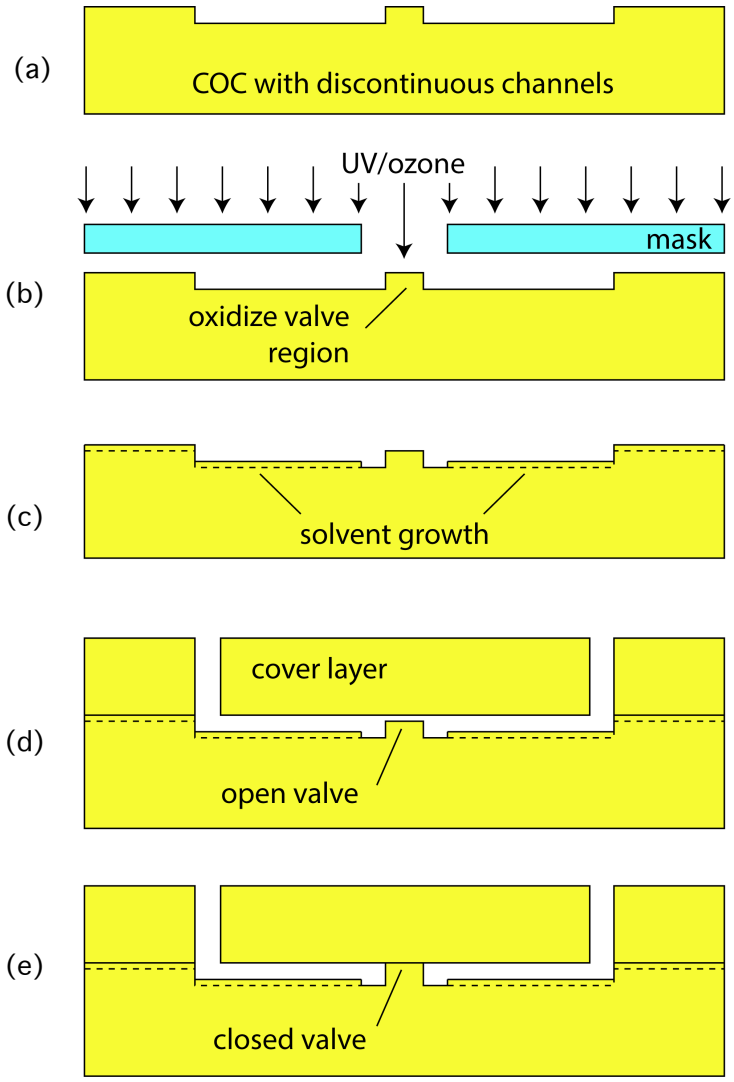

Figure 4.1 Burst valve fabrication process. (a)Discontinuous micro- channels are formed in a COP substrate which is, (b) selectively treated with UVO, yielding an oxidized chemical masking layer in the treated valve area. (C) Exposure of the substrate to solvent vapor induces orogenic growth in the unmasked areas, controllably raising the surface height outside of the valve region. During this process, solvent is prevented from entering the substrate within the oxidized UVO-treated valve region. (D) Aligned solvent bonding with a mating COP chip containing pre-milled access ports creates a gap connecting the discontinuous channels across the solvent-free valve region. (e) Thermal bonding of the chip collapses the valve gap, resulting in a bond in the valve region that is weaker than the solvent bond within the field of the chip

and glass syringes (Hamilton) were connected to chip inlets via capillary tubing (Cole-Palmer) and appropriate fittings (Upchurch Scientific) to provide the desired input pressure for valve actuation.

4.4 Results and discussion

As mentioned before, due to their low material cost and compatibility with a wide range of industrial-scale replication methods, thermoplastics are ideal materials for disposable point-of-care diagnostic assays. In particular, COP is an attractive material due to its high transparency and low autofluorescence, exceptional dimensional stability, low water absorption, and low gas permeability. In addition, COP offers excellent chemical compatibility, including good resistance to a range of common solvents as discussed in Chapter 2. However, by selecting a solvent with a solubility parameter similar to that of the COP itself, the solvent can be absorbed into the bulk substrate (Orogenic growth). Like most thermoplastics, COP is a moderately hydrophobic material with low surface energy. However, selective treatment of COP with UVO oxidizes the exposed surface, generating surface charges that can render it inert to solvent uptake and allowing regions with differential solvent absorption to be formed. In Chapter 2 we demonstrated that native COP surfaces exhibit permanent volume changes following cyclohexane uptake, resulting in surface height increases that can be controlled over a wide range by adjusting the solvent exposure conditions[33,34]. To form the thermoplastic burst valves, a short 5-min exposure to solvent vapor results in a 3 to 5 μm-height difference between the native and UVO-treated COP surfaces. By growing the entire surface of the microchannel substrate, except for a small UVO-treated region bridging two or more discontinuous channels,

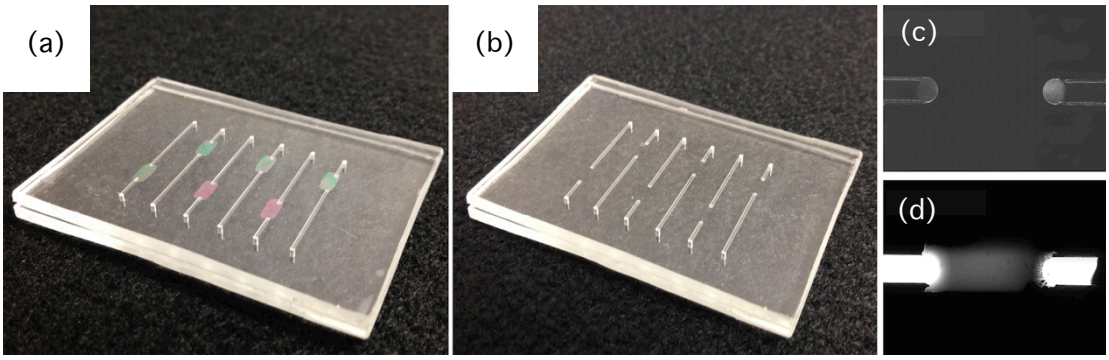

Figure 4.2 Fabricated COP chip with multiple burst valves (a) after solvent bonding, and (b)following thermal bonding. The unbonded gaps at the channel discontinuity after solvent bonding are visible as colored regions in, a due to light refraction at the *top* and *bottom* surfaces of the valve gap. Magnified images of the valve region for, (c) a closed burst valve after thermal bonding and (d) the same valve during flow of fluorescent dye confirm that the valve can be opened following application of sufficient pressure at the inlet

a shallow trench is formed between the deeper channel structures. After the initial solvent bonding step, this trench provides fluidic interconnection between the microchannels, as seen in Figure 4.2a. The UVO-treated regions appear colored in this image due to the difference in refractive index within the shallow gap. After thermocompression bonding under sufficient pressure to collapse the shallow gap, the valve region appears clear due to elimination of the refractive index gradient (Figure 4.2b). Since the bond strength at the solvent bonded interface is significantly stronger[36,45] than thermally bonded valve region, the closed valve can be opened by applying a sufficient pressure within one of the microchannels. When the pressure reaches a critical point (Figure 4.2d), the weakly bonded region fails, opening the seal and allowing fluid to flow between the newly interconnected channels. Because thermocompression bonding is performed at a relatively low temperature to prevent significant flow of polymer during the bonding step, significant residual stress within the valve region allows the gap to return to its original height after the valve is

actuated, ensuring a well-defined fluid flow path for the open valve. The critical burst pressure at which a valve will open and the final back pressure during steady-state flow of liquid through the opened valve are both affected by the UVO treatment time. Modifying COP surfaces by UVO treatment has been shown to enhance thermal bonding of COP by increasing wettability of the surfaces, enhancing mechanical interlocking and inter-diffusion of the polymer chains during bonding[36,47] . However, UVO treatment also impacts solvent absorption, with longer treatment times and higher levels of oxidation resulting in less solvent uptake. To estimate the extent of surface oxidation, sessile water contact angle was used as an indirect measure of surface charge density, since hydrophobicity is inversely correlated with surface charge. As shown in Figure 4.3, the contact angle decreased with longer UVO exposure time until reaching a lower limit of 20° at 20 min. Following solvent exposure of COP chips containing valve designs with nominal dimensions shown inset in Figure 4.3, the chips were sealed and the valves were characterized to determine burst pressure and back pressure. For treatment times below 20 min, significant solvent uptake within the treated regions resulted in the valves remaining closed over the full range of inlet pressures up to 12 MPa, whereas for a 20-min UVO treatment, the valves opened at an average input pressure of 1.53 MPa. While no further decrease in contact angle occurred for longer UVO exposures, a significant reduction in burst pressure was observed when extending the exposure time from 20 to 30 min, suggesting that some amount of solvent is still absorbed by the COP at the 20-min time point, thereby strengthening the bond within the valve region. Increasing the exposure time to 30 min further inhibits solvent uptake, resulting in a primarily

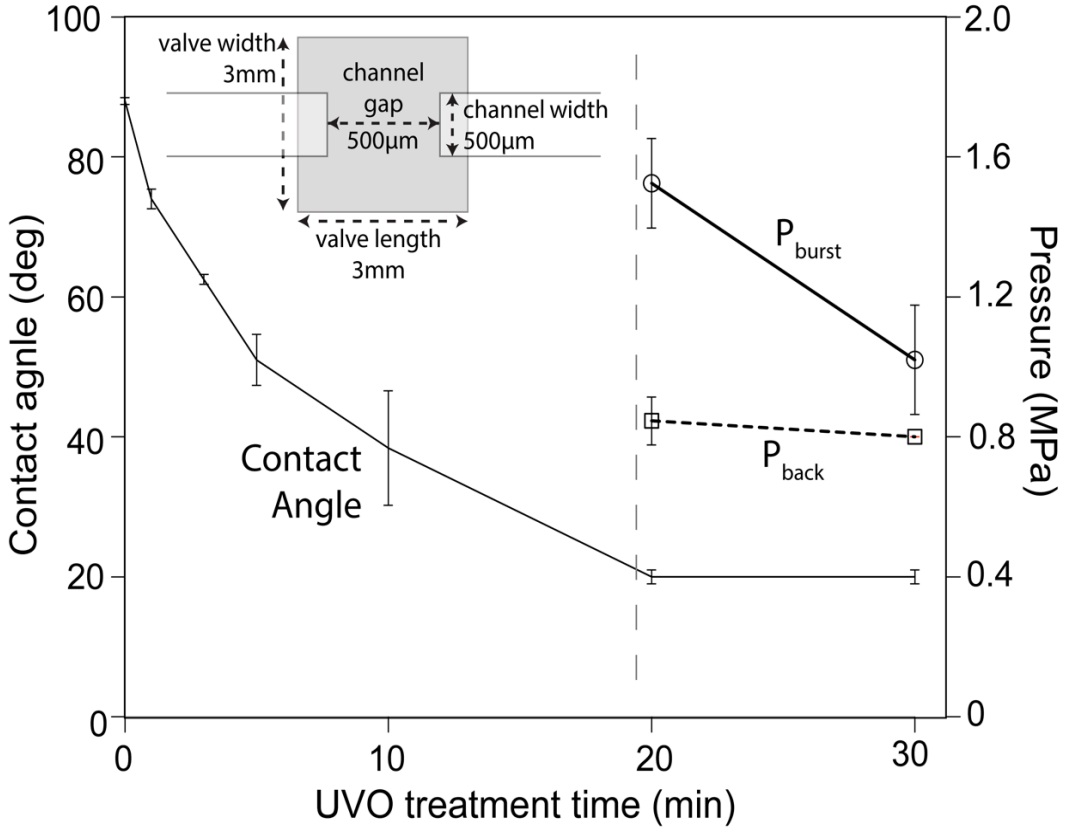

Figure 4.3 Sessile water contact angle on a COP surface, valve burst pressure (P_{burst}), and back pressure (P_{back}) of an opened valve as a function of UVO treatment time. Treatment times below 20 min do not generate sufficient surface functional groups to prevent solvent uptake within the valve region. The nominal dimensions of the valves used for this study are shown *inset*

thermal bond at the valve interface that can be actuated at a lower input pressure. All further experiments were performed using a UVO exposure time of 20 min to enhance the difference between burst pressure and back pressure, making it easier to identify valve actuation events from pressure measurements alone. In addition to UVO treatment time, the effects of valve geometry on burst pressure and back pressure were also studied, with results presented in Figure 4.4. For all experiments, the nominal device dimensions were the same as those provided inset in Figure 4.3. As shown in Figure 4.4a, the burst pressure exhibits a slight drop as the width of the

valve region is increased from 1 to 3 mm, but remains nearly constant as the width is further increased to 1 cm. The higher burst pressure observed for the 1 mm-wide valve is presumed to result from the low width : length ratio for this design, resulting in constrained lateral crack propagation relative to the crack length during valve opening. In contrast to the insensitivity of burst pressure to valve width, a significant drop in back pressure was found to occur with increased width, reflecting the larger cross-sectional flow path presented by the wider valve structure. In principle, smaller valve regions on the order of several tens of micrometers can be readily patterned using our previously demonstrated techniques[33,34]. However, since both burst pressure and back pressure rapidly increase as the valve area is reduced, the minimum practical valve geometry is dictated by the limits of these parameters that can be tolerated for a given design. Valve performance was also evaluated as a function of inlet and outlet channel width, as shown in Figure 4.4b. Significantly, neither burst pressure nor back pressure was found to be correlated with the channel width, even for designs where channel width is of the same length scale as the width of the valve itself. These data confirm that valve performance is determined by the properties of the valve region itself, indicating that burst valves may be designed independently from the microfluidic channels interfaced with the valves. In a further study of valve geometry, the distance between the tips of the inlet and outlet channels was varied between 500 and 1500 μm. As illustrated in Figure 4.4c, channel gap appears to have a strong influence on valve performance, with both burst pressure and back pressure directly correlated with the channel gap. With larger gaps, the burst pressure required to open the valve increases rapidly. At the same time, back pressure increases due to

the longer flow path between the inlet and outlet channels, resulting in higher hydrodynamic resistance for larger gaps. However, because the valve area is held

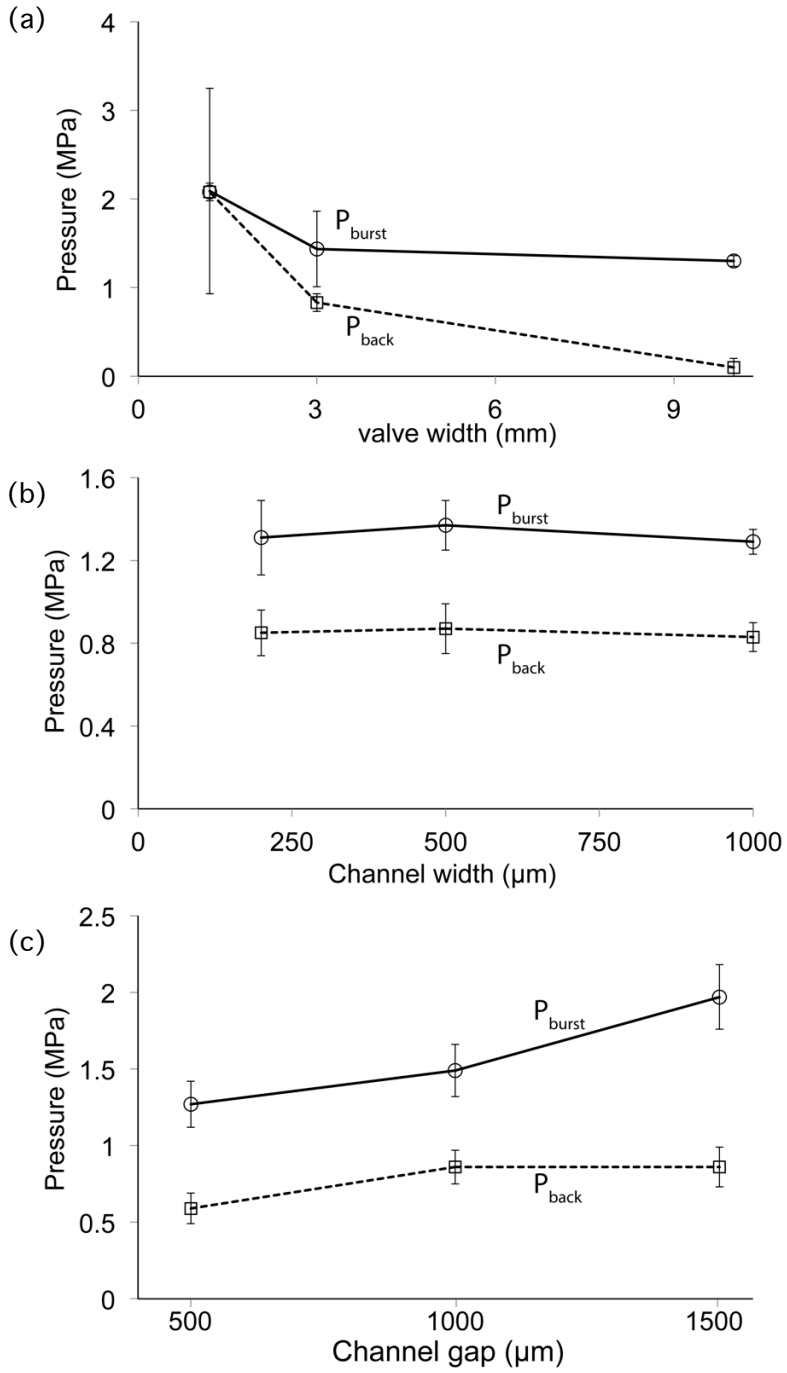

Figure 4.4 Measure valve burst pressure and back pressure as a function of (a) valve width, (b) channel width, and (c) channel gap. Inlet and outlet channels were positioned symmetrically about the center of the UVO- treated valve region for these experiments

constant in these experiments, with inlet and outlet channels positioned symmetrically about the center of the valve region, variations in channel gap result in different lengths by which the channels intrude into the valve area. To evaluate whether the channel gap or the channel position relative to the valve region is responsible for the changes in burst pressure observed in Figure 4.4c, an additional set of experiments was performed using square valves with constant 3 mm side lengths and different channel gaps, similar to the devices used for Figure 4.4c, but with variations in positioning of the channels relative to the valve center. By allowing the channels to be asymmetric within the valve region, the influence of channel position could be assessed independent of channel gap. The resulting measurements are presented in Figure 4.5, which displays the measured burst pressure as a function of the minimum radial distance between the inlet channel and the center of the valve region. A clear linear trend is observed for all data sets, regardless of the channel spacing. Although not explicitly displayed in this Figure, the results also demonstrate that positioning of the outlet channel does not impact the burst pressure. While the valve opening process is presumed to involve crack opening consistent with the principles of fracture mechanics applied to the bonded valve interface, the results presented in this work are based on experimental characterization of bond failure using internal pressures applied within laterally confined channels, similar to pressure burst tests used to characterize microchannel substrate bond strength. While the complex loading state used in these experiments limits the ability to infer details of the bond interface physics, the results provide engineering insight into valve behavior and reveal several important aspects of the underlying valve opening mechanism.

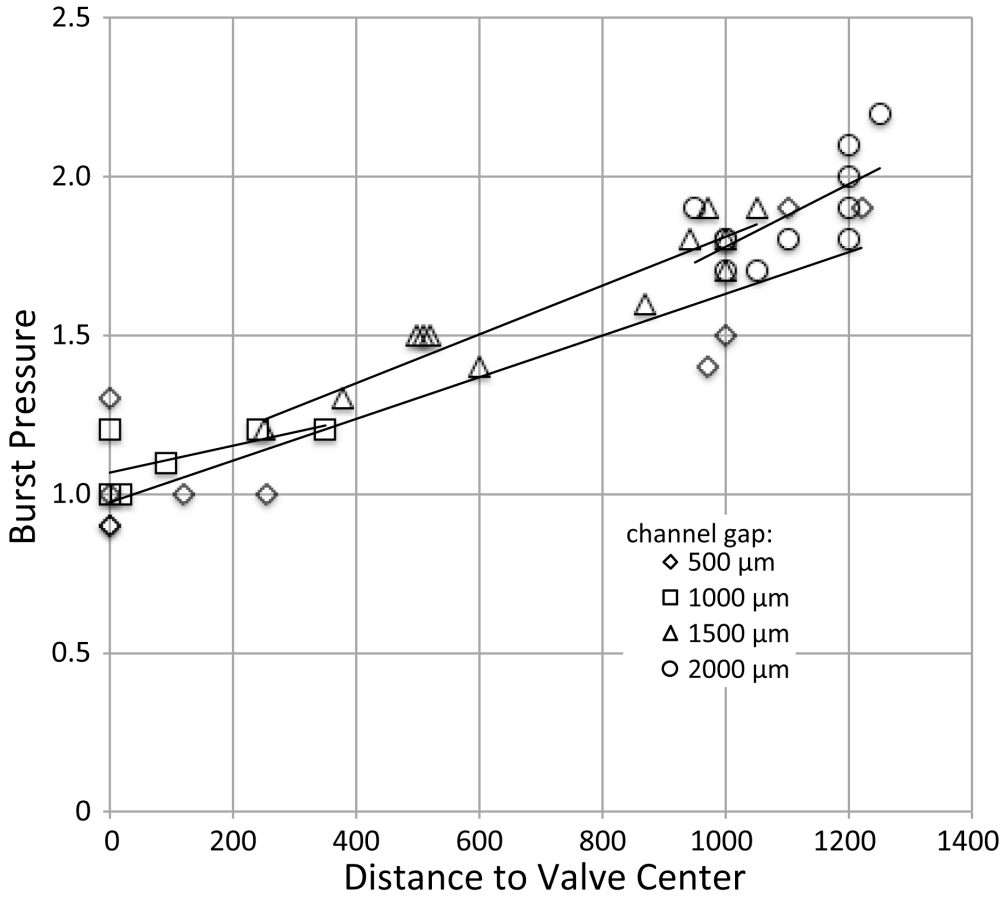

Figure 4.5 Measured burst pressure as a function of the minimum radial distance between the inlet channel and center of the UVO-treated valve region reveals a linear relationship, regardless of the gap between inlet and outlet channels, which varies between 500 and 2,000 µm

Following thermal bonding of the valve region, a high residual tensile stress is imposed at the bond interface, as the closed micrometer scale gap seeks to relax to significant role in defining the burst pressure than the total force exerted over the full width of the valve. As the separation force is moved closer to the center of the valve region, the maximum bending moment generated in the thermoplastic substrate rapidly increases, resulting in higher strain energy at the interface and thus a lower burst pressure. This hypothesis is consistent with the burst pressure versus channel position measurement presented in Figure 4.5, as well as the data in Figure 4.4c

which show that as the channel gap widens, and the tip of the input channel is positioned further from the center of the valve region, the burst pressure increases. Within the limits of our optical measurements, with image capture performed at a rate of 60 frames/s, valve response time is essentially instantaneous. While the relationship between substrate thickness and burst pressure was not explored in this work, the expected reduction in bending stiffness associated with a thinner capping layer may provide an additional approach to controlling the burst pressure. After investigating the fundamental relationships between valve design and actuation pressure, a microfluidic device employing multiple valves operating with different burst pressures and coupled with manual on-chip pumps was fabricated to evaluate the utility of the thermoplastic burst valves for microfluidic operations including reagent storage and fluid mixing. Individual liquid reagent storage wells were integrated upstream of four on-chip burst valves, as can be seen in Figure 4.6a. Each storage reservoir was first tapped to create threaded a port, and solutions of water mixed with different colored dyes were introduced into each of the open wells by pipette. The ports were then capped using fine pitch stainless steel screws, sealing the fluid packets between the upstream screw and downstream burst valves. Actuation of each valve was realized by manual rotation of the corresponding screw (Figure 4.6b). In this demonstration device, the burst valves were configured to couple multiple inlets with single outlets, allowing for mixing of reagents by Taylor dispersion following successive actuation of each valve as seen in Figure 4.6c,d. Opening of the valves using the screw pumps was found to be robust, with consistent actuation observed. By sealing different air volumes within the reservoirs, the number of turns

required to reach the defined burst pressure could also be controlled. The valves themselves were highly resistant to accidental opening during chip handling, with no actuation observed after dropping chips multiple times onto a rigid floor from a standing position.

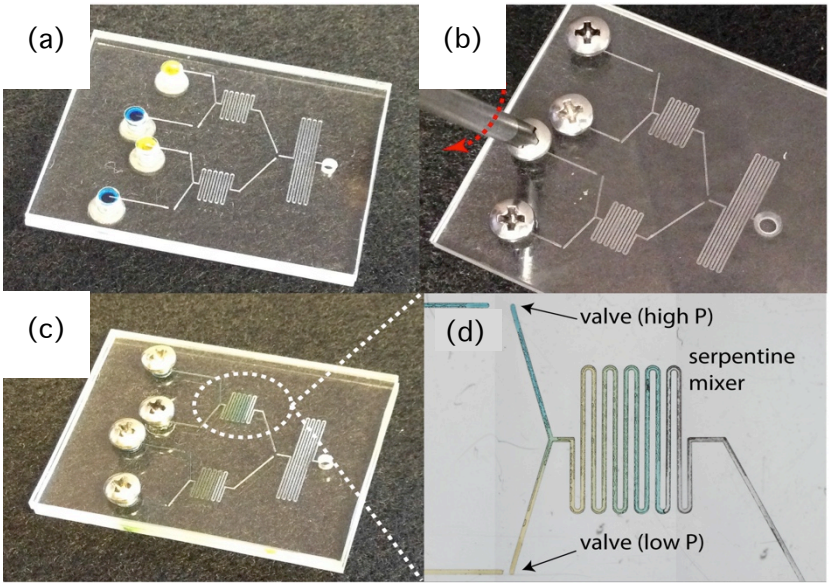

Figure 4.6 Images of a fabricated COP chip containing multiple burst valves with on-chip reagent storage and manual screw valves. (a) Colored solutions pipetted into storage reservoirs are later capped with fine pitch stainless steel screws. (b) Manual rotation of each screw pressurizes the reagent pouches, until, (c) accumulated pressure overcomes the thermal bonding at the valve interface, pumping the liquid through the device. (d) Actuation of multiple reservoirs results in mixing within the downstream serpentine channel. As seen in d, each coupled valve is designed with a different burst pressure, preventing unwanted actuation of multiple valves

Long-term on-chip reagent storage is an essential requirement for point-of-care analytics and diagnostics. Currently, the majority of platforms designed for near-care use lack on-chip storage, and rely on the end user to manually pipette or pump reagents into the device prior to assay execution[100] . Various approaches to on-chip reagent storage have been explored, including storage of liquid reagents packaged in glass ampules[101] and both liquid and dry reagents in foil pouches[100], with controlled

release in a lab-on-a-cd platform. Similarly, long-term storage of horseradish peroxidase conjugated antibodies in paper-based microfluidic devices has been explored[102]. One goal of this Chapter was to demonstrate the integration of dried reagents within reagent storage reservoirs on thermoplastic chips without the need for additional components such as paper, glass ampules, or foil packaging as used in prior work. To demonstrate on-chip reagent storage, a saturated 0.5 µL fluorescein salt solution was pipetted into open reagent reservoirs located between two burst valves prior to sealing the device, i.e., after the first step in Figure 4.1. The

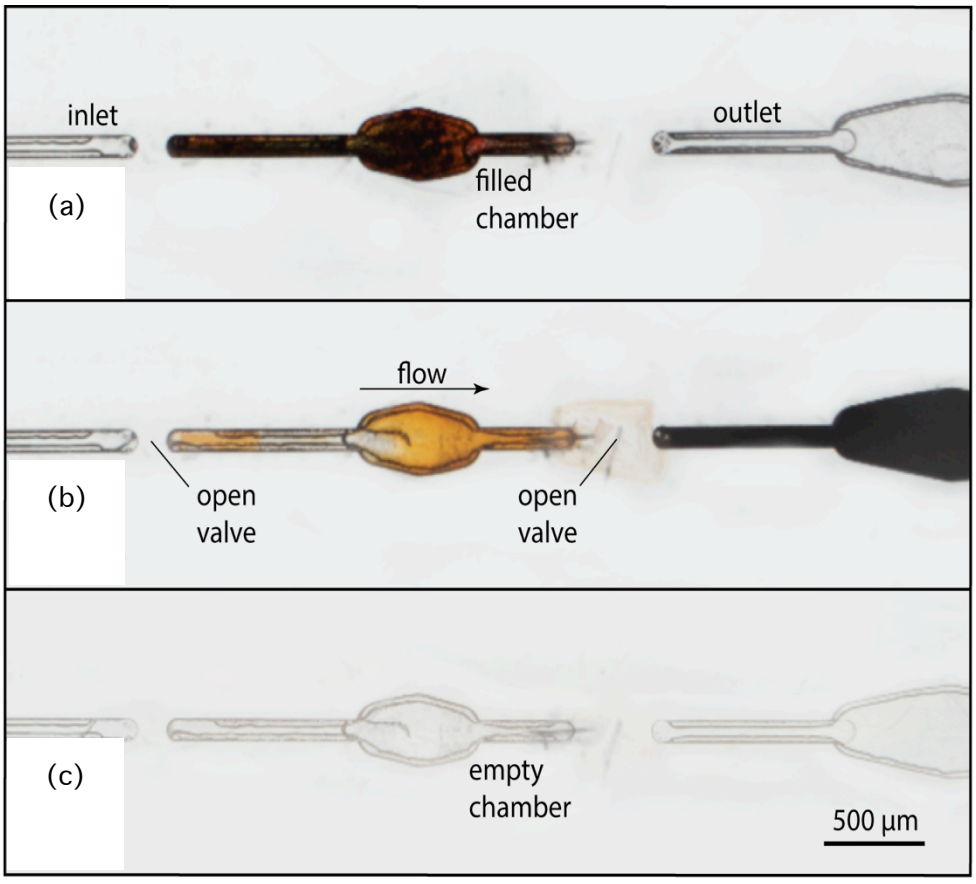

Figure 4.7 Image sequence revealing (a) on-chip packaging of dehydrated fluorescein salt within an integrated storage chamber, (b) pressure-induced valve actuation upstream (at 1.2 MPa) and downstream (at 2 MPa), thereby rehydrating the dye and releasing it into the outlet channel, and (c) complete emptying of the reagent storage chamber

fluorescein was air dried, and the resulting substrate containing dehydrated reagent was then bonded to a capping layer as described in Figure 1b–e. DI water was injected in the microchannel using a syringe pump, allowing pressure to build up until reaching the critical level for valve actuation. Upon actuation of the first valve, with a designed burst pressure of 1.2 MPa, reconstitution of the dried fluorescein salt is initiated. Since the second valve was engineered to open above 2 MPa pressure, a brief period of pressure accumulation is observed, during which fluorescein salt becomes fully dissolved in water that has entered the reagent reservoir. As the pressure within the reagent chamber increases, the second downstream valve opens, allowing fluorescent solution to pass through downstream channels. A sequence of images showing each stage of this process is depicted in Figure 4.7. It is notable that employing valves with different burst pressures in this configuration has two advantages. First, valve actuation can be automated, with no interference from the end user required once the syringe pump is set at predefined volumetric flow rate. Second, the differential burst pressure can be engineered to define the desired time for dry-stored reagents to fully dissolve prior to opening the second valve. A potential concern regarding the packaging of reagents using the presented burst valve technology is that the temperature employed during valve bonding may affect thermally sensitive reagents. We note that for a wide range of reagents, such as polymerase, nucleotides, and surfactants used in polymerase chain reaction (PCR), and many proteins which can resist denaturation at 95 °C, thermal degradation under the current process conditions is not an issue. Furthermore, thermal stability of proteins including antibodies required for immunoassays can be significantly

enhanced by lyophilization in the presence of sugar-based cryoprotectants[103–105]. For other reagents where thermal stability remains an issue, local control over chip temperature during bonding may provide an alternative solution to this challenge.

4.5 Conclusions

A single-use normally closed valve technology suitable for integration into a wide range of thermoplastic microfluidic systems has been developed. The fabrication process requires minimal infrastructure and is fully compatible with conventional processing methods employed for microfluidic device development using COP substrates. Parametric studies revealed the key relationships between valve design parameters and performance, enabling both burst pressure and final back pressure of the valves to be independently tuned for specific applications, and allowing multiple valves with different actuation pressures to be achieved within a single device. Fabricated devices are realized that require low burst pressures of only 1–2 MPa, making the valves compatible with a simple manual actuation method leveraging integrated screw pumps. Effective on-chip packaging, reconstitution, and release of dehydrated reagents were demonstrated, with an engineered burst pressure differential between upstream and downstream valves used to control the reagent release process. The fabrication of multiple valves into a device supporting on-chip liquid storage and selective reagent delivery and mixing using manual screw pumps was successfully demonstrated. We anticipate that the normally closed valves will find utility for sealing and long-term on-chip storage of bioactive reagents in liquid or dried format, enabling reconstitution, mixing, and delivery of stored reagents for a range of

disposable point-of-care assays that can take advantage of the low material cost and attractive chemical and physical properties of thermoplastic microfluidic devices.

Chapter 5: Integrated screw-actuated micropumps for thermoplastic microfluidic devices

5.1 Summary

A simple method for fabricating and integrating on-chip displacement pumps in thermoplastic substrates is presented, using a process compatible with established workflows for fabrication of microfluidic devices. Stainless steel screws are utilized for reliable on-chip pumping, capable of delivering reagents over a wide range of flowrates from 0.5nL/min to 40µl/min. O-ring equipped stainless steel rods are utilized to achieve a watertight seal. Combined with previously reported burst-valves, on-chip displacement pumps offer complete control over fluid distribution in microfluidic circuitry. An Arduino platform is utilized to achieve automated and portable pumping platform for thermoplastic microfluidic devices at a low cost in resource-constrained settings.

5.2 Introduction

As discussed in previous chapters, microfluidic devices aimed for use in resource-constrained settings should ideally operate with minimal use of off-chip instruments. While significant advances has been made in the development of new diagnostics designed for use at the point of care or in near-patient settings, integration and miniaturization of peripheral instruments such as pumps, that are essential for manipulation of fluids during assay operation, is a challenge that has yet to be resolved. In an effort to accomplish this unmet need, in this chapter we demonstrate

an integrated on-chip microfluidic displacement pump technology capable of manual actuation as well as precise automated control over flow rate using a microcontroller and DC motors driven by a low-voltage power source such as a battery.

Although a wide range of microfluidic pumps have been previously demonstrated,[1–4] miniaturized pumps with the potential to be easily integrated in thermoplastic microfluidic devices in a portable and disposable format have not yet been realized, with some of the major studies using microfluidic-based diagnostics of infectious diseases in the developing world still relying on syringe pumps for controlled reagent delivery[5]. Conventional syringe pumps are bulky, costly, and require high voltage AC power sources for operation. While there has been several efforts to fabricate low-cost and open-source syringe pumps,[6–8] these solutions are not miniaturized or sufficiently portable for many diagnostic applications, and do not remedy the need for integrated, on-chip pumping for use at the point-of-care. Centrifugal lab-on-a-CD platforms,[9,10] which take advantage of centrifugal forces to generate on-chip radial pressure gradients, offer several advantages for pumping in compact analytical systems, but this mechanism constrains the range of device designs that can be realized, does not support bi-directional flow without the use of complex fluidic circuits, and suffers from similar power requirements as syringe pumps.

Several alternative mechanisms that have been explored for integrated on-chip pumping in microfluidic devices include capillary,[11–15] gravity,[16,17], and vacuum[18–20] driven pumping. While both capillary- and gravity-driven pumping are energy efficient pumping mechanisms, they provide limited or no control over the flow rate, a significant disadvantage for many bioanalytical platforms. While vacuum pumping

can overcome the issue of flow rate control, the need for a vacuum source with ancillary valving presents similar power, cost, and integration limitations as positive displacement syringe pumps. The use of manually-drive vacuum sources such as hand-operated syringes can overcome this limitation.

A promising alternative to these various pumping methods involves the direct displacement of fluid within an on-chip chamber sealed with an elastic membrane. Using PDMS as a membrane material, displacement pumps capable of manual operation by a simple thumb press or similar actuation force have been reported.[21–32] However, PDMS and related silicone elastomers are expensive, with material costs that are approximately 100 times greater than thermoplastics including COP, precluding the manufacture of low-cost disposable systems directly from these materials. Similarly, the integration of PDMS into thermoplastic fabrication processes is not generally amenable to high throughput manufacturing methods, thereby increasing overall manufacturing costs. More fundamentally, PDMS is not a favorable material for many POC assays, particularly for applications where long-term on-chip storage of reagents is necessary, since the high gas permeability and water absorption associated with PDMS has a negative impact on reagent stability and contamination.

Here we demonstrate a simple and effective approach to the fabrication of on-chip displacement pumps through the integration of threaded screws within thermoplastic microfluidic devices. The fabrication process takes advantage of the excellent machinability of thermoplastic materials, and is fully compatible with existing COP fabrication methods. In their simplest form, the pumps consist of threaded stainless

steel screws seated within tapped holes previously milled into the side of the microchannel capping layer. By adding a miniature plunger element consisting of a fluoropolymer elastomer O-ring seated onto a small stainless steel rod, a tight seal can be realized, eliminating fluid leakage and enabling sealing of the on-chip fluidic network.

In addition to allowing direct manual screw actuation, automated pump operation is explored using a microcontroller platform to drive multiple screws through DC motors coupled to the screw heads, allowing flow rates to be precisely controlled with linear response within the range of 0.5-35 μL/min. The pumps are capable of generating high pressure heads sufficient to actuate downstream on-chip burst valves. By combining these burst valves with the leak-free pump seals enabled by the integrated O-rings, enclosed fluidic reservoirs capable of storing hundreds of microliters of buffer solutions or other reagents were formed within the thermoplastic substrates, thereby eliminating the need for off-chip reagent storage and delivery, and enabling true on-demand delivery of reagents without the need for external fluidics.

5.3 Experimental section

5.3.1 Materials and methods

Thermoplastic 1020R cyclic olefin polymer (COP) plaques (2 mm thick) and resins were purchased from Zeon chemicals (Louisville, KY). Stainless steel rods (3 mm diameter) and stainless steel screws (sizes 0-80 and 4-40) were purchased from McMaster-Carr Inc. (Princeton, NJ). O-rings were purchased from Precision Associates (Minneapolis, MN). A Tamiya 72005 6 speed gearbox configured for a 1300:1 gear ratio and providing an output shaft stall torque of 8.9 N□m at 3 V coil

voltage was purchased from Tamiya America Inc. (Irvine, CA). A custom shaft coupler was fabricated using a Stratasys Dimension (SST-1200es) 3D printer (Stratasys Ltd., Eden Priarie, MN) to allow a screw bit or hex key to be coupled to the output shaft of the gearbox. An Arduino Uno microcontroller board was purchased from Adafruit Industries (New York, NY).

5.3.2 Microchannel and pump fabrication

COP plaques were either diced, or milled to 3.5cm X 3.5cm squares. Microchannels were directly milled using a CNC machine (MDX-650A; Roland, Lake Forest, CA) on either purchased 2mm COP plaques, or in-house 6 mm thick COPs using a 200 μm diameter endmills. Vias connecting microfluidic channels to the pump reservoir were similarly milled with a 1 mm diameter endmill.

To create the pump reservoirs, COP plaques were mounted sideways on a low-profile vise (Palmgren, Naperville, IL) and milled using 3mm diameter endmills. For flow-rate studies the reservoirs were then tapped using an appropriate-sized tapping set. For watertight experiments, reservoirs were treated with a 1:10 solution of cyclohexane: ethanol for 2 min to induce orogenic growth on the sidewalls, softening the inner walls of reservoir and creating a smooth, watertight surface to interact with plastic O-rings.

A lathe equipped with a 1 mm thick blade was used to machine grooves for O-ring seating into 3 mm diameter stainless steel rods cut to 1.2 cm length to be used as plungers. Viton O-rings with inner diameter of 1.1mm and cross-section of 1.5 mm were purchased from Precision Associates, Inc. (Minneapolis, MN).

5.3.3 Automation of pumping

To enable automated and programmable pump control, an microcontroller board (Arduino Uno) was selected as a convenient and low cost physical computing platform with a robust integrated development environment that supports . As summarized in Figure 5.2, the microcontroller was interfaced with a DC motor connected to a gearbox to increase output torque and provide more precise output shaft speed control. A custom shaft coupler provided convenient coupling between

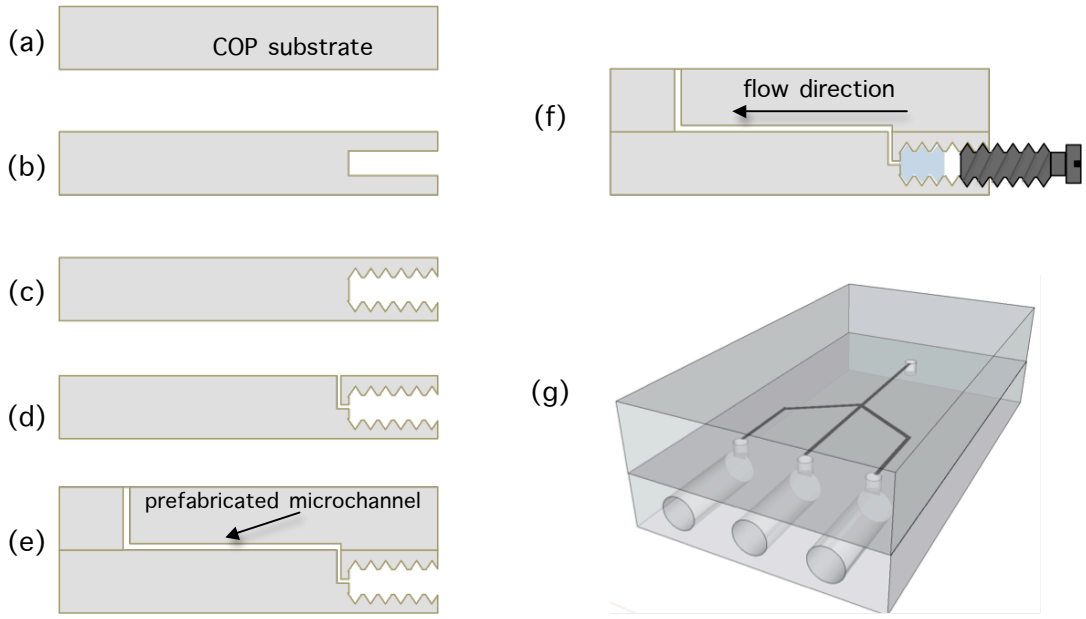

Figure 5.1 Fabrication of a micropump in a COP substrate. Following direct milling (b) and tapping (c) of reagent reservoirs, vias are micromachined (d) to connect reservoir to the top surface of COP. Solvent assisted bonding (e) is used to bond the top surface to a mating COP chip with prefabricated microchannels. Insertion and tightening of a screw (f) drives the liquid out of reservoir and circulates it through the microfluidic channels. 3-dimendional schematics of a flow-focusing device with three reagent reservoirs is shown (g).

the output shaft of the gearbox and the pumping screw integrated into the microfluidic chip. Software control of the screw bit rotation speed was achieved by modulating the average voltage applied to the DC motor through an 8-bit pulse width modulation (PWM) signal generated by the microcontroller at a frequency of

approximately 500 Hz. A 5 V power supply was connected to the motor through an inline power MOSFET (IRF520, Vishay) for switching the voltage using the microcontroller's PWM output.

5.3.4 Flow rate measurements

A camera mounted in front of test microfluidic chips recorded high-resolution videos while an Arduino-controlled screw-pump was used to dispense food coloring in a 5cm long serpentine microfluidic channel. The video was analyzed using QuickTime player (version 10.4, Apple Inc.) to measure fluid velocity experimentally. Empirical data was confirmed by theoretical flow rate values based on the number of rotations of screw, its diameter and pitch length.

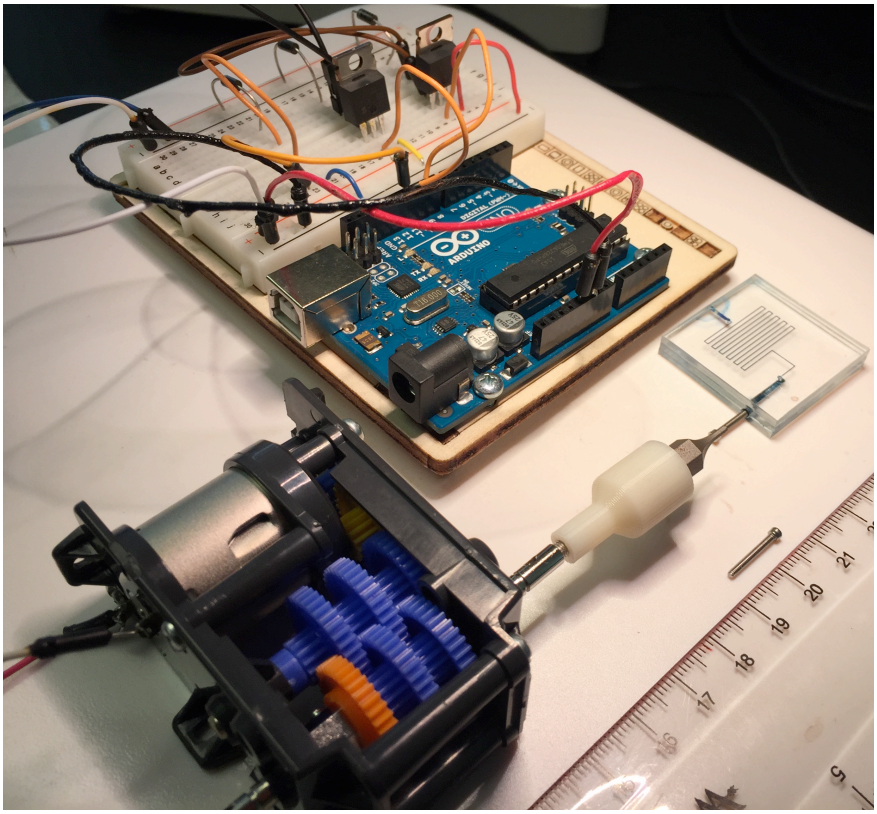

Figure 5.2 Experimental setup for evaluation of the automated micropumps with and Arduino-controlled DC motor screwdriver. Red frame highlights a 3D printer shaft coupler custom designed to fit hexagonal end of screwbits to make interchanging screw bits used to drive various pumps effortless.

5.4 Results and discussion

5.4.1 Fabrication of pump and reservoir

Thermoplastics are attractive materials for disposable point-of-care diagnostic assays due to their low cost. However unlike PDMS, where the inherent elasticity of the material can be utilized for fluid displacement in a wide variety of ways,[18–21,27,29,33] the integration of displacement pumps into thermoplastic devices cannot take advantage of elastic substrate deformations due to their high rigidity. Rather than relying on volume changes resulting from elastic strains, here we demonstrate a miniaturized pump based on rigid displacement of threaded screw elements integrated into COP thermoplastic chips. Reagent reservoirs were milled on the side of a 6 mm thick COP plate with an appropriate sized endmill as demonstrated in figure 5.1b. For devices that stainless steel screws were directly used for fluid displacement, an appropriate size tapping set was used to create grooves in the COP reservoir with identical pitch diameter to that of the screw used for pumping (Figure5.1c). A fluidic via is then milled to connect the bottom of the reservoir to the top surface of the COC platen (Figure 5.1d), followed by aligned, vapor-phase solvent bonding to permanently bond this surface to a mating COP chip containing microfluidic channels (Figure 5.1e). Reagents can be manually pipetted inside the reservoir, and pumping is triggered by driving the capping screw inside either manually, using a screwdriver, or automatically using the developed Arduino-based pump (Figure 5.1f). It is significant to note that although the fabrication process is demonstrated using micromilling, fabrication of the proposed reagent reservoir and pump is compatible with other common thermoplastic fabrication techniques including injection molding, and does

not add further complications or costs to device fabrication, a significant advantage for fabrication of point-of-care diagnostic devices.

5.4.2 Flow rate measurements

Two different screws of 4-40 (2.85 mm diameter, 40 threads per inch) and 0-80 (1.5 mm diameter, 80 threads per inch) sizes were used in experiments to investigate the impact of screw geometry on flow rate control. As demonstrated in Figure 5.3, the flow rate of the screw-driven displacement pumps was easily tuned by varying the duty cycle of the DC motor for both screw sizes, with linear response observed in each case for input signals up to 23% duty cycle. Over this range, repeatable average flow rates ranging from approximately 500 nL/min to 50 µl/min were achieved. Flow rates for duty cycles below 5% were not characterized since the friction generated in the gearbox system resulted in intermittent rotation of the motor for this input range. However, we note that lower flow rates can theoretically be achieved by either using motors with higher torque or more efficient gear systems with lower friction. For duty cycles over 25%, the relationship between duty cycle and flow rate became nonlinear, with saturation of the flow rate at 42 µl/min observed at 50% duty cycle. Further increase in duty cycle above the 50% threshold did not affect the flow rate due to a current limit of 650 mA for the power supply used in the experimental system.

The experimental average flow rate data presented in Figure 5.3 were measured using video recordings of at least 5 trials for each data point. Flow velocity was determined by measuring the distance travelled by a colored dye inside an initially-empty 5 cm long microchannel over a fixed time period, with volumetric flow rate determined from the known cross-sectional area of the channel, which was fabricated with equal width and height of 150 µm. The total volume of displaced liquid was also estimated from the known screw geometry and number of revolutions during each pumping cycle, with the experimental data differing from these geometric estimates by an average of 10±4%. The discrepancy between theoretical and experimental data is

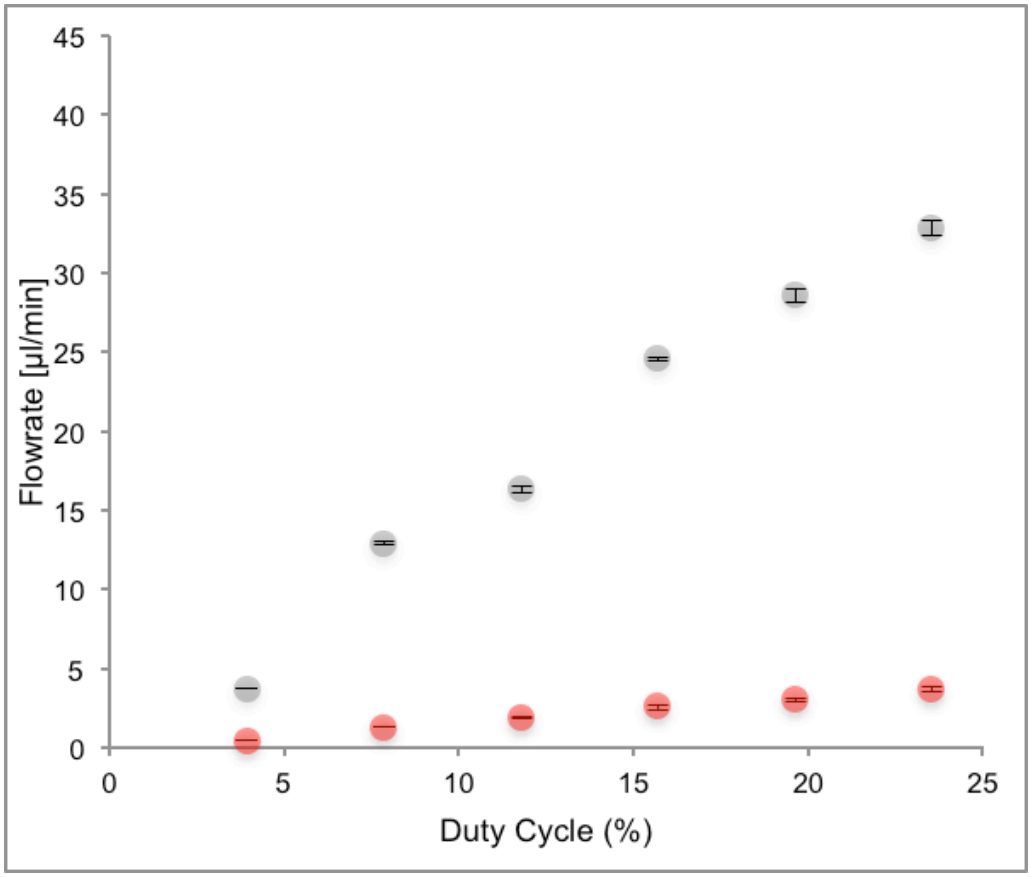

Figure 5.3 Flow rate of the screw-driven pump can be tuned by varying the duty cycle of the Arduino-based screwdriver, as well as the diameter of the stainless steel screw [2.85mm (gray) and 1.5mm (red)] Standard deviations are shown using black dashes.

likely due to imprecision in both the screw geometry and measurements of microfluidic channel dimensions.

5.4.3 Integration with Burst-valves

In addition to the controlled delivery of liquid reagents by using integrated micropumps, a goal of this chapter was to demonstrate that the reported micropump technology may be combined with single-use burst valves explored in chapter 5 to create a truly portable, independent platform for fluidic delivery in a thermoplastic microfluidic device. To explore this concept, a microfluidic device containing 4 independent sets of burst valves, reagent reservoirs, and pump elements was fabricated, as shown in Figure 5.7. This device was designed to mimic an on-chip immunoassay in which multiple wash buffers, secondary antibody, and reporter reagent must be controllably delivered through the analytical section of the device in a defined order. Regulation of the delivery sequence is controlled not only by the

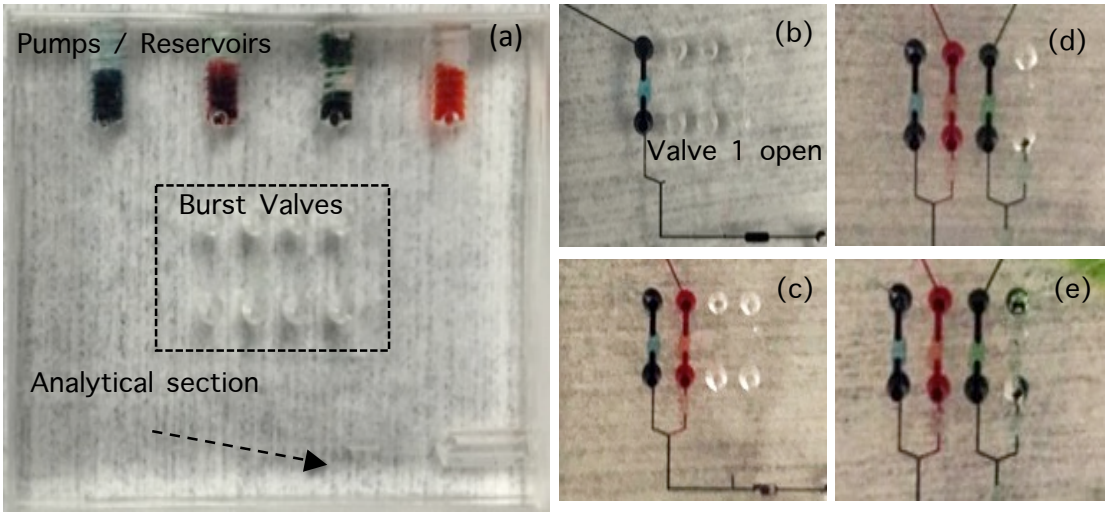

Figure 5.4 Microfluidic device with 4 integrated pump reservoirs burst-valves for use in diagnostic assay (a) close-up of the burst-valve region during sequential pumping and opening of valves (b-d) [using colored reagents for visualization] represents step-vise execution of a typical diagnostic assay.

screw-enabled pumps, but also by two sets of integrated burst valves. The first group of valves, highlighted in Figure 5.7a, are initially closed, and opened by actuation of the associated upstream pump. Fabrication of the secondary set of valves, highlighted in Figure 5.7e, was slightly altered compared to the process reported in chapter 4, with the the thermal bonding step omitted (Figure 4.1). By foregoing this last step, small open gaps are formed which bridge the channel discontinuity, creating a 5 μm tall fluidic pathway between the channel segments (Figure 4.2a). These small gaps serve as flow constrictors which limit unwanted mixing and backflow within the fluidically coupled microchannel network. Figure 5.7b-e depicts the sequential manual operation of the pumps, together with actuation of the integrated burst valves used for regulating fluid flow.

5.4.4 Integration of elastomer O-ring seals

During the previously described experiments, fluid leakage past the screws was occasionally observed at higher flow rates. In order to eliminate this potential leakage in our micropumps and achieve a watertight seal at the reservoir end, stainless steel rods equipped with indentations to house miniature O-rings were fabricated. Each rod was designed to serve as a sealed plunger which can move within a smooth-bored hole. An online tool[35] was used to calculate critical dimensions for both reagent reservoir as well as stainless steel pistons to achieve a watertight seal when equipped with a miniature O-ring, as shown in Figure 5.5. Critical dimensions of the stainless steel rod and O-ring were chosen such that a 30% compressive load, and 9% stretching force is applied when the O-ring is placed in the grooved section of the rod (1.2 mm diameter). Testing of the O-ring seals was performed using a microfluidic

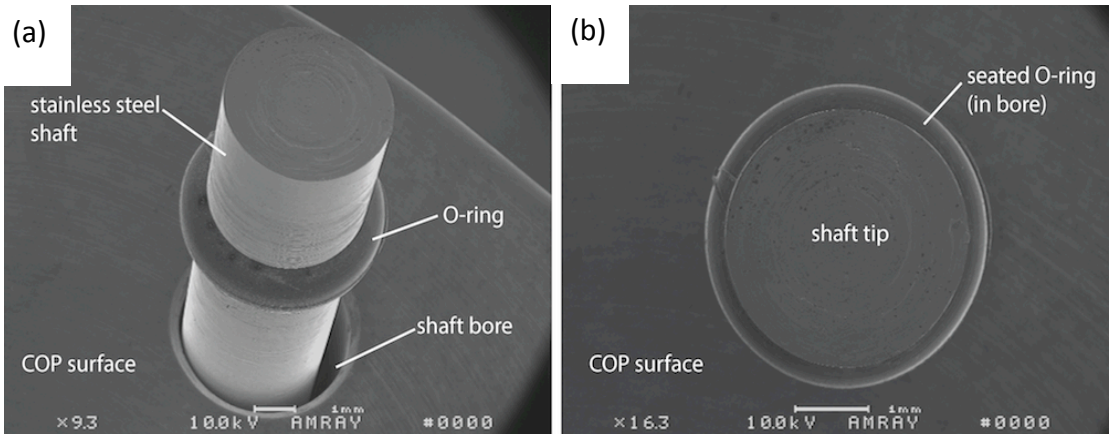

Figure 5.5 SEM images of O-ring equipped stainless steel rod used for watertight sealing and pumping from on-chip reagent reservoirs

device with two reservoirs with bore diameter of 3.0 mm, (Figure 5.6) in place of two inlets of a typical microfluidic T-junction, with a single outlet connected to atmospheric pressure. Once the two reservoirs were filled with different food coloring, pumps were actuated sequentially at ~20 µl/min while the device was observed for leakage. The T-junction design allowed leakage to be assessed using a microscope at the screw end of either pump, while the other was in operation. In order to quantify the maximum pressure elastomer O-rings could withstand, an analytical liquid chromatography pump (PU-2089; Jasco, Easton, MD) was interfaced to the outlet via high-pressure needle ports, providing precise volumetric flowrates and pressure measurements with 0.1MPa resolution. A constant flowrate of 1µl/min was applied to the outlet, while accumulated pressure was constantly monitored, with failure pressure of the o-ring seal determined by a sudden drop in back pressure. It was determined that the elastomer O-rings could withstand pressures up to 0.7±0.2 Mpa before leakage was observed, accompanied by sudden drop in pressure, demonstrating use of miniaturized O-rings as a suitable solution to achieve watertight

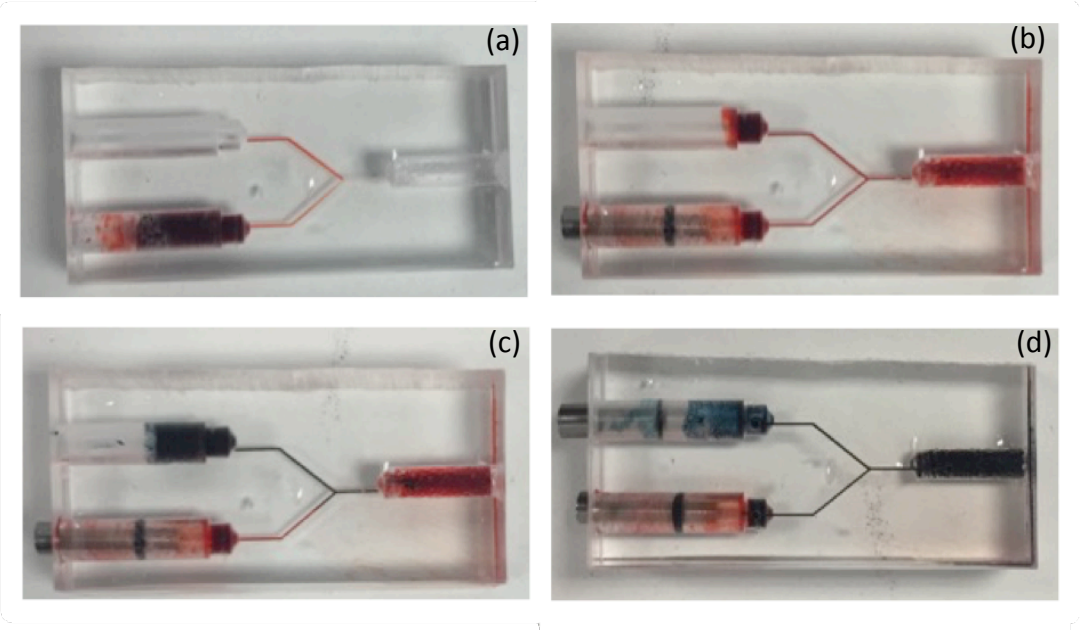

Figure 5.6 Microfluidic T-junction fabricated to test efficacy of watertight sealing of O-ring equipped micropumps. Food coloring is pipetted into one reservoir (a) and distributed in the microfluidic network since there are no signifanct resistive pathways(b) when the second reservoir is filled with food coloring (c) since pump 1 has been sealed with o-rings, the highly resistive pathway forces the entire liquid in the second reservoir to be carried into downstream outlet.

sealing for low-pressure experiments that require sequential pumping of multiple reagents.

5.5 Conclusions

A facile fabrication method for integrating on-chip micropumps into thermoplastic microfluidic substrates has been developed. The fabrication process is compatible with conventional processing methods employed for thermoplastic microfluidic device manufacture, enabling the integration of stainless steel screws as displacement pumps in for a wide range of microfluidic applications. The pumps are capable of achieving a wide range of flow rates by selecting appropriate screw diameter and thread size, while automated software-controlled operation of the integrated pumps is readily achieved by driving the screws with a geared DC motor coupled to a

microcontroller with simple circuitry that is highly amenable to miniaturization. Furthermore, together with previously reported single-use burst valves (Chapter 5) the integrated screw pumps directly support on-chip storage of both lyophilized and solvated reagents, as well as buffers, diluents, and wash solutions in liquid format. When coupled with burst valves, integrated micropumps enable facile separation of bioactive reagents and solvents, and can facilitates rapid reconstitution of lyophilized and hermetically sealed bioactive regents and their on-demand delivery in a truly miniaturized, fully portable, and automated package, a highly desirable feature for POC diagnostic platforms. Lastly, it is important to note that although the micropumps here were presented with an automated platform requiring a electric source for operation, in cases where précises flow rates are not essential, the technique allows the end-user full control of the fluid handling by simply using a screwdriver to operate the pump.

Chapter 6: Conclusions

6.1 Summary

This dissertation represents a series of original research conducted for development of a portable and disposable thermoplastic microfluidic device for use in point-of-care and resource-constrained settings. Despite the dominance of elastomer substrates in the microfluidics field, there are numerous inherent disadvantages of PDMS as a material that renders it unfavorable in several applications including point-of-care diagnostic platforms. On the other hand, most of the established techniques for device and component fabrication, including microfluidic valves and pumps also relies on inherent characteristics of PDMS (i.e. elastic deformation) and implementation of the same techniques on other substrates are non-trivial. Hence there is a significant need for creative and novel technological progress to facilitate the use of alternative materials.

As a potential solution to this unmet need, cyclic olefin polymer (COP) was chosen as ideal substrate for point-of-care diagnostic purposes, and a series of original research efforts were made towards the goal of developing a standalone portable and disposable thermoplastic microfluidic device. In Chapter 2, a novel fabrication method for micro and nano scale features in COP was established by utilizing an irreversible solvent swelling mechanism coined “orogenic microfabrication”. In addition, a wide variety of masking methods for micropatterning was explored, with each masking method offering unique characteristics to the resultant features. The knowledge gained from parametric studies in Chapter 3 laid a solid foundation

utilized in Chapters 3 and 4 for rapid prototyping of micro devices and development of single-use valves in thermoplastic substrates. In Chapter 3, direct masking using commercially available water soluble inks were utilized for rapid prototyping of fully sealed microfluidic devices in less than 30 minutes. To our knowledge, this "pen microfluidics" approach is one of the fastest methods for rapid prototyping of microfluidic devices that also allows for great control over channel dimensions. In Chapter 4, orogenic growth and UV/Ozone passivation masking was utilized to fabricated tunable single-use normally closed burst valves in thermoplastic substrates. Lastly, in Chapter 6 an on-chip integrated pumping method was established, capable of delivering buffers and reagents to the thermoplastic device with volumetric flow rates varying from nanoliters per minute to tens of microliters per minute. Combined with single-use burst valves, these micropumps give end-user complete control over on-chip fluid manipulation without the need for other external instruments.

All of the above technologies developed are highly cost effective, do not require significant investment in infrastructure, and are compatible with conventional thermoplastic microfabrication techniques such as micromilling used for prototyping, or injection molding for high throughput production. Moreover, integration of developed micropumps and burst valves in thermoplastic devices enables hermetic sealing, and can potentially be used for long-term on-chip storage of bioactive reagents in their lyophilized format, as well as buffers, diluents and washing solutions in their liquid form. Burst valves and micropumps also directly support facile separation of bioactive reagents and solvents, with on demand reconstitution and

rapid delivery in a truly portable and disposable package, a highly desired feature yet to be realized for POC diagnostic platforms.

6.2 Contributions to the field

The developed orogenic microfabrication technique is currently the only thermoplastic microfabrication technology for creating two dimensional microstructures or fully sealed microfluidic channels based on solvent-assisted swelling of the surface, rather than material displacement or removal. The fabrication technology is compatible with a wide variety of masking methods, with the choice of mask layer playing a significant impact on the morphology of resultant surface features, often difficult to replicate using other microfabrication techniques. In addition, Orogenic microfabrication allows for rapid manufacturing, enabling concept to device cycle times in a truly low-cost and scalable desktop process. This feature was highlighted in fabrication of fully sealed microfluidic channels in less than 30 minutes. To our knowledge, this "pen microfluidics" approach is the fastest methods for rapid prototyping of thermoplastic microfluidic devices that also allow for precise control over channel dimensions. In particular, the fabrication of low aspect ratio channels, often difficult to achieve using conventional microfabrication techniques, was demonstrated here with exceptional repeatability and precise control over channel height.

Another unique feature of orogenic microfabrication technique is its compatibility with other thermoplastic microfabrication techniques, a feature highlighted during realization of burst valves in thermoplastic substrates. The normally closed, single-used valves are the first homogenous valves in thermoplastic microfluidic devices

fabricated by utilizing differential bond strengths of solvent-assisted bonding and thermo-compression bonding. Reported burst valves can also be tuned to open at various pressures, allowing for flow regulation without the need for off-chip intervention. Burst valves also enable sealing and long-term storage of bioreagents lyophilized directly in thermoplastic microfluidic devices, achieved for the first time without the need for on-chip integration of other materials such as foil pouches[1] or glass ampules[2].

Screw-enabled micropumps enable delivery of liquid reagents to thermoplastic microfluidic devices in a truly integrated and portable manner. The low-cost, software controlled pump allows for automated delivery in a wide range of volumetric flow rates without the need for other on-chip components or complex fluidic circuitry to regulate on-chip flow.

The technologies covered in this dissertation have several unique characteristics in common. First, fabrication of surface features, fully sealed orogenic microchannels, and components such as valves and pumps have all been achieved in homogeneous thermoplastic substrate, without introduction of other materials that may complicate compatibility of resultant devices for various bioassays. Second, the fabrication processes developed are uniquely simple, and require minimal investment in laboratory infrastructure. Lastly, the simplicity of design and fabrication of burst valves and micropumps is mirrored in the ease of use of these components in microfluidic devices, where at their simplest form, the end user can control on-chip fluidic delivery and flow regulation using a single screwdriver.

Using thermoplastic substrate suitable for point-of-care diagnostic devices, the above developed fabrication technologies can all contribute in realization of a truly portable and disposable point-of-care diagnostic device that can be readily combined with low-cost point-of-care imaging instruments[3–5] to be used in resource-limited settings.

6.2 Future work

The long-term objective of this project was realization of a thermoplastic-based point-of-care diagnostic device. Besides the fluidic handling components developed here, there are three additional discrete components for sample processing, signal processing, and detection units required for realization of this goal.

One potential research direction is investigation of long-term storage of bioactive material in hermetically sealed reservoirs. Strategies for improving stability and controlled release of bioactive reagents such as enzymes and proteins has been investigated by the pharmaceutical industry[103–105], with freeze-drying in presence of lyoprotectant materials such as sucrose and trehalose proving to be the most common and effective approach. However a single universal formulation, or lyophilization recipe does not exist[140], requiring experimentation and validation of the process for each biomolecule. Furthermore, since formulation and stability studies are typically performed in bench-top assays using glass vials, on-chip lyophilization of bioactive reagents in thermoplastic substrates, and more importantly their controlled reconstitution and release in microfluidic platforms adds further complexity to the design, and requires a significant research effort.

Another possible research effort is the development of multiplex detection elements in thermoplastic substrates. Unlike PDMS, where a wide variety of techniques[141–143]

can be used to modify the surface of PDMS for attachment of immunoassay probes, the inertness and absence of functional groups on the surface of COP renders biomolecule attachment to it's surface challenging[144]. As an alternative to these surface modification techniques that result in planar detection zones, porous polymer monoliths[145–148] can be used as flow-through immunosensor platforms when integrated into thermoplastic devices, offering volumetric detection elements that can potentially enhance assay sensitivity and reduce assay time. In particular, batch fabrication of monoliths[148], combined with desktop inkjet printing[149,150] is an attractive option for multiplex detection of analytes within a single re-integrated monolith and merits further investigation.

In its current format our microfluidic platform does not incorporate sample processing capabilities, hence complex biological fluids typically used in bioanalysis such as blood or urine require an off-chip purification step prior to use. A wide variety of technologies including deterministic lateral displacement[151], affinity purification[152] , or hydrodynamic separation[153,154] methods can all be readily integrated within the microfluidic circuitry of the device, enabling filtering and separation of complex sample fluids prior to assay operation. Although each of these techniques have previously been demonstrated with success, achieving acceptable separation or purification percentages using technologies described in this work offers an intriguing challenge.

The above potential research directions can all contribute in realization of a truly portable and disposable point-of-care diagnostic device that can be readily combined

with low-cost point-of-care imaging instruments[155–157] to be used in resource-limited settings.

Bibliography

1. Terry, S. C., Jerman, J. H. & Angell, J. B. A gas chromatographic air analyzer fabricated on a silicon wafer. *IEEE Trans. Electron Devices* **26,** 1880–1886 (1979).

2. Manz, A., Graber, N. & Widmer, H. M. Miniaturized total chemical analysis systems: A novel concept for chemical sensing. *Sensors and Actuators B: Chemical* **1,** 244–248 (1990).

3. Xia, Y. & Whitesides, G. M. Soft Lithography. *Annu. Rev. Mater. Sci.* **28,** 153–184 (1998).

4. Jebrail, M. J., Bartsch, M. S. & Patel, K. D. Digital microfluidics: a versatile tool for applications in chemistry, biology and medicine. *Lab Chip* **12,** 2452 (2012).

5. Beebe, D. J., Mensing, G. a & Walker, G. M. Physics and applications of microfluidics in biology. *Annu. Rev. Biomed. Eng.* **4,** 261–286 (2002).

6. Dittrich, P. S. & Manz, A. Lab-on-a-chip: microfluidics in drug discovery. *Nat. Rev. Drug Discov.* **5,** 210–218 (2006).

7. Andersson, H. & Van den Berg, A. Microfluidic devices for cellomics: A review. *Sensors Actuators, B Chem.* **92,** 315–325 (2003).

8. Abou-Hassan, A., Sandre, O. & Cabuil, V. Microfluidics in inorganic chemistry. *Angew. Chemie - Int. Ed.* **49,** 6268–6286 (2010).

9. Squires, T. M. Microfluidics Fluid physics at the nanoliter.pdf. **77,** (2005).

10. Systems, B. Bioanalytical systems. *Environ. Sci. Technol.* **17,** 502A (1983).

11. Horsman, K. M., Bienvenue, J. M., Blasier, K. R. & Landers, J. P. Forensic DNA analysis on microfluidic devices: A review. *J. Forensic Sci.* **52,** 784–799 (2007).

12. Verpoorte, E. Microfluidic chips for clinical and forensic analysis. *Electrophoresis* **23,** 677–712 (2002).

13. Whitesides, G. M. The origins and the future of microfluidics. *Nature* **442,** 368–373 (2006).

14. Reyes, D. R., Iossifidis, D., Auroux, P.-A. & Manz, A. Micro total analysis systems. 1. Introduction, theory, and technology. *Anal. Chem.* **74,** 2623–2636 (2002).

15. Auroux, P. A., Iossifidis, D., Reyes, D. R. & Manz, A. Micro total analysis systems. 2. Analytical standard operations and applications. *Anal. Chem.* **74,** 2637–2652 (2002).

16. Quake, S. R. & Scherer, a. From micro- to nanofabrication with soft materials. *Science* **290,** 1536–1540 (2000).

17. Beebe, D. J. *et al.* Functional hydrogel structures for autonomous flow control inside microfluidic channels : Abstract : Nature. *Nature* **404,** 588–590 (2000).

18. Young, E. W. K. *et al.* Rapid prototyping of arrayed microfluidic systems in polystyrene for cell-based assays. *Anal. Chem.* **83,** 1408–1417 (2011).

19. Wang, Y. *et al.* Benchtop micromolding of polystyrene by soft lithography. *Lab Chip* **11,** 3089–3097 (2011).

20. Xu, J., Locascio, L., Gaitan, M. & Lee, C. S. Room-temperature imprinting method for plastic microchannel fabrication. *Anal. Chem.* **72,** 1930–1933 (2000).

21. Liedert, R. *et al.* Disposable roll-to-roll hot embossed electrophoresis chip for detection of antibiotic resistance gene mecA in bacteria. *Lab Chip* **12,** 333 (2012).

22. Roberts, M. a., Rossier, J. S., Bercier, P. & Girault, H. UV laser machined polymer substrates for the development of microdiagnostic systems. *Anal. Chem.* **69,** 2035–2042 (1997).

23. Nunes, P. S., Ohlsson, P. D., Ordeig, O. & Kutter, J. P. Cyclic olefin polymers: Emerging materials for lab-on-a-chip applications. *Microfluid. Nanofluidics* **9,** 145–161 (2010).

24. Niles, W. D. & Coassin, P. J. Cyclic olefin polymers: innovative materials for high-density multiwell plates. *Assay Drug Dev. Technol.* **6,** 577–590 (2008).

25. Kuo, J. S. & Chiu, D. T. Disposable microfluidic substrates: transitioning from the research laboratory into the clinic. *Lab Chip* **11,** 2656–2665 (2011).

26. Berthier, E., Young, E. W. K. & Beebe, D. Engineers are from PDMS-land, Biologists are from Polystyrenia. *Lab Chip* **12,** 1224 (2012).

27. Sia, S. K. & Kricka, L. J. Microfluidics and point-of-care testing. *Lab Chip* **8,** 1982–1983 (2008).

28. Yager, P. *et al.* Microfluidic diagnostic technologies for global public health. *Nature* **442,** 412–418 (2006).

29. Gubala, V., Harris, L. F., Ricco, A. J., Tan, M. X. & Williams, D. E. Point of care diagnostics: Status and future. *Anal. Chem.* **84,** 487–515 (2012).

30. Gervais, L., De Rooij, N. & Delamarche, E. Microfluidic chips for point-of-care immunodiagnostics. *Adv. Mater.* **23,** (2011).

31. Becker, H. & Gärtner, C. Polymer microfabrication technologies for microfluidic systems. *Anal. Bioanal. Chem.* **390,** 89–111 (2008).

32. Ng, S. H. & Wang, Z. F. Hot roller embossing for microfluidics: Process and challenges. *Microsyst. Technol.* **15,** 1149–1156 (2009).

33. Rahmanian, O., Chen, C. F. & Devoe, D. L. Microscale patterning of thermoplastic polymer surfaces by selective solvent swelling. *Langmuir* **28,** 12923–12929 (2012).

34. Rahmanian, O. & DeVoe, D. L. Pen microfluidics: rapid desktop manufacturing of sealed thermoplastic microchannels. *Lab Chip* **13,** 1102–8 (2013).

35. Rahmanian, O. D. & DeVoe, D. L. Single-use thermoplastic microfluidic burst valves enabling on-chip reagent storage. *Microfluid. Nanofluidics* **18,** 1045–1053 (2015).

36. Tsao, C. W. & DeVoe, D. L. Bonding of thermoplastic polymer microfluidics. *Microfluid. Nanofluidics* **6,** 1–16 (2009).

37. Cristea, D., Obreja, P., Kusko, M., Manea, E. & Rebigan, R. Polymer micromachining for micro- and nanophotonics. *Mater. Sci. Eng. C* **26,** 1049–1055 (2006).

38. McFarland, A. W. & Colton, J. S. Chemical sensing with micromolded plastic microcantilevers. *J. Microelectromechanical Syst.* **14,** 1375–1385 (2005).

39. Lee, Y., Park, S. H., Kim, K. B. & Lee, J. K. Fabrication of hierarchical structures on a polymer surface to mimic natural superhydrophobic surfaces. *Adv. Mater.* **19,** 2330–2335 (2007).

40. Schulte, A. J., Koch, K., Spaeth, M. & Barthlott, W. Biomimetic replicas: Transfer of complex architectures with different optical properties from plant surfaces onto technical materials. *Acta Biomater.* **5,** 1848–1854 (2009).

41. Shin, J. Y., Park, J. Y., Liu, C., He, J. & Kim, S. C. Chemical structure and physical properties of cyclic olefin copolymers (IUPAC Technical Report). *Pure Appl. Chem.* **77,** 801–814 (2005).

42. Martynova, L. *et al.* Fabrication of plastic microfluid channels by imprinting methods. *Anal. Chem.* **69,** 4783–4789 (1997).

43. Heckele, M. & Schomburg, W. K. Review on micro molding of thermoplastic polymers. *J. Micromechanics Microengineering* **14,** R1–R14 (2003).

44. Wang, L., Zhang, D., Wen, Z. & Zhang, H. Micro-fabrication and monitoring of three-dimensional microstructures based on laser-induced thermoplastic formation. *Microsc. Res. Tech.* **72,** 717–722 (2009).

45. Chen, C. F. *et al.* High-pressure needle interface for thermoplastic microfluidics. *Lab Chip* **9,** 50–55 (2009).

46. Attia, U. M., Marson, S. & Alcock, J. R. Micro-injection moulding of polymer microfluidic devices. *Microfluid. Nanofluidics* **7,** 1–28 (2009).

47. Tsao, C. W., Hromada, L., Liu, J., Kumar, P. & DeVoe, D. L. Low temperature bonding of PMMA and COC microfluidic substrates using UV/ozone surface treatment. *Lab Chip* **7,** 499–505 (2007).

48. Enoch Kim, Younan Xia, Xiao-Mei Zhao, and G. M. Wh. Solvent-Assisted Microcontact Molding: A Convenient Method for Fabricating Three-Dimensional Structures on Surfaces of Polymers. *Adv. Mater.* 651–654 (1997).

49. Suh, K. Y. & Lee, H. H. Capillary force lithography: Large-area patterning, self-organization, and anisotropic dewetting. *Adv. Funct. Mater.* **12,** 405–413 (2002).

50. Suh, K. Y., Park, M. C. & Kim, P. Capillary force lithography: A versatile tool for structured biomaterials interface towards cell and tissue engineering. *Adv. Funct. Mater.* **19,** 2699–2712 (2009).

51. Brydson, J. A. *Plastic Materials*. (Butterworth-Heinemann, 1999).

52. Hilderbrandt, J. & Scott, R. *The solubility of non-electrolytes*. (Reinhold: New York, 1949).

53. Cruickshank, A. J. B. & Cutler, a J. B. Vapor pressure of cyclohexane, 25 to 75 degree. *J. Chem. Eng. Data* **12,** 326–329 (1967).

54. Wallow, T. I. *et al.* Low-distortion, high-strength bonding of thermoplastic microfluidic devices employing case-II diffusion-mediated permeant activation. *Lab Chip* **7,** 1825–1831 (2007).

55. Thomas, N. . & Windle, A. . A theory of case II diffusion. *Polymer (Guildf).* **23,** 529–542 (1982).

56. Wei, S., Vaidya, B., Patel, A. B., Soper, S. a. & McCarley, R. L. Photochemically patterned poly(methyl methacrylate) surfaces used in the fabrication of microanalytical devices. *J. Phys. Chem. B* **109,** 16988–16996 (2005).

57. Lausted, C. G., Warren, C. B., Hood, L. E. & Lasky, S. R. Printing Your Own Inkjet Microarrays. *Methods Enzymol.* **410,** 168–189 (2006).

58. Lee, J. N., Park, C. & Whitesides, G. M. Solvent Compatibility of Poly(dimethylsiloxane)-Based Microfluidic Devices. *Anal. Chem.* **75,** 6544–6554 (2003).

59. Lucio, C. *et al.* Article A Dry Process for Production of Microfluidic Devices Based on the Lamination of Laser-Printed Polyester Films A Dry Process for Production of Microfluidic Devices Based on the Lamination of Laser-Printed Polyester Films. *Anal. Chem.* **75,** 3853–3858 (2003).

60. Liu, A.-L. *et al.* Rapid method for design and fabrication of passive micromixers in microfluidic devices using a direct-printing process. *Lab Chip* **5,** 974–978 (2005).

61. Coltro, W. K. T., De Jesus, D. P., Da Silva, J. A. F., Do Lago, C. L. & Carrilho, E. Toner and paper-based fabrication techniques for microfluidic applications. *Electrophoresis* **31,** 2487–2498 (2010).

62. Do, J., Zhang, J. Y. & Klapperich, C. M. Maskless writing of microfluidics: Rapid prototyping of 3D microfluidics using scratch on a polymer substrate. *Robot. Comput. Integr. Manuf.* **27,** 245–248 (2011).

63. Nath, P. *et al.* Rapid prototyping of robust and versatile microfluidic components using adhesive transfer tapes. *Lab Chip* **10,** 2286–2291 (2010).

64. Yuen, P. K. & Goral, V. N. Low-cost rapid prototyping of flexible microfluidic devices using a desktop digital craft cutter. *Lab Chip* **10,** 384–387 (2010).

65. Hansen, T. S., Selmeczi, D. & Larsen, N. B. Fast prototyping of injection molded polymer microfluidic chips. *J. Micromechanics Microengineering* **20,** 015020 (2009).

66. Truckenmüller, R. *et al.* Thermoforming of film-based biomedical microdevices. *Adv. Mater.* **23,** 1311–1329 (2011).

67. Velten, T. *et al.* Microfluidics on foil: state of the art and new developments. *Proc. Inst. Mech. Eng. Part B J. Eng. Manuf.* **222,** 107–116 (2008).

68. Rötting, O., Röpke, W., Becker, H. & Gärtner, C. Polymer microfabrication technologies. *Microsyst. Technol.* **8,** 32–36 (2002).

69. Becker, H. & Locascio, L. E. Polymer microfluidic devices. *Talanta* **56,** 267–287 (2002).

70. Becker, H. & Gärtner, C. Polymer microfabrication methods for microfluidic analytical applications. *Electrophoresis* **21,** 12–26 (2000).

71. Ro, K. W., Liu, J. & Knapp, D. R. Plastic microchip liquid chromatography-matrix-assisted laser desorption/ionization mass spectrometry using monolithic columns. *J. Chromatogr. A* **1111,** 40–47 (2006).

72. Tsao, C. W., Kumar, P., Liu, J. & DeVoe, D. L. Dynamic electrowetting on nanofilament silicon for matrix-free laser desorption/ionization mass spectrometry. *Anal. Chem.* **80,** 2973–2981 (2008).

73. Chen, C.-F., Liu, J., Chang, C.-C. & DeVoe, D. L. High-pressure on-chip mechanical valves for thermoplastic microfluidic devices. *Lab Chip* **9,** 3511–3516 (2009).

74. Rosen, M. J. & Kunjappu, J. T. *Surfactants and Phenomena, Fourth Edition*. (2012).

75. Hunger, K. & Wiley-vch, A. *Industrial Dyes:* **125,** (2003).

76. Material Safety Data Sheet MSDS for Vis-A-Vis, overhead projector pen permanent extra fine point and fine point. (1999).

77. Xia, D., Yan, J. & Hou, S. Fabrication of nanofluidic biochips with nanochannels for applications in DNA analysis. *Small* **8,** 2787–2801 (2012).

78. Xu, B.-Y., Xu, J.-J., Xia, X.-H. & Chen, H.-Y. Large scale lithography-free nano channel array on polystyrene. *Lab Chip* **10,** 2894–2901 (2010).

79. Hamblin, M. N. *et al.* Selective trapping and concentration of nanoparticles and viruses in dual-height nanofluidic channels. *Lab Chip* **10,** 173–178 (2010).

80. Chantiwas, R. *et al.* Simple replication methods for producing nanoslits in thermoplastics and the transport dynamics of double-stranded DNA through these slits. *Lab Chip* **10,** 3255–3264 (2010).

81. Fu, J., Yoo, J. & Han, J. Molecular sieving in periodic free-energy landscapes created by patterned nanofilter arrays. *Phys. Rev. Lett.* **97,** 1–4 (2006).

82. O'Brien, M. J. *et al.* Fabrication of an integrated nanofluidic chip using interferometric lithography. *J. Vac. Sci. Technol. B Microelectron. Nanom. Struct.* **21,** 2941 (2003).

83. Huang, L. R. *et al.* A DNA prism for high-speed continuous fractionation of large DNA molecules. *Nat. Biotechnol.* **20,** 1048–1051 (2002).

84. Bartholomeusz, D. a., Boutté, R. W. & Andrade, J. D. Xurography: Rapid prototyping of microstructures using a cutting plotter. *J. Microelectromechanical Syst.* **14,** 1364–1374 (2005).

85. Aguilera-Herrador, E., Cruz-Vera, M. & Valcárcel, M. Analytical connotations of point-of-care testing. *Analyst* **135,** 2220–2232 (2010).

86. Oh, K. W. & Ahn, C. H. A review of microvalves. *J. Micromechanics Microengineering* **16,** R13–R39 (2006).

87. Hosokawa, K. & Maeda, R. A pneumatically-actuated three-way microvalve fabricated with polydimethylsiloxane using the membrane transfer technique. *J. Micromechanics Microengineering* **10,** 415–420 (2000).

88. Grover, W. H., Ivester, R. H. C., Jensen, E. C. & Mathies, R. a. Development and multiplexed control of latching pneumatic valves using microfluidic logical structures. *Lab Chip* **6,** 623–631 (2006).

89. Blazej, R. G., Kumaresan, P. & Mathies, R. a. Microfabricated bioprocessor for integrated nanoliter-scale Sanger DNA sequencing. *Proc. Natl. Acad. Sci. U. S. A.* **103,** 7240–7245 (2006).

90. Yang, Y. N., Hsiung, S. K. & Lee, G. B. A pneumatic micropump incorporated with a normally closed valve capable of generating a high pumping rate and a high back pressure. *Microfluid. Nanofluidics* **6,** 823–833 (2009).

91. Kuo, C. H., Wang, J. H. & Lee, G. B. A microfabricated CE chip for DNA pre-concentration and separation utilizing a normally closed valve. *Electrophoresis* **30,** 3228–3235 (2009).

92. Mosadegh, B., Tavana, H., Lesher-Perez, S. C. & Takayama, S. High-density fabrication of normally closed microfluidic valves by patterned deactivation of oxidized polydimethylsiloxane. *Lab Chip* **11,** 738–742 (2011).

93. Madou, M. *et al.* Lab on a CD. *Annu. Rev. Biomed. Eng.* **8,** 601–628 (2006).

94. Gorkin, R. *et al.* Centrifugal microfluidics for biomedical applications. *Lab Chip* **10,** 1758–1773 (2010).

95. Luo, Q., Mutlu, S., Gianchandani, Y. B., Svec, F. & Fréchet, J. M. J. Monolithic valves for microfluidic chips based on thermoresponsive polymer gels. *Electrophoresis* **24,** 3694–3702 (2003).

96. Chen, G., Svec, F. & Knapp, D. R. Light-actuated high pressure-resisting microvalve for on-chip flow control based on thermo-responsive nanostructured polymer. *Lab Chip* **8,** 1198–1204 (2008).

97. Liu, R. H., Bonanno, J., Yang, J., Lenigk, R. & Grodzinski, P. Single-use, thermally actuated paraffin valves for microfluidic applications. *Sensors Actuators, B Chem.* **98,** 328–336 (2004).

98. Park, J.-M., Cho, Y.-K., Lee, B.-S., Lee, J.-G. & Ko, C. Multifunctional microvalves control by optical illumination on nanoheaters and its application in centrifugal microfluidic devices. *Lab Chip* **7,** 557–564 (2007).

99. Garcia-Cordero, J. L. *et al.* Optically addressable single-use microfluidic valves by laser printer lithography. *Lab Chip* **10,** 2680–2687 (2010).

100. Van Oordt, T., Barb, Y., Smetana, J., Zengerle, R. & von Stetten, F. Miniature stick-packaging--an industrial technology for pre-storage and release of reagents in lab-on-a-chip systems. *Lab Chip* **13,** 2888–92 (2013).

101. Hoffmann, J., Mark, D., Lutz, S., Zengerle, R. & von Stetten, F. Pre-storage of liquid reagents in glass ampoules for DNA extraction on a fully integrated lab-on-a-chip cartridge. *Lab Chip* **10,** 1480–1484 (2010).

102. Ramachandran, S., Fu, E., Lutz, B. & Yager, P. Long-term dry storage of an enzyme-based reagent system for ELISA in point-of-care devices. *Analyst* **139,** 1456–62 (2014).

103. Cleland, J. L. *et al.* A specific molar ratio of stabilizer to protein is required for storage stability of a lyophilized monoclonal antibody. *J. Pharm. Sci.* **90,** 310–321 (2001).

104. Meyer, J. D., Nayar, R. & Manning, M. C. Impact of bulking agents on the stability of a lyophilized monoclonal antibody. *Eur. J. Pharm. Sci.* **38,** 29–38 (2009).

105. Chang, L. (lucy) & Pikal, M. J. Mechanisms of Protein Stabilizaation in the Solid State. *J. Pharm. Sci.* **98,** 2886–2908 (2009).

106. Nguyen, N.-T., Huang, X. & Chuan, T. K. MEMS-Micropumps: A Review. *J. Fluids Eng.* **124,** 384 (2002).

107. Iverson, B. D. & Garimella, S. V. Recent advances in microscale pumping technologies: A review and evaluation. *Microfluid. Nanofluidics* **5,** 145–174 (2008).

108. Au, A. K., Lai, H., Utela, B. R. & Folch, A. *Microvalves and micropumps for BioMEMS*. *Micromachines* **2,** (2011).

109. Chin, C. D. *et al.* Microfluidics-based diagnostics of infectious diseases in the developing world. *Nat. Med.* **17,** 1015–1019 (2011).

110. Patrick, W. Open source syringe pump; As visited in May 2015. (2013). at <http://fab.cba.mit.edu/classes/4.140/people/wildebeest/projects/final/>

111. Biochemtronics. Simple Syringe Pumps; Visited in May 2015. (2015). at <http://www.instructables.com/id/Simple-Syringe-Pump/>

112. DIY Syringe Pump Version 3; Visited in May 2015. (2015). at <https://aonomus.wordpress.com/2010/04/02/diy-syringe-pump-version-3/>

113. Czugala, M. *et al.* Optical sensing system based on wireless paired emitter detector diode device and ionogels for lab-on-a-disc water quality analysis. *Lab Chip* **12,** 5069 (2012).

114. Aeinehvand, M. M. *et al.* Latex micro-balloon pumping in centrifugal microfluidic platforms. *Lab Chip* **14,** 988–97 (2014).

115. Zimmermann, M., Hunziker, P. & Delamarche, E. Valves for autonomous capillary systems. *Microfluid. Nanofluidics* **5,** 395–402 (2008).

116. Guan, Y. X., Xu, Z. R., Dai, J. & Fang, Z. L. The use of a micropump based on capillary and evaporation effects in a microfluidic flow injection chemiluminescence system. *Talanta* **68,** 1384–1389 (2006).

117. Gervais, L. & Delamarche, E. Toward one-step point-of-care immunodiagnostics using capillary-driven microfluidics and PDMS substrates. *Lab Chip* **9,** 3330–3337 (2009).

118. Gervais, L., Hitzbleck, M. & Delamarche, E. Capillary-driven multiparametric microfluidic chips for one-step immunoassays. *Biosens. Bioelectron.* **27,** 64–70 (2011).

119. Lu, F. *et al.* A siphonage flow and thread-based low-cost platform enables quantitative and sensitive assays. *Lab Chip* **15,** 495–503 (2015).

120. Yao, B. *et al.* A microfluidic device based on gravity and electric force driving for flow cytometry and fluorescence activated cell sorting. *Lab Chip* **4,** 603–607 (2004).

121. Du, W. B., Fang, Q., He, Q. H. & Fang, Z. L. High-throughput nanoliter sample introduction microfluidic chip-based flow injection analysis system with gravity-driven flows. *Anal. Chem.* **77,** 1330–1337 (2005).

122. Gong, M. M., MacDonald, B. D., Vu Nguyen, T. & Sinton, D. Hand-powered microfluidics: A membrane pump with a patient-to-chip syringe interface. *Biomicrofluidics* **6,** 1–13 (2012).

123. Li, G., Luo, Y., Chen, Q., Liao, L. & Zhao, J. A 'place n play' modular pump for portable microfluidic applications. *Biomicrofluidics* **6,** 1–16 (2012).

124. Xu, L., Lee, H. & Oh, K. W. Syringe-assisted point-of-care micropumping utilizing the gas permeability of polydimethylsiloxane. *Microfluid. Nanofluidics* 1–6 (2014). doi:10.1007/s10404-014-1356-4

125. Weibel, D. B., Siegel, A. C., Lee, A., George, A. H. & Whitesides, G. M. Pumping fluids in microfluidic systems using the elastic deformation of poly(dimethylsiloxane). *Lab Chip* **7,** 1832–1836 (2007).

126. Rhee, M. & Burns, M. a. Microfluidic pneumatic logic circuits and digital pneumatic microprocessors for integrated microfluidic systems. *Lab Chip* **9,** 3131–3143 (2009).

127. Dimov, I. K. *et al.* Stand-alone self-powered integrated microfluidic blood analysis system (SIMBAS). *Lab Chip* **11,** 845–850 (2011).

128. Li, W. *et al.* Squeeze-chip: a finger-controlled microfluidic flow network device and its application to biochemical assays. *Lab Chip* **12,** 1587 (2012).

129. Iwai, K. *et al.* Finger-Powered Microfluidic Systems Using Multilayer Soft Lithography and Injection Molding Processes. *Lab Chip* 18–20 (2014). doi:10.1039/C4LC00500G

130. Lai, H. & Folch, A. Design and dynamic characterization of 'single-stroke' peristaltic PDMS micropumps. *Lab Chip* **11,** 336–342 (2011).

131. Chen, C.-Y., Chen, C.-H., Tu, T.-Y., Lin, C.-M. & Wo, A. M. Electrical isolation and characteristics of permanent magnet-actuated valves for PDMS microfluidics. *Lab Chip* **11,** 733–737 (2011).

132. Gu, P., Liu, K., Chen, H., Nishida, T. & Fan, Z. H. Chemical-assisted bonding of thermoplastics/elastomer for fabricating microfluidic valves. *Anal. Chem.* **83,** 446–452 (2011).

133. Weibel, D. B. *et al.* Torque-actuated valves for microfluidics. *Anal. Chem.* **77,** 4726–4733 (2005).

134. Hulme, S. E., Shevkoplyas, S. S. & Whitesides, G. M. Incorporation of prefabricated screw, pneumatic, and solenoid valves into microfluidic devices. *Lab Chip* **9,** 79–86 (2009).

135. Markov, D. a. *et al.* Tape underlayment rotary-node (TURN) valves for simple on-chip microfluidic flow control. *Biomed. Microdevices* **12,** 135–144 (2010).

136. Liong, M. *et al.* Magnetic barcode assay for genetic detection of pathogens. *Nat. Commun.* **4,** 1752 (2013).

137. Cha, K. J. & Kim, D. S. A portable pressure pump for microfluidic lab-on-a-chip systems using a porous polydimethylsiloxane (PDMS) sponge. *Biomed. Microdevices* **13,** 877–883 (2011).

138. Oh, K. W., Lee, K., Ahn, B. & Furlani, E. P. Design of pressure-driven microfluidic networks using electric circuit analogy. *Lab Chip* **12,** 515 (2012).

139. O-Ring Gland Calculator by AppleRubber ; Visited in May 2015. at <http://www.applerubber.com/oring-gland-calculator/>

140. Carpenter, J. F., Chang, B. S., Garzon-Rodriguez, W. & Randolph, T. W. Rational Design of Stable Lyophilized Protein. 109–133 (2002).

141. Makamba, H., Kim, J. H., Lim, K., Park, N. & Hahn, J. H. Surface modification of poly(dimethylsiloxane) microchannels. *Electrophoresis* **24,** 3607–3619 (2003).

142. Zhou, J., Ellis, A. V. & Voelcker, N. H. Recent developments in PDMS surface modification for microfluidic devices. *Electrophoresis* **31,** 2–16 (2010).

143. Henry, A. C. *et al.* Surface Modification of Poly (methyl methacrylate) Used in the Fabrication of Microanalytical Devices Surface Modification of Poly (methyl methacrylate) Used in the Fabrication of Microanalytical Devices. *Society* **72,** 5331–5337 (2000).

144. Ooi, H. W. *et al.* Coordination complexes as molecular glue for immobilization of antibodies on cyclic olefin copolymer surfaces. *Anal. Biochem.* **456,** 6–13 (2014).

145. Liu, J., Chen, C. F., Chang, C. W. & DeVoe, D. L. Flow-through immunosensors using antibody-immobilized polymer monoliths. *Biosens. Bioelectron.* **26,** 182–188 (2010).

146. Liu, J., White, I. & DeVoe, D. L. Nanoparticle-functionalized porous polymer monolith detection elements for surface-enhanced raman scattering. *Anal. Chem.* **83,** 2119–2124 (2011).

147. Liu, J. *et al.* Polymer microchips integrating solid-phase extraction and high-performance liquid chromatography using reversed-phase polymethacrylate monoliths. *Anal. Chem.* **81,** 2545–2554 (2009).

148. Kendall, E. L., Wienhold, E., Rahmanian, O. D. & Devoe, D. L. Ex situ integration of multifunctional porous polymer monoliths into thermoplastic microfluidic chips. *Sensors Actuators, B Chem.* **202,** 866–872 (2014).

149. Yu, W. W. & White, I. M. Inkjet printed surface enhanced raman spectroscopy array on cellulose paper. *Anal. Chem.* **82,** 9626–9630 (2010).

150. Yu, W. W. & White, I. M. Inkjet-printed paper-based SERS dipsticks and swabs for trace chemical detection. *Analyst* **138,** (2012).

151. McGrath, J., Jimenez, M. & Bridle, H. Deterministic lateral displacement for particle separation: a review. *Lab Chip* **14,** 4139–4158 (2014).

152. Dineva, M. A., MahiLum-Tapay, L. & Lee, H. Sample preparation: a challenge in the development of point-of-care nucleic acid-based assays for resource-limited settings. *Analyst* **132,** 1193–1199 (2007).

153. Kersaudy-Kerhoas, M., Kavanagh, D. M., Dhariwal, R. S., Campbell, C. J. & Desmulliez, M. P. Y. Validation of a blood plasma separation system by biomarker detection. *Lab Chip* **10,** 1587–1595 (2010).

154. Yang, S., Undar, A. & Zahn, J. D. A microfluidic device for continuous, real time blood plasma separation. *Lab Chip* **6,** 871–880 (2006).

155. Boppart, S. A. & Richards-kortum, R. Point-of-care and point-of-procedure optical imaging technologies for primary care and global health. **6,** (2014).

156. Laksanasopin, T. *et al.* A smartphone dongle for diagnosis of infectious diseases at the point of care. **7,** (2015).

157. Ambrosio, M. V. D. *et al.* Point-of-care quantification of blood-borne filarial parasites with a mobile phone microscope. **7,** (2015).